UNIVERSITY OF NAPLES "FEDERICO II"

PhD Program

Molecular Pathology and Physiopathology

School of Molecular Medicine

XXVII Cycle

Local DNA oxidation and DNA methylation define chromatin loops and drive the transcription cycles induced by estrogen

SUPERVISOR
Prof. Vittorio Enrico Avvedimento

CANDIDATE
Dr. Antonio Pezone

PhD COORDINATOR
Prof. Vittorio Enrico Avvedimento

Academic Year 2013-2014

“L’immaginare rende tutto possibile”

For you, that'll fill up my days…

Local DNA oxidation and DNA methylation define chromatin loops and drive the transcription cycles induced by estrogen

TABLE OF CONTENTS

LIST OF ABBREVIATION

3C Chromosome conformation capture
5-caC 5-carboxylCytosine
5-fC 5-formylCytosine
8-oxo-dG 8-oxo-7,8- dihydroGuanine
Ab Antibody
Bcl-2 B-cell lymphoma 2
BER Base Excision Repair
Bp base-pair
CAV1 Caveolin-1
ChIP Chromatin Immuno-Precipitation
CTD Carboxyl-Terminal Domain
DDB DNA-damage binding
DNMTs DNA methyltransferases
E2 Estrogen
ER estrogen receptor
ERE estrogen response elements
FAD Flavin Adenine Dinucleotide
FEN1 Flap EndoNuclease-1
GG-NER global genomic NER
Gs Guanines
H_2O_2 Hydrogen peroxide
H3K27me3 trimethylation of lysine 27/histone H3
H3K36me3 trimethylation of lysines 36/ histone H3
H3K4me2/me3 di- and trimethylation of lysine 4/ histone H3
H3K79me3 trimethylation of lysines 79/ histone H3
H3K9me2/me3 di- and trimethylated lysine 9 / histone H3
H4K20me3 trimethylation of lysine 20/histone H4
LBD ligand-binding domain
LIG1 DNA Ligase I
LSD1 lysine specific demethylase
MBDs methyl-CpG-binding domain proteins

MPG N-Methylpurine DNA Glycosylase
mRNA messenger RNA
NER Nucleotide Excision Repair
NTPs nucleoside triphosphates
OGG1 8-Oxoguanine DNA Glycosilase 1
PCNA Proliferation Cell Nuclear Antigen
PIC Pre-Initiation Complex
Pol II RNA PolymeraseII
Polβ DNA polymerase β
TAFs TBP associated factors
TBP TATA-box binding protein
TC-NER transcription coupled NER
TDG Thymine DNA Glycosylase
TET Ten-Eleven Translocation
Topo IIβ topoisomerase IIβ
UDG Uracil DNA glycosylase
XRCC1 X-ray Repair Cross-Complementing group 1

ABSTRACT

Changes of histone methylation code, cytosine hydroxylation and formation of chromatin loops are associated with transcription induction by nuclear hormones, but it is not known if these events are the consequence or the cause of transcription initiation.

We have studied the events induced by estrogens to stimulate transcription of target genes. We find periodic oscillations of histone H3 methylation, G oxidation, C methylation and hydroxyl-methylation at the enhancer and PolyA addition sites after induction of transcription in prototypic estrogen-induced genes. The oscillations correlate with formation of chromatin loops that juxtapose the 5' and 3' ends of the induced genes. BER followed by NER enzymes are recruited to the 5' and 3' end sites to repair the DNA oxidative lesions and to stabilize the 5' and 3' borders of the transcriptional units included in the loops. At the 5' and 3' end sites of the loops, repair of oxidized Gs and hydroxymethylated Cs proceeds in a strand specific fashion.

We suggest that coupling transcription with methylation and repair enzymes is the evolutionary strategy to reduce the mutational burden induced by DNA oxidation at the borders of chromatin loops.

1. BACKGROUND

1.1. The basics: Transcription

Transcription is the process by which the information in DNA is copied into messenger RNA (mRNA) for protein synthesis. It must be finely adjusted in order to regulate coordinately the expression of genes.

We imagine the transcription as a dynamic process that includes several steps: 1. recognition of specific DNA regions; 2. modification of chromatin; 3. recruitment of co-transcriptional factors; 4.initiation of transcription (Figure 1):

- ***Transcription: Initiation***

RNA polymerase and cofactors bind and unwind DNA, creating an initiation bubble. This is a DNA domain that allows RNA polymerase to access a single strand of the DNA molecule.

In eukaryotes RNA PolymeraseII (Pol II) does not contain a subunit similar to the prokaryotic σ factor, which can recognize the promoter and unwind the DNA double helix. These two functions are carried out by a family of proteins called general transcription factors. PolII is associated with six general transcription factors, designated as TFIIA, TFIIB, TFIID, TFIIE, TFIIF and TFIIH, where "TF" stands for "transcription factor" and "II" for the RNA PolII. TFIID consists of TBP (TATA-box binding protein) and TAFs (TBP associated factors). The role of TBP is to bind the core promoter. TAFs may assist TBP in this process. In human cells, TAFs are formed by 12 subunits. One of them, TAF250 (with molecular weight 250kD), has the histone acetyl transferase activity, which can relieve the binding between DNA and histones in the nucleosome.

The transcription factor, which catalyzes DNA melting is TFIIH.

However, before TFIIH can unwind DNA, the RNA PolII and at least five general transcription factors (TFIIA is not absolutely necessary) have to form a Pre-Initiation Complex (PIC).

- ***Transcription: Elongation***

One strand of DNA serves as the template for RNA synthesis, but multiple rounds of transcription may occur in a way that many copies of a gene may be produced.

After PIC is assembled at the promoter, TFIIH can use its helicase activity to unwind DNA. This requires energy released from ATP hydrolysis. The DNA melting starts from about-10bp. Then, RNA PolII uses nucleoside triphosphates (NTPs) to synthesize a RNA transcript. During RNA elongation, TFIIF remains attached to the RNA polymerase, all other transcription factors dissociated from PIC.

The Carboxyl-Terminal Domain (CTD) of the largest subunit of PolII is critical for elongation. In the initiation phase, CTD is un-phosphorylated, but during elongation it is phosphorylated. This domain is characterized by proline, serine and threonine residues.

- ***Transcription: Termination***

Termination is the final step of transcription. Termination results in the release of the newly synthesized mRNA from the elongation complex (Lykke-Andersen S. et al. 2007).

Eukaryotic protein genes contain a poly-A signal located downstream of the last exon. This signal is used to add a series of adenylate residues (PolyA) during RNA processing.

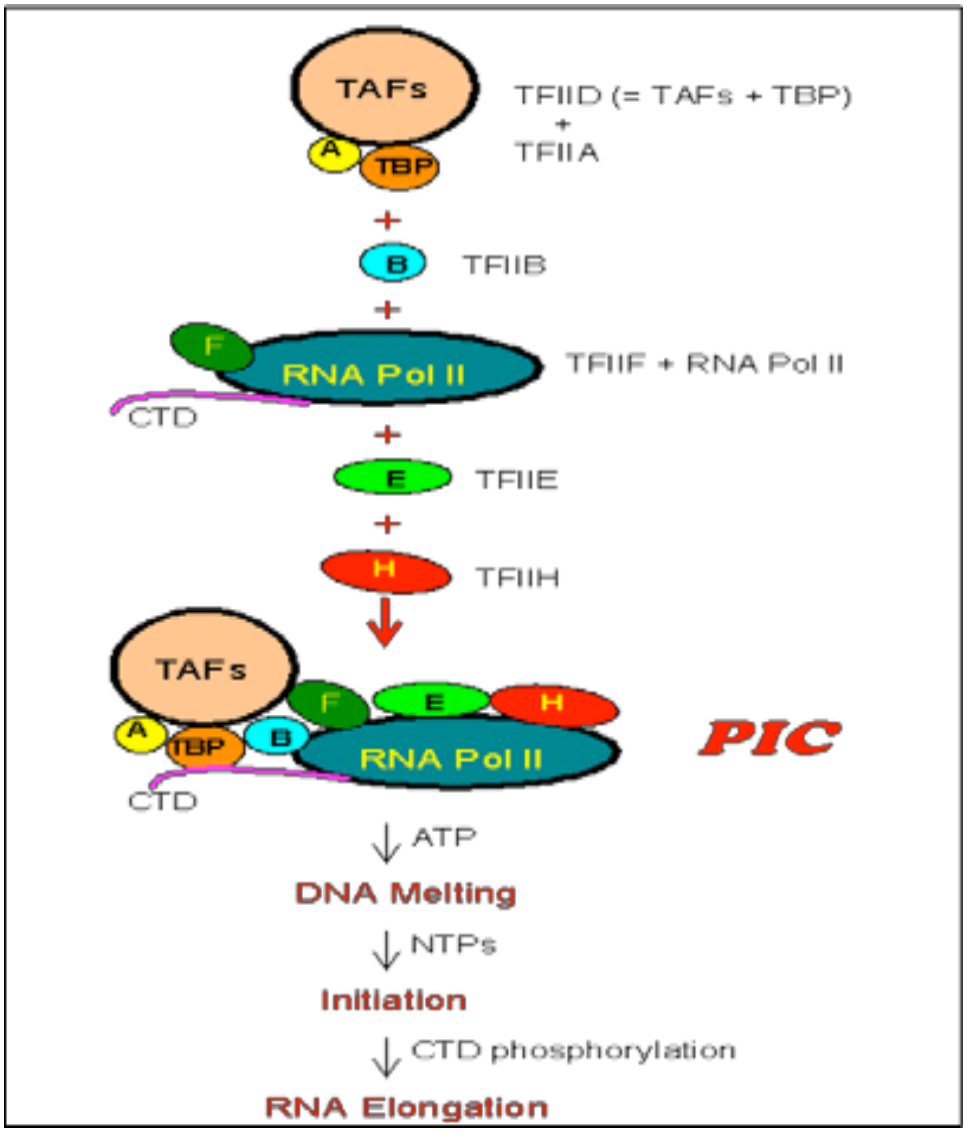

Figure 1:Assembly of the pre-initiation complex (PIC). TBP first binds to the promoter and then recruits TFIIB to join TFIID (and TFIIA if present). Before entering PIC, RNA Pol II and TFIIF are bound together. RNA Pol II recruits TFIIE, which further recruits TFIIH to complete the PIC assembly. (Adapted from *Molecular Biology Web Book, modified from: Roeder, R.G. 996. Trends in Biochem. Sci. 21:327-334*).

1.2. Epigenetic modifications of DNA and chromatin

Epigenetics is the study of modifications that induce changes in gene expression without any change in DNA sequence.
Epigenetic changes are involved in development and differentiation and are heritable. However, environment can influence the epigenetic states and gene expression. Many epigenetic changes characterize the development of cancer and other diseases.

The interaction between different epigenetic mechanisms controls the accessibility of genes by the transcriptional machinery.

- ***Chromatin structure***

Eukaryotic chromatin contains DNA and histones that are organized in the nucleosome, which consists of a histone octamer (two H2A/H2B dimers and an H3/H4 tetramer), around which the DNA (146 bp) is wrapped (Figure 2).

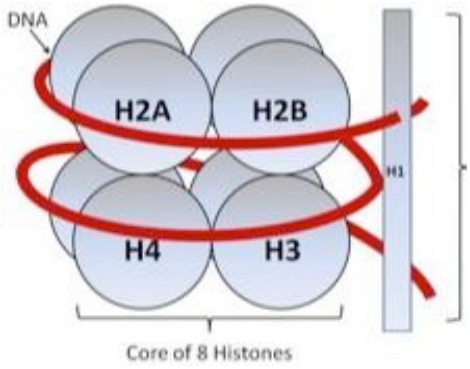

Figure 2. Structure of a nucleosome, with the DNA wrapped around an octameric histone core (Adapted from Schneider R.et al. 2004 Nat Cell boil. 6:73-77)

The bulk of chromatin exists as transcriptionally inactive *heterochromatin*, in which the nucleosomes are densely packaged to form a "closed chromatin structure". Conversely, an "open chromatin form" is characteristic of

transcriptionally competent *euchromatin*, which has widely spaced nucleosomes and is accessible to the transcriptional machinery. The amino-terminal tails of the histones can be modified by methylation and acetylation, which are critical for the regulation of gene transcription. Together, these modifications result in a complex series of molecular events that modify the chromatin configuration and render genes either active or repressed.

- ***Histone post-translational modifications: histone code***

The amino-terminal tail of histones may undergo a number of changes, including methylation and acetylation (Figure 3) (Andrew J Bannister1 and Tony Kouzarides, 2011).Together, these modifications modify the chromatin configuration and render genes either active or repressed.

Histone methylation occurs on all basic residues: arginines, lysines and histidines (Fischle W.et al. 2008).

Histone lysines may be unmethylated, or mono-, di- or trimethylated (-me1, -me2, -me3).

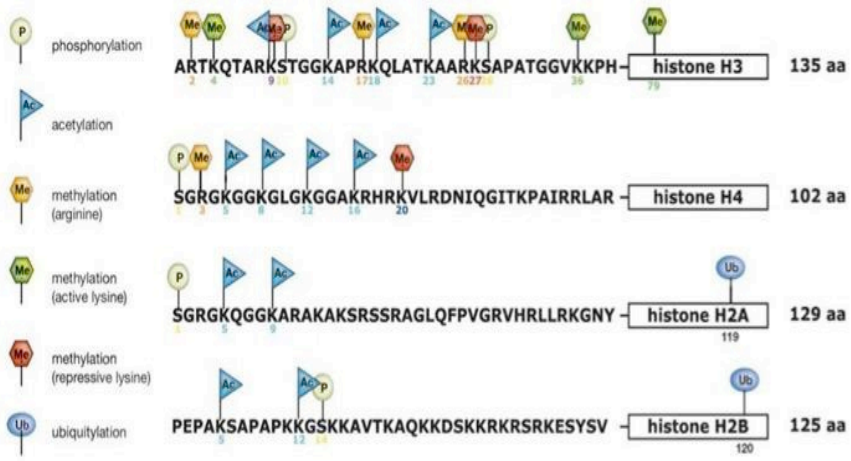

Figure 3: Histone modifications involved in chromatin re-organization. Histone N- tails are post-translationally modified, and certain combinations of histone modifications appear to generate a "histone code". (Adapted *from Allis et al, Epigenetics, 2006*).

The level of histone methylation is essential for regulation of transcriptional activity. Repressive marks include di- and trimethylation of lysine 9 on histone H3 (H3K9 me2/me3), trimethylation of lysine 27 on histone H3 (H3K27me3) and trimethylation of lysine 20 on histone H4 (H4K20 me3). Conversely, activation is associated with histone H3 di- and trimethylation of lysine 4 (H3K4me2/me3) and trimethylation of lysines 36 and 79 (H3K36me3, H3K79me3). Methyl groups are provided to the histones by SAM/Ado-Met and the methylation reaction is catalysed by histone lysine methyltransferases.

Methyl groups can also be removed from histone lysine residues by the action of histone lysine demethylases (Kirsten Grønbæk et al. 2008).

These are the amine oxidases, LSD1 (KDM1) (Shi et al. 2004) and jumonji C (JmjC)-domain- containing, iron-dependent dioxygenases (Tsukada Y. et al. 2006) (Figure 4). These enzymes are highly conserved from yeast to humans and demethylate histone and non- histone substrates.

All these modifications may act alone or in concert in a context-dependent manner to facilitate or repress chromatin- mediated processes (Berger 2007). Some histone modifications are thought to influence nucleosome stability, but an exciting emerging view is that histone modification can influence one another such that one modification recruits or activates chromatin-modifying complexes to generate a different histone code.

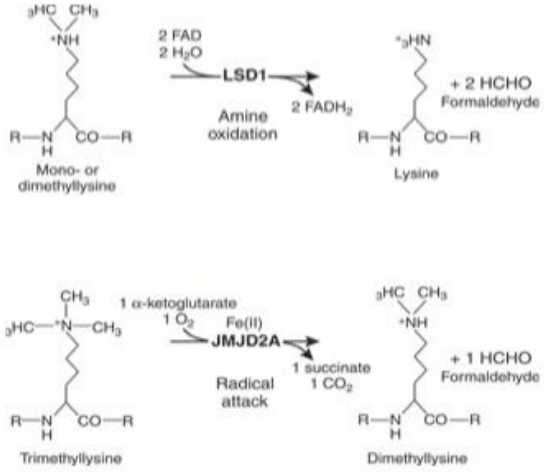

Figure 4: Histone lysine demethylase mechanisms. (A) JmjC proteins catalyze the hydroxylation of methyllysine residues in a 2-OG and Fe(II)-dependent manner, releasing succinate and CO2. In a second, non enzymatic step, formaldehyde is spontaneously released after the decomposition of the *N*-hydroxymethyl moiety. **(B)** LSD1 catalyzes the oxidation of the C-N methylamine bond in an FAD-dependent mechanism, producing an unstable intermediate that decomposes to release formaldehyde. As a consequence of this mechanism, LSD1 cannot eliminate trimethyllysine, whereas jmjC demethylases . (Adapted *from Wikipedia).*

- ***DNA methylation***

DNA methylation is the addition of a methyl group at the 5'-carbon of cytosine. In mammals, DNA methylation typically occurs in a CpG dinucleotide context (CpG islands). The enzymes that catalyze this modification are called DNA methyltransferases (DNMTs) (Law J. A. et al. 2010).

There are two categories of DNMTs: *de novo* and maintenance (Goll M. G. & Bestor T. H. 2005). DNMT1 is an enzyme that copies the methylation in hemi-methylated template (maintenance) during DNA replication and cell division. DNMT3a and DNMT3b are *de novo* methyl transferase enzymes that add methyl groups to unmethylated CpG in DNA.

DNA methylation correlates with reduced transcription (Bird A. P. & Wolffe A. P. 1999) and it has been implicated in development and differentiation (Li E. et al. 1992), imprinting (Li E. et al. 1993), X chromosome inactivation (Panning B. & Jaenisch R. 1998), and cancer (Laird P. W. et al. 1995; Baylin S. B. & Ohm J. E. 2006).

DNA methylation may reduce the transcription in two ways: preventing the binding of transcriptional proteins to the gene (Choy MK et al. 2010) and attracting proteins known as methyl-CpG-binding domain proteins (MBDs). MBD proteins can recruit additional proteins to the locus, such as histone deacetylases and other chromatin remodeling proteins that can modify histones.

Aberrant methylation has been found in cancer cells (Cho Y. H. et al. 2010) and it was shown that DNA methylation marks DNA damage and repair as a "scar" (Cuozzo C. et al. 2007) and that transcription can reduce the methylation on repaired DNA regions (Morano A. et al. 2014).

However, a methyl group may be also removed by a process called DNA demethylation, which can either be passive or active. Passive DNA demethylation takes place on newly synthesized DNA strands *via* DNMT1

during replication rounds. Active DNA demethylation mainly occurs *via* the sequential modification of methylated cytosine by TET enzyme-mediated oxidation. The ten-eleven-translocation (TET) enzyme family of 5-mC hydroxylases includes TET1, TET2 and TET3. These proteins may promote DNA demethylation by binding to CpG rich regions to prevent unwanted DNA methyltransferase activity, and by converting 5-mC to 5-hmC, 5-hmC to 5-fC (5-formylcytosine), and 5-fC to 5-caC (5-carboxylcytosine) through hydroxylase activity (Figure 5).

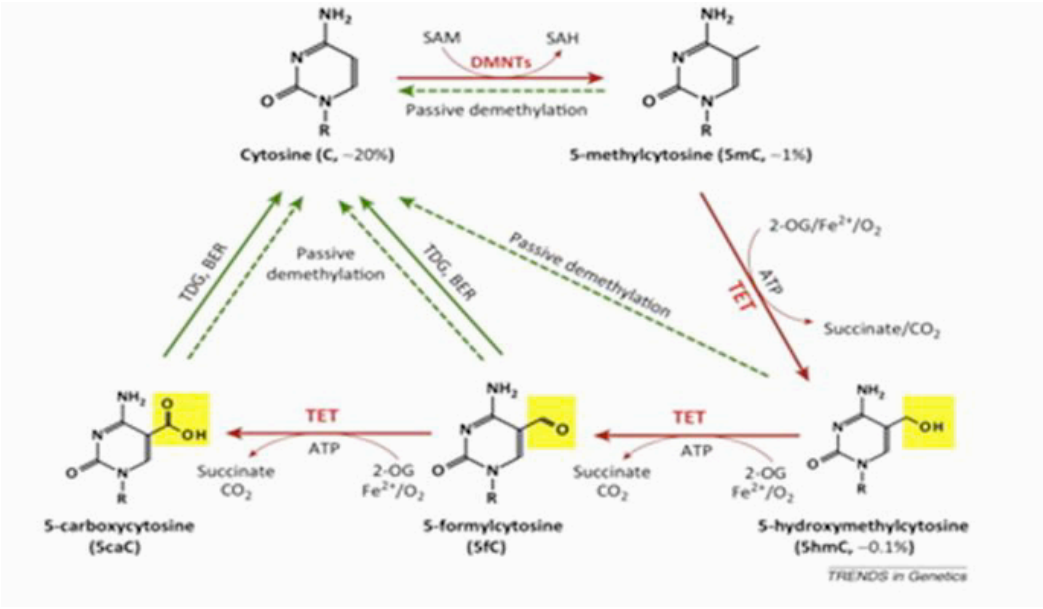

Figure 5: **Schematic representation of DNA methylation / demethylation cycle.** (Adapted *from Yun huang, Anjana Rao. 2014 Trends in Genetics).*

The TET proteins have been shown to function in transcriptional activation. Furthermore, the detection of the 5-hmC or 5-fC in various tissues and cells may also be used as a marker to indicate active DNA demethylation. 5-fC can also be directly excised by thymine DNA glycosylase (TDG) to allow subsequent base excision repair (BER) processing, which converts modified cytosine back to cytosine (Adapted from Rahul M. Kohli & Yi Zhang 2013).

- ***DNA oxidation***

DNA oxidation is a consequence of cellular metabolism, which can increase as a result of toxic insults. The most common oxidized base is guanine oxidized to 8-oxo-7,8- dihydroguanine (8-oxo-dG). The 8-oxo-dG can base-pair with deoxyadenosine, instead of deoxycytotidine. This error can induce a transversion point mutation (C→A) during replication.

Also, transcription can induce DNA oxidation. In fact, Lysine specific demethylase 1 (KDM1a o LSD1) is a flavin adenine dinucleotide (FAD)-containing enzyme, which demethylates di- methyl lysine 4 (or lysine 9under certain conditions) and generates H_2O_2 during the demethylation process (Anand and Marmorstein 2007; Gronbaek et al. 2008; Lan et al. 2008). It has been shown that transient demethylation of histone H3 lysine 4 triggers Myc-induced transcription (Amente et al. 2010). Also, it has been found that Estrogen-Induced Gene Expression is driven by H3K9me2 demethylation (Perillo et al. 2008). In both cases LSD1 is responsible for the oxidative process that results in the formation of hydrogen peroxide (H_2O_2) whose main DNA product is 8-oxo-guanine (8-oxo-G) (Fig, 6) (Perillo et al. 2008).

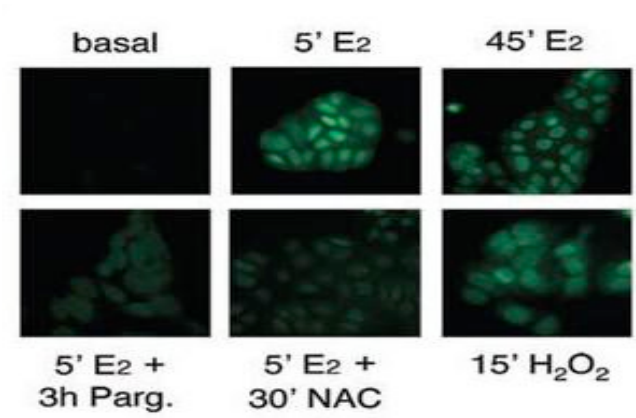

Figure 6: E_2 induces 8-oxo-dG foci through LSD1-dependent mechanism. (*Adapted from Perillo et al, 2008. Science).*

- ***Base Excision Repair (BER)***

Base excision repair (BER) is a group of enzymes that remove damaged bases that can otherwise cause mutations by mis-pairing or lead to breaks in DNA. In BER system, the damaged bases are recognized by DNA glycosylases, which remove specific damaged or inappropriate bases, forming apurinic sites. These sites are then cleaved by an AP endonuclease. The resulting single-strand break can then be processed by either short-patch (where a single nucleotide is replaced) or long-patch BER (where 2-10 new nucleotides are synthesized)(Figure 7) (Liu Y, et al. 2007).

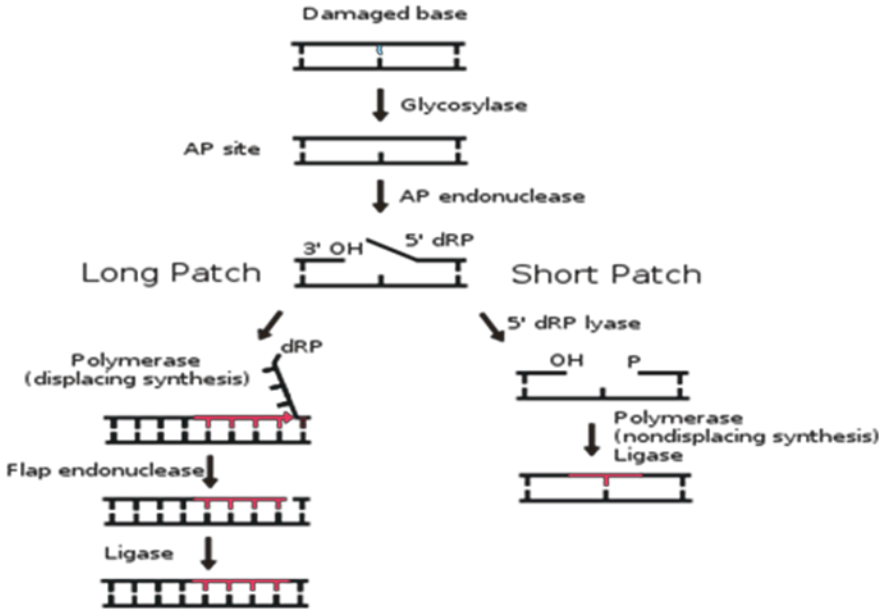

Figure 7: Scheme of base excision repair showing the two sub-pathways. The "short-patch" or single-nucleotide pathway, and the "long-patch" pathway. There are essentially four steps in the base excision repair pathway. (Adapted *from Wikipedia).*

There are many DNA Glycosilases: 1. 8-Oxoguanine DNA Glycosilase 1 (OGG1) removes 8-oxo-dG; 2. Uracil DNA glycosylase (UDG) excises the uracil that is the product of cytosine deamination, thereby preventing the subsequent C→T point mutation; 3. Timidine DNA Glycosylase (TDG) is able

to remove a variety of modified cytosine and 4: N-Methylpurine DNA Glycosylase (MPG) removes a variety of modified purine bases.

In the short patch, the DNA polymerase β (Polβ) inserts the correct nucleotide and removes the deoxyribose phosphate through its associated AP-lyase activity. The X-ray repair cross-complementing group 1 (XRCC1) acts as a scaffold protein to present a non-reactive binding site for Polβ and to bring the Polβ and LIG3 enzymes together at the site of repair (Lindahl T. & Wood R. D. 1999).

An alternative pathway called "*long-patch BER*" replaces a strand of nucleotides with a minimum length of 2 nucleotides. It requires the presence of proliferation-cell-nuclear antigen (PCNA), which acts as a scaffold protein for the repair enzymes (Fortini P. et al. 1998). Other DNA polymerases, possibly Pol δ and Pol ε (Klungland A. & Lindahl T. 1997), generate an oligonucleotide flap. The existing nucleotide sequence is removed by flap endonuclease-1 (FEN1). The oligonucleotide is then ligated to the DNA by DNA ligase I (LIG1), sealing the break and completing the repair (Sung J. S. & Demple B. 2006).

- ***Nucleotide Excision Repair (NER)***

Nucleotide Excision Repair (NER) acts to repair single strand breaks containing at least 2 bases and creating a structural distortion of the DNA. The same pathway may be used to repair damage from oxidative stress (Gros L. et al. 2002).

There are 9 major proteins involved in NER in mammalian cells. Deficiencies in certain proteins lead to specific diseases; protein names are associated with the disease. XPA, XPB, XPC, XPD, XPE, XPF, and XPG all derive from X*eroderma Pigmentosum* and CSA and CSB represent proteins linked to Cockayne syndrome. Additionally, the proteins

ERCC1, RPA, RAD23A, RAD23B, and others also participate in nucleotide excision repair.

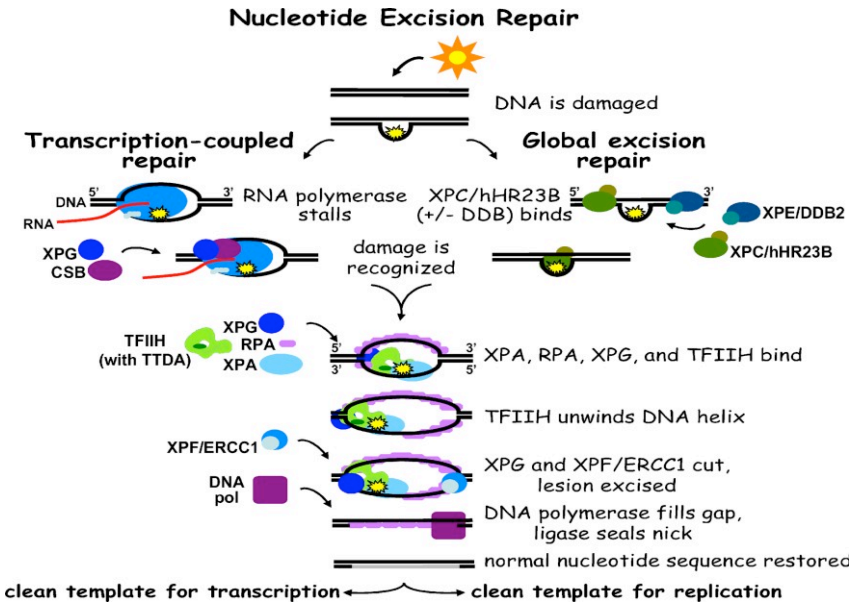

Figure 8: A model of the nucleotide excision repair pathway, which includes global genomic repair and transcription-coupled repair. (Adapted from Fuss JO, Cooper PK (June 2006). *PLoS Biol).*

Eukaryotic nucleotide excision repair can be divided into two sub-pathways: global genomic NER (GG-NER) and transcription coupled NER (TC-NER) (Figure 8). Two different sets of proteins are involved in recognizing DNA damage for each sub-pathway. After damage recognition, the two pathways converge to the steps of dual incision, repair, and ligation.

Global genomic NER repairs damage in both transcribed and un-transcribed DNA strands in active and inactive genes throughout the genome. This process is not dependent on transcription. This pathway employs several "damage sensing" proteins including the DNA-damage binding (DDB) and XPC-Rad23B complexes that constantly scan the genome and recognize helix distortions: the XPC-Rad23B complex is responsible for distortion recognition, while DDB1 and DDB2 (XPE) can also recognize some types of damage caused by UV light.

Instead, *Transcription Coupled-NER* initiates when RNA polymerase stalls at a lesion in DNA: the blocked RNA polymerase serves as a damage recognition signal, which replaces the need for the distortion recognition properties of the XPC-RAD23B and DDB complexes. CS proteins CSA and CSB bind some types of DNA damage instead of XPC-Rad23B

Upon identification of a damaged site, subsequent repair proteins are then recruited to the damaged DNA to verify presence of DNA damage, excise the damaged DNA surrounding the lesion then fill in the repair patch.

NER repairs the transcribed strands of transcriptionally active genes faster than it repairs non-transcribed strands and transcriptionally silent DNA.

- ***Estrogen induced transcription***

The estrogen receptor (ER) belongs to a family of nuclear hormone receptors that act as ligand-activated transcription factors (Heldring N. et al. 2007). The binding of ligand induces a conformational change in the receptor, which translocates to the nucleus, binds as homodimer to specific DNA sequences termed estrogen response elements (ERE) and regulates the transcription of multiple target genes. The domain architecture of the ER includes N-terminal hormone-independent transactivation domain (AF1), a highly conserved DNA-binding domain that mediates specific recognition of ERE, a hinge domain that separates the DNA-binding domain from the ligand-binding domain (LBD), a LBD that contains the hormone binding pocket, and a second transactivation domain (AF2) in the C-terminus that is activated in response to ligand binding (Figure 9) (Nilsson S. et al. 2001).

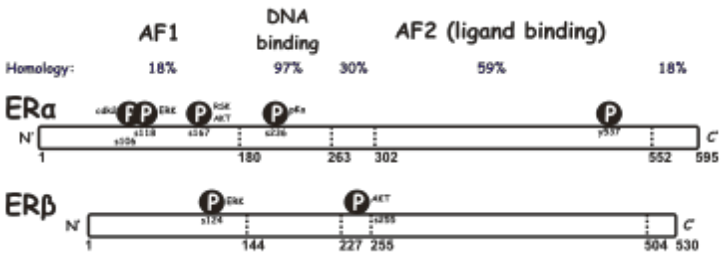

Figure 9: The domain structures of ERα and ERβ, including some of the known phosphorylation sites involved in ligand-independent regulation. (*Adapted from Wikipedia).*

Below is shown the structure and the location of the ERE relative to the coding region and the promoter of three prototypic estrogen-induced genes.

- ***TFF1 / pS2 gene***

Trefoil factor 1 is encoded in humans by the *TFF1*gene (also called *pS2* gene).

This gene and two other related trefoil family member genes are found in a cluster on chromosome 21 (Gött P. at al.1997).

They encode for three stable secretory proteins expressed in gastro-intestinal mucosa. Their functions are not defined, but they may protect the mucosa from insults, stabilize the mucus layer, and affect healing of the epithelium.

Estrogen stimulates pS2 gene transcription by interacting with an ERE site at the 5'- flanking region of that gene (Figure 10).

Figure 10: pS2 gene structure. It is formed by 3 exons and an Estrogen Responsive Element at the 5'- flanking region.

- ***BCL2 gene***

Bcl-2 (B-cell lymphoma 2) is encoded in humans by *BCL2* gene and is localized on chromosome 18. It is member of the Bcl-2 family of regulator proteins that regulate cell death by either inducing it or inhibiting apoptosis (Tsujimoto Y. et al 1984). Bcl-2 is specifically considered as an important anti-apoptotic protein and is thus classified as an oncogene.

Estrogen stimulates *BCL2* gene transcription by interacting with an ERE in the second exon of the gene (Figure 11).

Figure 11: BCL2 gene structure. It is formed by 3 exons and an Estrogen Responsive Element in the coding region (II exon) of the gene.

- ***CAV1 gene***

Caveolin-1 is a protein that in humans is encoded by the *CAV1*gene. *CAV1* and *CAV2* are located next to each other on chromosome 7 and express co-localizing proteins that form a stable hetero- oligomeric complex.

The scaffolding protein encoded by this gene is the main component of the *caveolae* plasma membranes found in most cell types. The protein links integrin subunits to the tyrosine kinase FYN, an initiating step in coupling integrins to the Ras-ERK1/2 pathway and promoting cell cycle progression. The gene is a tumor suppressor gene candidate and a negative regulator of the Ras- p42/44 ERK1/2 kinase cascade.

Estrogen stimulates *CAV1* gene transcription by interacting with the first ERE at the 5'end of the gene (Figure 12).

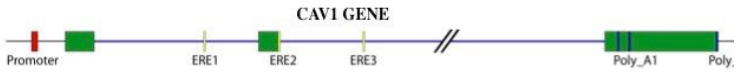

Figure 12: CAV1 gene structure. It is composed by 3 exons and the Estrogen Responsive Element in the 5'-flanking region of the gene.

2. AIM OF THE STUDY

Estrogen exposure is a major determinant of the risk of breast cancer (James D. Yager and Nancy E. Davidson 2006) and the expression of the receptor is indicative of the clinical outcome of breast cancer.

The modulation of estrogen signaling remains the mainstay of breast cancer treatment for the majority of breast cancers classified as ER-positive (Shang Y. 2007). Several strategies for inhibiting the estrogen axis in breast cancer exist, including: selective ER modulators (SERM) such as tamoxifen and raloxifene, which act as selective tissue-specific antagonists of ER in the breast (Shang Y. 2006). However, unfortunately in breast cancer, long term SERM therapy causes the development of acquired resistance (Sengupta S. and Jordan VC. 2008). More information about the transcriptional mechanisms used by estrogen may facilitate the understanding and the use of its modulators.

The specific objectives of this study are: 1. the analysis of the dynamic changes of epigenetic marks induced by estrogen; 2. the identification of the players involved : 3. the dissection of the mechanism leading to the formation of chromatin domains associated with active transcription.

We have used as cellular model MCF-7 cells, a breast cancer cell line, expressing the receptor alpha and responsive to the estrogens.

3. MATERIAL AND METHODS

3.1. Cells, treatment and transfections

Human breast cancer MCF-7 cells were grown at 37°C in 5% CO_2 in Dulbecco's modified Eagle's medium (DMEM) supplemented with phenol red, L-glutamine (2 mM), insulin (10 μg/ml), hydrocortisone (3.75 ng/ml), and 10% fetal bovine serum (FBS, South America origin, Brazil, Invitrogen, Rockville, MD, USA). Cells were incubated with fresh medium every 3 days. To evaluate the effect of Estrogen challenge, cells were grown in phenol red-free DMEM containing 10% dextran– charcoal-stripped FBS for 1 to 3 days, before being challenged with 50 nM Estrogen for different times according to the experimental needs.

For experiment with N-Acetyl-Cysteine, it was used at final concentration of 50 mM for 30 min.

To obtain DNMT3a knock down with siRNA, cells were transiently transfected, using a Neon® Transfection System, with siRNA L-006672-01-0005 (Dharmacon) in medium without serum to a final concentration of 10 nM and incubation was continued for 48 h. Scrambled RNA, at the same concentration, was used as negative control. To determine the recovery of DNMT3a activity in knock down experiments with siRNAs, we used DNMT3a full-length cDNA from ADDGENE Plasmid #25328.

To obtain LSD1 dominant negative expression, the cells were transiently transfected, using a Neon® Transfection System, with LSD1 full-length cDNA and LSD1 dominat negative (ala) were inserted into the CMV 3xFLAG, Sigma-Aldrich, St. Louis, MO, USA), in medium without serum and incubation was continued for 48 h as previously published (Ambrosio et al. 2013).

3.2. RNA extraction and qRT-PCR and qPCR

Total RNA was extracted using Trizol (Gibco/Invitrogen). cDNA was synthesized in a 20 µl reaction volume containing 1 µg of total RNA, 100 units of Superscript III Reverse Transcriptase (Invitrogen), and 2 µl random hexamer (20 ng/µl) (Invitrogen). mRNA was reverse-transcribed for 1 h at 50 °C, and the reaction was heat inactivated for 15 min at 70 °C. The products were stored at -20 °C until use.

Quantitative reverse Transcription Polymerase Chain Reaction (qRT-PCR) and Quantitative Polymerase Chain Reaction (qPCR) were performed three times in six replicates on a 7500 Real Time PCR System (Applied Biosystems) using the SYBR Green-detection system (FS Universal SYBR Green MasterRox/Roche Applied Science). The complete list of oligonucleotides used is reported in Table 1.

3.3. Chromatin Immuno-Precipitation (ChIP)

Cells were transfected and/or treated as indicated in the legends of the figures. The cells (~2.5 x 10^6 for each antibody) were fixed for 10 min at room temperature by adding 1 volume of 2% formaldehyde to a final concentration of 1%, the reaction was quenched by the addition of glycine to a final concentration of 125 mM. Fixed cells were harvested and the pellet was resuspended in 1 ml of Lysis Buffer (10 mM Tris- HCl pH 8.0, 10 mM NaCl, 0.2 % NP40) containing 1X protease inhibitor cocktail (Roche Applied Science). The lysates were sonicated in order to have DNA fragments from 300 to 600 bp. Sonicated samples were centrifuged and supernatants diluted 2 fold in the ChIP Buffer (1% Triton X-100, 2 mM EDTA, 150 mM NaCl, 20 mM Tris- HCl pH 8.0). An aliquot (1/10) of sheared chromatin was further treated with proteinase K (4U every 1 x 10^6 nuclei), extracted with 1 volume of phenol/chloroform/isoamyl alcohol (25:24:1) and precipitated in LiCl 0,4 M/ ethanol 75% to determine DNA concentration and shearing efficiency

(input DNA). The ChIP reaction was set up according to the manufacturer's instructions. Briefly, the sheared chromatin was precleared for 2 h with 1 μg of non-immune IgG (Santa Cruz Biotechnology, Santa Cruz, CA, USA) and 20 μl of Protein A/G PLUS-Agarose (Santa Cruz Biotechnology) saturated with salmon sperm (1 mg/ml). Precleared chromatin was divided in aliquots and incubated at 4 °C for 16 h with 1 μg of the specific antibody (for the codes, see below) and non-immune IgG respectively. The immuno-complexes were recovered by incubation for 3 h at 4 °C with 20 μl of protein-A/G PLUS agarose, beads were washed with wash buffers according to the manufacturer's instructions and immunoprecipitated DNA was recovered through phenol/chloroform/isoamyl alcohol extraction and ethanol precipitation and redissolved in TE buffer (10 mM Tris-HCl, 1mM EDTA, pH 8,0). Samples were subjected to qPCR using the primers indicated in the legend of the specific figures; primers sequences are reported in Table 1.

Real Time-qPCRs were performed using Fast Start Universal SYBR Green Master (Rox) (Roche Applied Science) with cycle conditions as follows: 95 °C 10 min; 40x (95 °C 10 sec, 55 °C 30 sec, 72 °C 30 sec); 72 °C 10 min

3.4. Chromosome conformation capture (3C)

The 3C assay was performed as described previously (Dekker J. et al., 2002) with minor adaptations. Briefly: The cells (2.5×10^6) were cross-linked in 12 ml of PBS with 1% formaldehyde for 10 min at room temperature. The reaction was quenched by the addition of glycine to a final concentration of 125 mM. Fixed cells were harvested and the pellet resuspended in 1 ml of ice-cold lysis buffer (the same used for ChIP experiments). Nuclei were washed with 0.5 ml of restriction enzyme buffer (100 mM NaCl, 50 mM Tris-HCl, 10 mM $MgCl_2$, 1mM Dithioerythritol, pH 7,5 at 37 °C), centrifuged and resuspended in 100 μl of restriction enzyme buffer. SDS was added to a final concentration of 0.1%, and nuclei were

incubated at 37 °C for 15 min. Triton X-100 was added to the final concentration of 1% to sequester SDS. Digestion was performed with 100 U of the restriction enzyme at 37 °C for 16 h. The restriction enzyme was inactivated by the addition of SDS to 2% and incubation at 65 °C for 30 min The reaction was diluted into 1 ml ligation reaction buffer (66 mM Tris-HCl, 5 mM MgCl2, 5 mM DTT, 1 mM ATP, pH 7,5) and incubated at 16 °C for 18 h with 50 U of T4 DNA Ligase (Roche Applied Science). EDTA (10 mM) was added to stop the reactions. Samples were treated with Proteinase K (200 μg/ml) and incubated for 5 h at 55 °C, and then overnight at 65 °C to reverse the formaldehyde crosslinks. The following day, the DNA was purified by phenol/chloroform/isoamyl alcohol extraction and ethanol precipitation. Samples were redissolved in 20 μl of TE buffer. To prepare a control template, we used a pool of plasmids containing an equimolar amount of the *CAV1*and *BCL2* inserts spanning the genomic regions of interest. Five micrograms of plasmid DNA were digested with AVAII or Bam HI in 50 μl of 1x buffer for 8 h at 37 °C and then ligated in 20 μl with 5 U of T4 Ligase at 16 °C for 4 h. The efficiency of digestion at the end of 3C treatment was quantified by real time PCR, amplifying a fragment spanning two AVAII (uncut) in different 3C DNA preparations. Primer sequences are reported in Table 1. PCR were performed using FastStart Taq DNA Polymerase (Roche Applied Science) with cycle conditions as follows:

CAV1 oligo 8-2 (Prenested): 95 °C 5 min; 5x (95 °C 45 sec, 60 °C 30 sec, 72 °C 30 sec); 25x (95 °C 45 sec, 58 °C 30 sec, 72 °C 30 sec); 72 °C 10 min

CAV1 oligo 8-2 (Nested): 95 °C 5 min; 5x (95 °C 45 sec, 62 °C 30 sec, 72 °C 35 sec);

35x (95 °C 45 sec, 60 °C 30 sec, 72 °C 35 sec); 72 °C 10 min

PCR products were run on1.5% agarose gels, stained with ethidium bromide and quantified with the imageJ program (Rasband WS, ImageJ, National Institutes of Health, Bethesda, Maryland, USA, http:

//rsb.info.nih.gov/ij/). The amplified fragments at the end of the procedure were verified by DNA sequence analysis.

3.5. Antibodies

ERa ab32063 (Abcam); H3K4me2 ab32356 (Abcam); H3K4me3 ab1012 (Abcam); H3K9me2 ab1220 (Abcam); H3K9me3 ab8898 (Abcam); Total H3 ab1791 (Abcam); OGG1 sc-33181 (Santa Cruz Biotechnology); LSD1 ab17721 (Abcam); DNMT3a ab2850 (Abcam); TET1 GTX124207 (Genetex); TDG sc-292440 (Santa Cruz Biotechnology); XPG sc-13563 (Santa Cruz Biotechnology); XPC sc-74411 (Santa Cruz Biotechnology); Normal rabbit IgG sc-2027 (Santa Cruz Biotechnology); Normal mouse IgG sc-2025 (Santa Cruz Biotechnology).

3.6. Ligation-dependent Probe Amplification (LPA)

The LPA assay was performed as described previously (Jan P. Schouten et al., 2002) with minor adaptations. Briefly:2µgof DNA samples were digest with FpG enzyme (New England Biolabs) for 1 h at 37°C and 5 min at 98°C. As control the not digest samples was added the storage buffer of FpG. Then, KCL 5x buffer (KCl 750mM, Tris pH 8.0 50mM,EDTA 5mM) and strand specifc probes were added to the samples (digest and not digest) and heated for 1 min at 95°C and then incubated for 16 h at 60°C.

Ligation of annealed oligonucleotides was performed by diluting the samples to 60µl with dilution buffer (2.6 mM MgCl2, 5 mM Tris–HCl pH 8.5, 0.013% non-ionic detergents, 0.2 mM NAD) containing 1 U Ligase-65 enzyme (MRC Hollad), and incubation for 1h at 56°C. The ligase enzyme was inactivated by heating at 98°C for 15 min and ligation products were amplified by qPCR. For most experiments, 10 µl of the ligation reaction was added to 25 µl qPCR buffer. Real Time-qPCRs were performed using FastStart Universal

SYBR Green Master (Rox) (Roche Applied Science) with cycle conditions as follows: 35 cycles (30 s at 95°C, 30 s at 60°C and 40 s min at 72°C). DNA was amplified by PCR using primers listed in the Table 1.

3.7. Oxidative Bisulfite (OxoBisulfite)

The Oxidative Bisulfite assay was performed as described previously (Michael J Booth, et al. 2013) with a mirror adatpion. Briefly: 1µg of DNA samples were denatureted in NaOH 0,05 mM at 37°C for 15 min and oxidated with 1µl ofPotassium Perruthenate (KRuO4, Sigma) in ice for 1 h, vortexing every 15 min. As control, KRuO4 solvent was added to the samples. The oxidative and not oxidative samples were undergoes bisulfite conversion (EZ DNA Methylation-Gold^{TM} Kit, Zymo Research)with cycle conditions as follows: 10 min. at 98°C, 4 h at 53°C.

DNA was amplified by PCR using primers listed in the Table 1 using HotStratTaq DNA polymerase (Qiagen) with cycle conditions as follows: 35 cycles (1 min. at 95°C, 1 min. at 50°C and 1 min at 72°C).

3.8. Statistical analysis

All data are presented as mean ± standard deviation in at least three experiments in triplicate ($n \geq 9$). Statistical significance between groups was determined using Student's t test (matched pairs test or unmatched test were used as indicated in figure legends).

Table 1

	PRIMERS FOR mRNA	LOCUS
mRNA Fw	5'-CCAGACAGAGACGTGTACAGT-3'	pS2 / TFF1
mRNA Rev	5'-ATTCACACTCCTCTTCTGGA-3'	pS2 / TFF1
mRNA Fw	5'-GTGGTGGAGGAGCTCTTCAG-3'	BCL2
mRNA Rev	5'-CAAACTGAGCAGAGTCTTCAG-3'	BCL2
mRNA Fw	5'-GCAGACGAGCTGAGCGAGAAGC-3'	CAV1
mRNA Rev	5'-GAATAGACACGGCTGATGCACTG-3'	CAV1
18S Fw	5'-GCGCTACACTGACTGGCTC-3'	h18S
18S Rev	5'-CATCCAATCGGTAGTAGCGAC-3'	h18S
	PRIMERS FOR ChIP	**LOCUS**
ChIP ERE Fw	5'-CTAGACGGAATGGGCTTCAT-3'	pS2 / TFF1
ChIP ERE Rev	5'-TCTGAGAGGCCCTCCCGCCAG-3'	pS2 / TFF1
ChIP PolyA Fw	5'-CTACTCACTGCGGATGCCCCAG-3'	pS2 / TFF1
ChIP PolyA Rev	5'-GCTTCTGTATCCCTCCTCTGCTG-3'	pS2 / TFF1
ChIP II Intron Fw	5'-CCTTTTTATACGATGGGTTCTGA-3'	pS2 / TFF1
ChIP II Intron Rev	5'-CGGCCGTGACTCTGTGTAA-3'	pS2 / TFF1
ChIP ERE Fw	5'-CATTATAAGCTGTCGCAGAG-3'	BCL2
ChIP ERE Rev	5'-GAGGGTCAGGTGGACCACAG-3'	BCL2
ChIP PolyA Fw	5'-AGTAAATGTGCCCAGCCTCT-3'	BCL2
ChIP PolyA Rev	5'-TAGGGATGGTTCTCTGTTGC-3'	BCL2
ChIP ERE Fw	5'-GGATCTTAGATAAAGCTGGAAGG-3'	CAV1
ChIP ERE Rev	5'-GATCTCGCAGAGGACACCACAC-3'	CAV1
ChIP PolyA Fw	5'-GATGTGATTGCAGAACCA-3'	CAV1
ChIP PolyA Rev	5'-CAACAGCTTCAAAGAGTG-3'	CAV1

	PRIMERS FOR 3C	LOCUS
OLIGO 1 (Prenested)	5’-CACGGACACTGGATCTTGACTAT-3’	BCL2
OLIGO 1 (Nested)	5’-CCCCTTCCTCTTGCTGGTATC-3’	BCL2
OLIGO 2 (Prenested)	5’-CTTCTTGCCCTTCTGATGGTTG-3’	BCL2
OLIGO 2 (Nested)	5’-TATGCGCGTGGGAGGTGT-3’	BCL2
OLIGO 3 (Prenested)	5’-AATCCTCGGCTGTTCCCTGTTCAC-3’	BCL2
OLIGO 3 (Nested)	5’-TCTGCCTTCCCCATTCAACTATTA-3’	BCL2
OLIGO 4 (Prenested)	5’-CGACGACTTCTCCCGCCGCTACC-3’	BCL2
OLIGO 4 (Nested)	5’-GGACGGGGTGAACTGGGGGAGGAT-3’	BCL2
OLIGO 1 (Prenested)	5’-CTGGGCGGGGAGGTGAAGAG-3’	CAV1
OLIGO 1 (Nested)	5’-GAAGAGAAGCCAGGAATGTTTTAT-3’	CAV1
OLIGO 2 (Prenested)	5’-ACGGGAACGCGAAACAGGTGAAGC-3’	CAV1
OLIGO 2 (Nested)	5’-CCGGGAGAAGCCTGCGGCTGC-3’	CAV1
OLIGO 3 (Prenested)	5’-CCTTGGGACGGTGAGATG-3’	CAV1
OLIGO 3 (Nested)	5’-CGTATTTTCTTTGTCTTTAGTCCT-3’	CAV1
OLIGO 4 (Prenested)	5’-CAGAGTTTTGTGGGTTTGATGTGT-3’	CAV1
OLIGO 4 (Nested)	5’-GAGGCATACATTGTTTTTGGTTTT-3’	CAV1
OLIGO 5 (Prenested)	5’-CAGGAAGACTGGAAGAGGCA-3’	CAV1
OLIGO 5 (Nested)	5’-TGCCTCCTCCCCCATCTT-3’	CAV1
OLIGO 6 (Prenested)	5’-GAGACCATTACCCCCCACAAA-3’	CAV1
OLIGO 6 (Nested)	5’-CACAGACTCTGACACATAAACACCTG-3’	CAV1
OLIGO 7 (Prenested)	5’-GAGGCAATACCAAGGTTCATCATC-3’	CAV1
OLIGO 7 (Nested)	5’-AAGTTGGGTGTGAGTGGATTTAAAG-3’	CAV1

	PRIMERS FOR LPA	LOCUS
ERE LPOMINUS	5'-GGGTTCCCTAAGGGTTGGAcCACTGCAGAAGTGATTCATAGTGAGAGATGGCC-3'	pS2 / TFF1
ERE RPOMINUS	5'-GGAAAAAGGCTTGGCCGTGACAACAGTGGCTCACGGGGTgTCTAGATTGGATCTTGCTGGCAC-3'	pS2 / TFF1
ERE LPOPLUS	5'-GGGTTCCCTAAGGGTTGGAcACCCCGTGAGCCACTGTTGTCACGGCCAAGCCTTTTTCC-3'	pS2 / TFF1
ERE LPOPLUS	5'-GGGTTCCCTAAGGGTTGGAcACCCCGTGAGCCACTGTTGTCACGGCCAAGCCTTTTTCC-3'	pS2 / TFF1
ERE RPOPLUS	5'-GGCCATCTCTCACTATGAATCACTTCTGCAGTGgTCTAGATTGGATCTTGCTGGCAC-3'	pS2 / TFF1
INTRONLPOPLUS	5'-GGGTTCCCTAAGGGTTGGAcCAAAAGCAGGTGGAGAGTAACTCAGGGTGGCAGGGCCCCC-3'	pS2 / TFF1
INTRONRPOPLUS	5'-GGAGACCTTCGAGAAGTGCGACGAGGAGGGGGCTgTCTAGATTGGATCTTGCTGGCAC-3'	pS2 / TFF1
INTRONLPOMINUS	5'-GGGTTCCCTAAGGGTTGGAcAGCCCCCTCCTCGTCGCACTTCTCGAAGGTCTCC-3'	pS2 / TFF1
INTRONRPOMINUS	5'-GGGGGCCCTGCCACCCTGAGTTACTCTCCACCTGCTTTTGgTCTAGATTGGATCTTGCTGGCAC-3'	pS2 / TFF1
TATALPOPLUS	5'-GGGTTCCCTAAGGGTTGGAcTAACGCTCTTTAAGCAAACAGAGCCTGCCCTATAAAATCC-3'	pS2 / TFF1
TATARPOPLUS	5'-GGGGCTCGGGCGGCCTCTCATCCCTGACTCGGGGTCgTCTAGATTGGATCTTGCTGGCAC-3'	pS2 / TFF1
TATALPOMINUS	5'-GGGTTCCCTAAGGGTTGGAcGACCCCGAGTCAGGGATGAGAGGCCGCCCGAGCCCC-3'	pS2 / TFF1

TATA RPOMINUS	5’-GGATTTTATAGGGCAGGCTCTGTTTGCTTAAAGAGCGTTAgTCTAGATTGGATCTTGCTGGCAC-3’	pS2 / TFF1
CnGLPOPLUS	5’-GGGTTCCCTAAGGGTTGGAcTTCCCCCTGCAAGGTCACGGTGGCCACCCCGTGAGCCACT-3’	pS2 / TFF1
CnGRPOPLUS	5’-GTTGTCACGGCCAAGCCTTTTTCCGGCCATCTCTCACTATgTCTAGATTGGATCTTGCTGGCAC-3’	pS2 / TFF1
CnGLPOMINUS	5’-GGGTTCCCTAAGGGTTGGAcATAGTGAGAGATGGCCGGAAAAAGGCTTGGCCGTGACAACA-3’	pS2 / TFF1
CnGRPOMINUS	5’-GTGGCTCACGGGGTGGCCACCGTGACCTTGCAGGGGGAAgTCTAGATTGGATCTTGCTGGCAC-3’	pS2 / TFF1
Universal LPA Fw	5’-GGGTTCCCTAAGGGTTGGA-3’	pS2 / TFF1
Universal LPA Rw	5’-GTGCCAGCAAGATCCAATCTAGA-3’	pS2 / TFF1
	PRIMERS FOR OXIDATIVE BISULFITE	**LOCUS**
ERE bis Minus Rw	5’-TAAACTTCATAAACTCCTTCCCTT-3’	pS2 / TFF1
ERE bis Minus Fw	5’-GGTTTTATTTATATTTGAGAGGTTTTTT-3’	pS2 / TFF1
ERE BIS plus Fw	5’-ATGGGTTTTATGAGTTTTTTTT-3’	pS2 / TFF1
ERE BIS plus Rw	5’-AAAATCTCCTCCAACCTAACCTTAA-3’	pS2 / TFF1

4. Results

4.1. Screening human promoter array for ER, OGG1, LSD1 and topoisomerase II sites induced by estrogen

To isolate and identify DNA regions recruiting, upon estrogen stimulation, estrogen receptor, RNA polymerase II, 8-oxoguanine DNA glycosylase (OGG1) and topoisomerase IIβ (Topo IIβ), we have immunoprecipitated the chromatin derived from estrogen stimulated cells (50 nM for 45 min) with specific antibodies to estrogen receptor a (ERα), the lysine specific demethylase (LSD1), OGG1 and Topo IIβ. DNA fragments immunoprecipitated were used as probe against arrays of human promoters (Affymetrix, human promoter 1.0 R array). These arrays interrogate regions proximal to transcription start sites and contain probes covering 59 percent of CpG islands annotated by UCSC in NCBI human genome assembly (Build 34). Each promoter region spans approximately from 7.5 kb upstream to 2.45 kb downstream of 5' transcription start sites.

We obtained several combinations of positive genomic sites depending on the antibodies used for immunoprecipitation. We decided to further analyze regions that were bound simultaneously by the estrogen receptor, RNA polymerase II, OGG1 and Topo IIβ , upon estrogen stimulation. We further refined this class of DNA regions by identifying sites, where the LSD1 signal was present also in the absence of estrogens.

We compared these regions (ER-OGG1- Topo Iiβ) with annotated sites of the estrogen receptor occupancy and found a significant overlap (Figure 13). We have further analyzed and validated several genomic sites reported in Figure13.

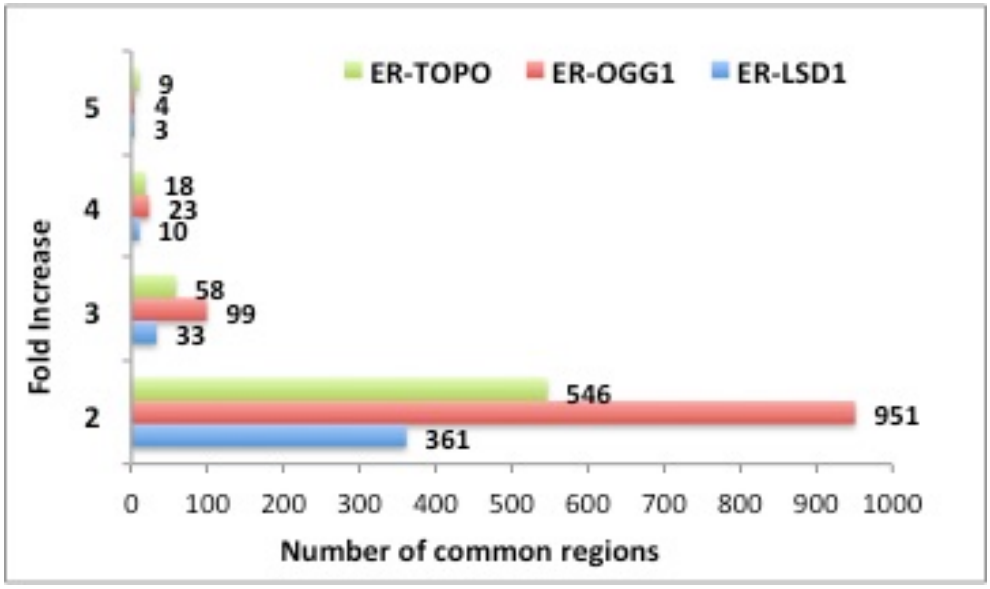

Figure 13: Stringency of the selection (fold increase between E2 treated and untreated). Screening human promoter array for ERa, OGG1 LSD1 and TopoisomeraseII sites induced by Estrogen. The cells were immunoprecipitated with specific antibody after Estrogen stimulation (50nM for 45 min.). DNA fragments immunoprecipitated were used as probe against arrays of human promoters (Affymetrix, human promoter 1.0 R array). The data can be accessed through this link http://www.genecore.embl.de/affydata/Affymetrix/ENRI).

4.2. Validation of estrogen induced genes isolated by the promoter array screening

To validate the genomic regions isolated from the promoter array screening reported in Figure 13, we identified 3 genes located in the surrounding area where ER was bound and analyzed their expression in the presence or absence of estrogens.

We have first analyzed mRNA levels after estrogen stimulation (Figure 14). MCF-7 cells were hormone-starved for 3 days and then treated with Estrogen (E2). Total RNA was extracted and reverse transcribed into cDNA and then amplified with specific primers of the specific genes examined. The results

indicate that estrogen induced cyclic mRNA expression with a peak after 30 min of stimulation and a second peak of expression that remains stable over time (Figure 14).

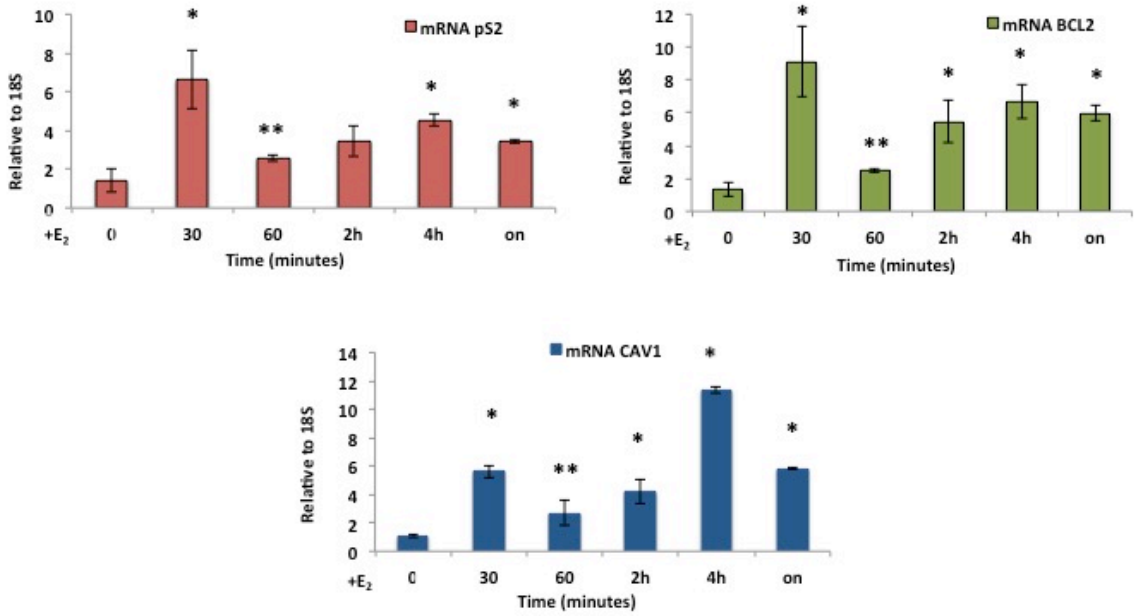

Figure 14: Estrogen induced cyclic mRNA expression of genes target.
Total RNA was prepared from MCF7 hormone-starved or stimulated with 50 nM of Estrogen for 30, 60, 120, 240 minutes until 18h and analyzed by qPCR with specific primers (Tablet1) to pS2, BCL2 and CAV1 mRNA normalized to 18S RNA levels. The statistical analysis derived from at least 3 experiments in triplicate (n≥9; Mean±SD). *p <0.01 (matched pairs t test) compared to E_2-unstimulated sample, **p<0.01 (matched pairs t test) comparing 30 to 60 min. of E_2 exposure.

4.3. Identification of gene regions, where selectively ER accumulates upon estrogen stimulation

First, we analyzed by ChIP the actual occupancy of the estrogen receptor at the predicted regions by the use of specific oligonucleotides (Figure 15a). Figure 14a shows also the location of the putative ERE sites relative to the transcription start sites. In some cases, the putative

ERE sequence is located at the 5', in other cases in exons or introns.

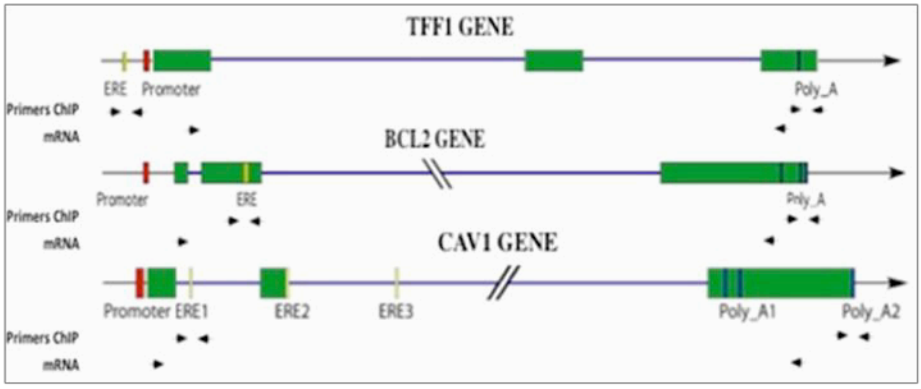

Figure 15a: Schematic representation of studied genes (pS2 – BCL2 – CAV1 genes).

Figure 15b shows that active receptor upon estrogen stimulation is rapidly recruited to the ERE at 30 - 45 min. This recruitment is not stable, but we observe a reduction at

60 min with a stabilization at 120 min after E_2. We have also found that other regions of the genes bind estrogen receptor: the 3' end PolyA addition site. Moreover, the binding of the receptor oscillates at the 3' end PolyA site during E2 stimulation as that found at the ERE, suggesting that the 2 regions are synchronized or probably interact.

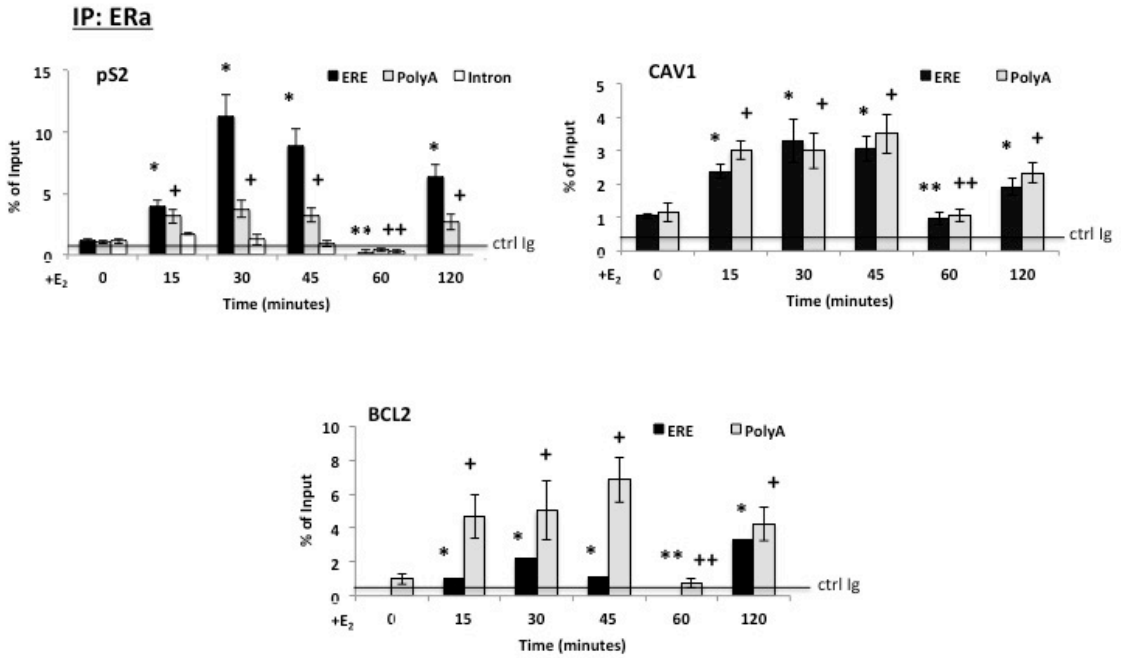

Figure 15b: Estrogen induced accumulation of ERa at Estrogen Responsive Elements (ERE) and PolyA sequence of genes target.
qChIP analysis of E2 dependent occupancy of ERa at ERE / PolyA of pS2 – BCL2 - CAV1 genes. MCF7 cells were stimulated with 50 nM of E2 for 15, 30, 45, 60 and 120 minutes. The chromatin was immunoprecipitated with antibodies directed against ERa. The black, horizontal, line indicates the percent of input from a control ChIP (Ab: non immune serum). The statistical analysis derived from at least 3 experiments in triplicate (n≥9; Mean±SD). *p <0.01 (matched pairs t test) compared to E_2-unstimulated sample; **p<0.01 (matched pairs t test) comparing 45 to 60 min.

4.4. A common histone H3 methylation code at the ERE and PolyA chromatin regions induced by estrogens

Estrogens induce the transcription of several genes. Some genes are induced *de novo*, others are already transcriptionally active and the hormone super-induce them. We have determined the histone code changes induced by the hormone in both types of genes by analyzing the H3 histone methylation code of the lysine 9 and 4 on ERE and PolyA chromatin regions of pS2 (induced by E2), CAV1 and BCL2 (super-induced by E2) genes.

In pS2 ERE and PolyA regions, we find that estrogen induces an early

demethylation of the H3k9me3-me2 at 30 and 60 min and methylation at 45 min (Figure 16a / 16b). At the ERE region, H3k4me2 increases at 15 min and remains high up to 45 min, whereas H3k4m3 increases at 45 min (Figure 16c). At the PolyA region we observe an increase of H3k4me3 at 15 and 45 min, whereas the H3k4me2 increases only at 45 min (Figure 16d).

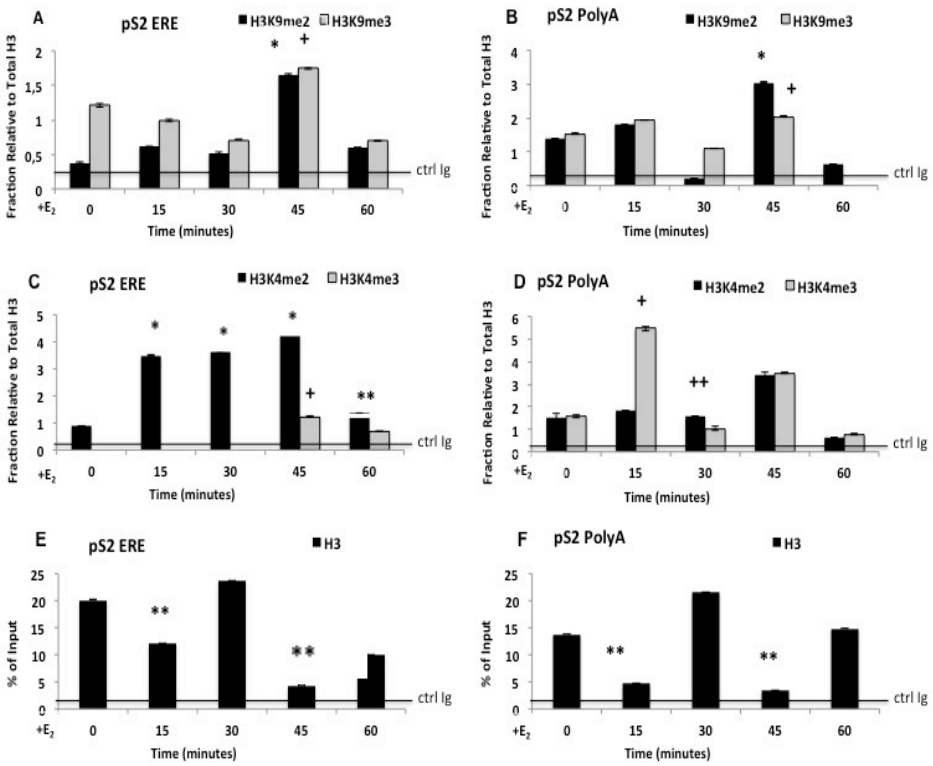

Figure 16: **Methylation-demethylation cycles of histone H3K4/K9 induced by E_2 on *pS2* ERE-PolyA chromatin.** MCF7 cells were serum starved and exposed to 50 nM E_2 at the indicated times (0, 15, 30, 45 and 120 min). qChIP was carried out using specific antibodies recognizing H3K4me3, H3K4me2, H3K9me3 and H3K9me2. **A, B.** H3K9me2 and H3K9me3 occupancy at *pS2*ERE and PolyA. **C, D.** H3K4me2 and H3K4me3 occupancy at *pS2*ERE and PolyA. **E, F.** TotalH3 occupancy at *pS2*ERE and PolyA. **G.** H3K9me2 and H3K9me3 occupancy at *pS2*Intron. **H.** H3K4me2 and H3K4me3 occupancy at *pS2*Intron. **I**. TotalH3 occupancy at *pS2*Intron. These data were normalized to total H3 histone. The statistical analysis derived from at least 3 experiments in triplicate (n ≥9; Mean±SD). *p <0.01 (matched pairs t test) compared to E_2-unstimulated sample, **p<0.01 (matched pairs t test) comparing 15 to 30 min. of E_2 exposure.

In *pS2* second intron, the methylation changes are less pronounced (Figure 16g / 16h).

In *CAV1* ERE and PolyA regions, we find that estrogen induced an early demethylation selectively of the H3k9me3 at 30 min and re-methylation at 45 min, whereas H3K9me2 was methylated at 30 min at ERE and at 45 min at PolyA (Figure 17a / 17b). H3k4me3-me2 increase at 15 min and 45 min and decrease at 30 min (Figure 17c / 17d).

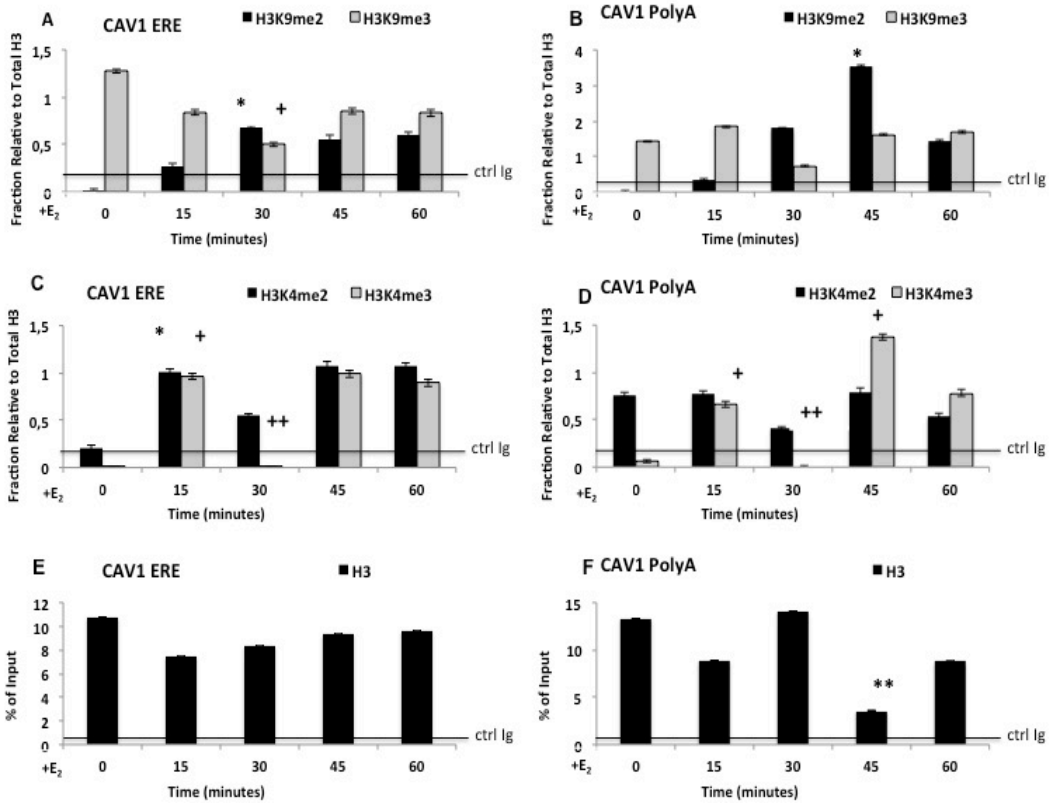

Figure 17: **Methylation-demethylation cycles of histone H3K4/K9 induced by E_2 on *CAV1* ERE-PolyA chromatin.** MCF7 cells were serum starved and exposed to 50 nM E_2 at the indicated times (0, 15, 30, 45 and 120 min). qChIP was carried out using specific antibodies recognizing H3K4me3, H3K4me2, H3K9me3 and H3K9me2. **A, B.** H3K9me2 and H3K9me3 occupancy at *CAV1*ERE and PolyA. **C, D.** H3K4me2 and H3K4me3 occupancy at *CAV1*ERE and PolyA. **E, F.** TotalH3 occupancy at *CAV1*ERE and PolyA. These data were normalized to total H3 histone. The statistical analysis derived from at least 3 experiments in triplicate (n ≥9; Mean±SD). *p <0.01 (matched pairs t test) compared to E_2-unstimulated sample, **p<0.01 (matched pairs t test) comparing 15 to 30 min. of E_2 exposure.

In *BCL2* ERE region, we find that estrogen induces an early increase only of the H3k9me3 at 15-45 min and 60 min, whereas H3K9me3-me2 are demethylated at 30 min and re-methylated at 45min on PolyA (Figure 18a /18b). H3k4me2 increases at 30 min at ERE region and at 45 min at PolyA site, while H3K4me3 levels do not change (Figure 18c / 18d).

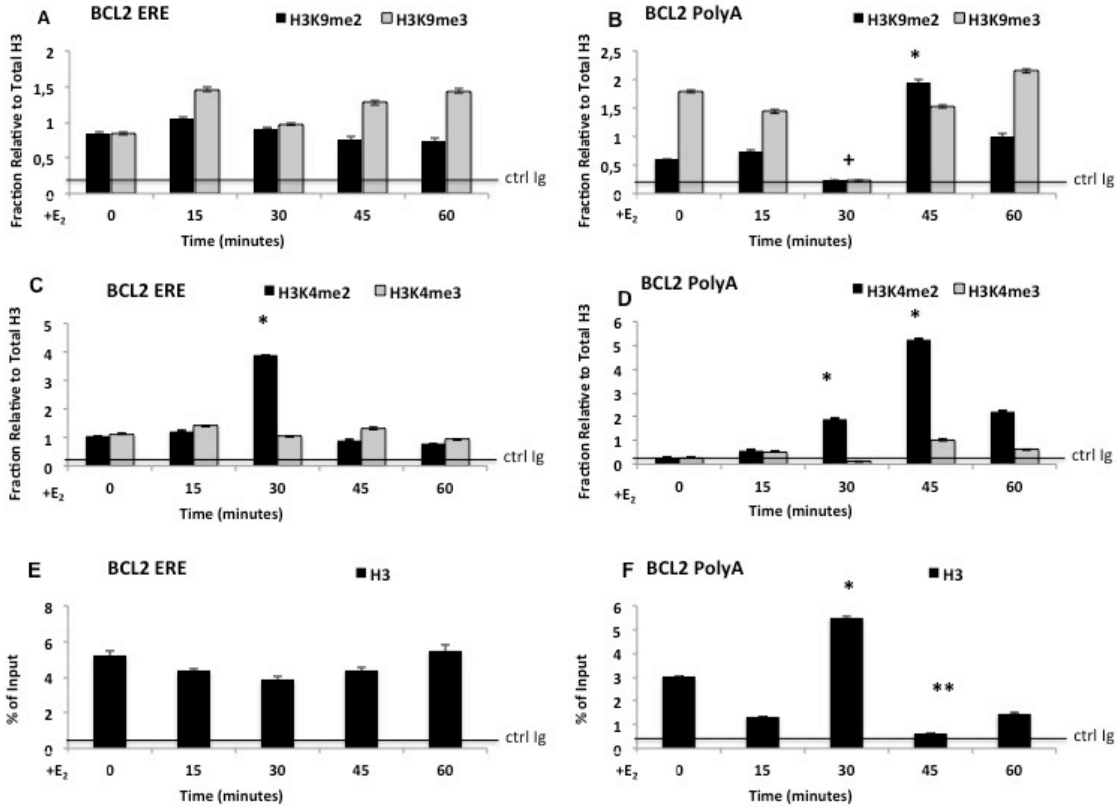

Figure 18: **Methylation-demethylation cycles of histone H3K4/K9 induced by E_2 on *BCL2* ERE-PolyA chromatin.** MCF7 cells were serum starved and exposed to 50 nM E_2 at the indicated times (0, 15, 30, 45 and 120 min). qChIP was carried out using specific antibodies recognizing H3K4me3, H3K4me2, H3K9me3 and H3K9me2. **A, B.** H3K9me2 and H3K9me3 occupancy at *BCL2*ERE and PolyA. **C, D.** H3K4me2 and H3K4me3 occupancy at *BCL2*ERE and PolyA. **E, F.** TotalH3 occupancy at *BCL2*ERE and PolyA.
These data were normalized to total H3 histone. The statistical analysis derived from at least 3 experiments in triplicate (n ≥9; Mean±SD). *p <0.01 (matched pairs t test) compared to E_2-unstimulated sample, **p<0.01 (matched pairs t test) comparing 30 to 45 min. of E_2 exposure.

Collectively, all the regions ERE and PolyA sites of the estrogen-induced genes analyzed, show discrete oscillations of methylation and demethylation involving H3K9 and H3K4. We suggest that the trigger is the demethylation of H3k9me3-me2. In addition, we note that the location of the ERE (intron or exon) and the basal transcriptional state of the gene may modify the intensity of the methylation-demethylation changes.

4.5. Formation of dynamic chromatin loops is associated with Estrogen-induced transcription

The data shown above indicate that estrogens induce the same histone modifications in distal segments of target genes, suggesting that these regions are functionally synchronized and may be physically associated in an unique estrogen- induced domain.

To identify these putative estrogen-dependent chromatin domains, we performed the 3C analysis on fixed chromatin isolated from E2-induced cells (*see Method*). Briefly, fixed chromatin DNA was cleaved with a restriction enzyme and ligated under very diluted conditions to favour intra-molecular interactions. PCR and DNA sequence were then used to identify the ligated DNA segments.

Figure 19 shows that specific chromatin domains are cyclically induced by estrogen at 15 and 60 min. These domains involve the transcription start site and PolyA in *BCL2* gene.

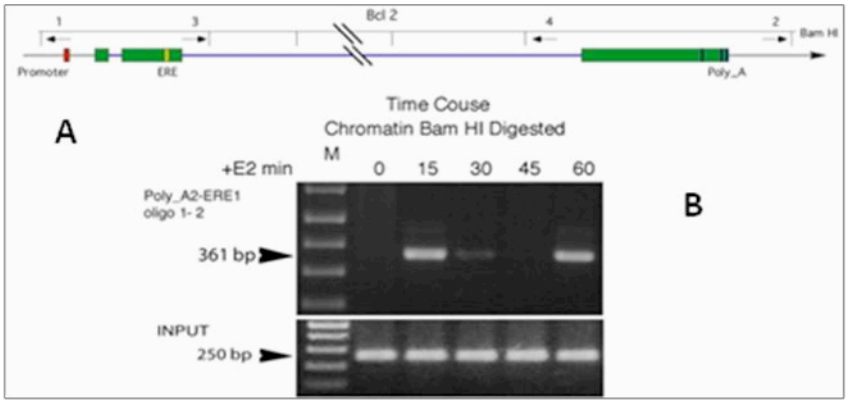

Figure 19: **Formation of dynamic chromatin loops in BCL2 during early E2-induced transcription.**
3C analysis of BCL2 chromatin MCF7 cells exposed to 50nM of E2 for various periods of time. **A.** Schematic presentation of gene and sites of Bam H1 enzyme. All the combinations of primers indicated, were performed on ligated chromatin. **B.** Time course of chromatin looping during E2 induction. 3C analysis was carried out as described in Methods. All 3C-fragments have been sequenced.

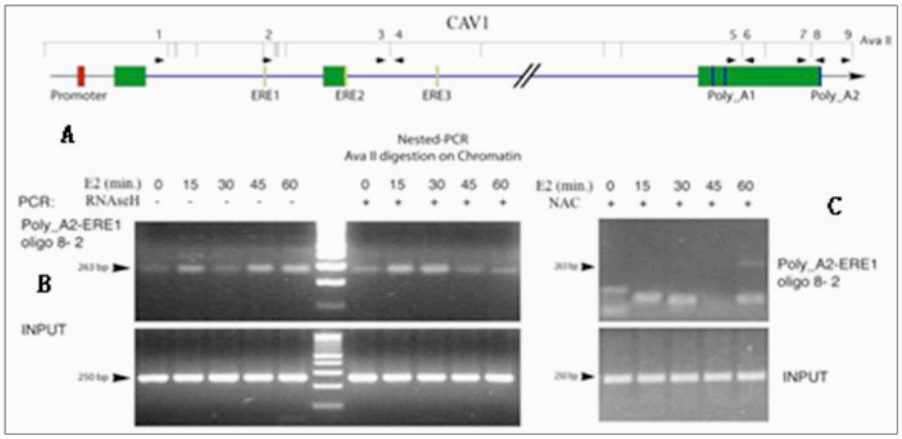

Figure 20: **Formation of dynamic chromatin loops in CAV1 during early E2-induced transcription.**
3C analysis of CAV1 chromatin MCF7 cells exposed to 50nM of E2 for various periods of time. **A.** Schematic presentation of gene and sites of AVA II enzyme. All the combinations of primers indicated, were performed on ligated chromatin. **B.** Time course of chromatin looping during E2 induction with or without RNAseH. **C.** Time course of chromatin looping during E2 induction in presence of N-acetyl-cysteine (NAC). 3C analysis was carried out as described in Methods. All 3C-fragments have been sequenced.

Figure 20a shows that estrogen induced chromatin domains in CAV1 gene at 15 – 45 and 60 min, these domains involve ERE1 and PolyA regions. Moreover, chromatin treatment with RNAseH eliminates the domain corresponding to the late loop (45-60 min) whereas the early loop is not affected. This suggests that the second interaction between these distal regions is dependent on a hybrid DNA / RNA (Figure 20a).

We have also investigated if local DNA oxidation induced by histone demethylation (Perillo et al., 2008) is necessary for loop formation. In fact, pretreatment of cells with the aspecific antioxidant, N-acetyl-cysteine (NAC), inhibits the PolyA-ERE loop formation (Figure20b) receptor recruitment and mRNA accumulation (Figure 21).

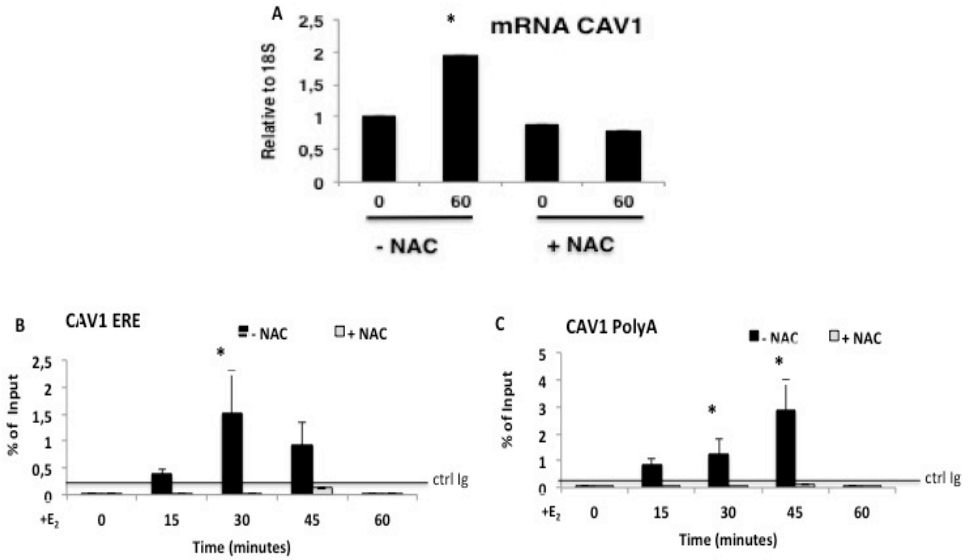

Figure 21: **NAC inhibits E2-dependent CAV1 mRNA expression and ERa binding to ERE region.**
MCF7 cells were pretreated with 50mM of NAC and exposed to 50nM of E2 for various periods of time. **A**. Inhibition of Transcription induced by Estrogen. **B.** ChIP analysis of E2-dependent ERa binding to ERE and PolyA. The statistical analysis derived from at least 3 experiments in triplicate (n ≥9; Mean±SD). *p <0.01 (matched pairs t test) compared to E_2-unstimulated sample.

These data indicate that estrogen induced a chromatin loop between ERE and PolyA regions and the physical association of these 2 sites may explain the same type of histone modifications. The enzyme that drives in vivo H3_K9 me2 demethylation induced by estrogens is LSD1 (KDM1) (Perillo et al., 2008; ref). To demonstrate that LSD1 is involved in loop formation, we transfected the cells with a dominant negative expression vector of LSD1 (LSD1 ala). The expression of this mutant inhibits the recruitment of the E2 receptor to the ERE and prevents histone H3-K9me2 methylation changes (Ambrosio et al, 2013). Expression of this mutant inhibited also, H3k9me2 demethylation induced by E2 (Figure 22b/c). The expression of this LSD1 variant inhibited also E2-induced chromatin loop (Figure 22a) and inhibited CAV1 mRNA expression (Figure 22d).

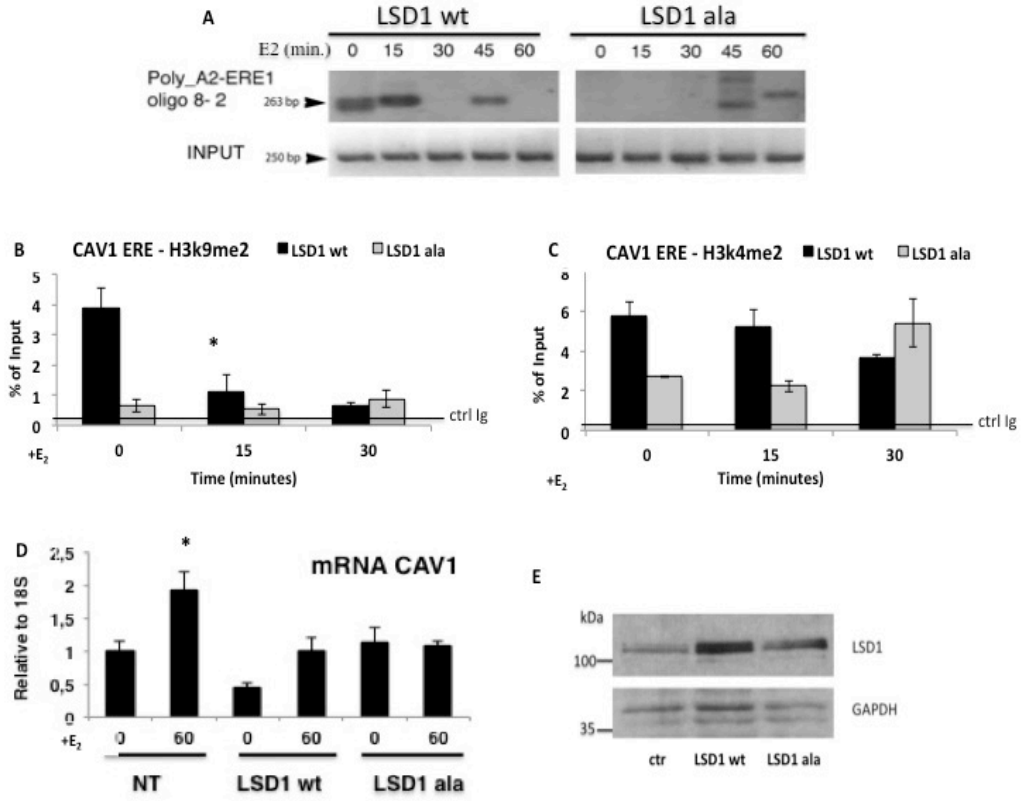

Figure 22: **Expression of LSD1 dominant negative inhibits estrogen-induced transcription.**
MCF7 cells were transfected with LSD1 wt or LSD1 ala expression vectors and exposed to 50nM of E2 for various periods of time. **A.** Expression of LSD1 dominant negative inhibits E2-dependent chromatin loop in CAV1. **B, C.** Expression of LSD1 dominant negative prevents histone H3-k9me2 methylation changes induced by E2. **D.** Expression of LSD1 dominant negative inhibits E2-dependent transcription. **E**. LSD1 protein expression. The statistical analysis derived from at least 3 experiments in triplicate (n ≥9; Mean±SD). *p <0.01 (matched pairs t test) compared to E_2-unstimulated sample.

4.6. Recruitment of base (BER) or nucleotide (NER) excision repair enzymes to the ERE-PolyA chromatin regions induced by Estrogen

Transcription is associated with a burst of DNA oxidation dependent from histone demethylation (Perillo B. et al 2008). Oxidized guanine (8-oxo-dG) is recognized by OGG1 (Amente S. et al. 2010). In addition, it was recently reported that NER enzymes are essential for the formation of

chromatin loops and DNA de-methylation induced by retinoic acid at the target genes (Le May N. et al., 2012). Together these data suggest that both BER and NER enzymes participate to the formation of chromatin loops induced by nuclear hormones and are essential for the correct repair of DNA oxidation lesions. Therefore, we analyzed the recruitment of OGG1 (BER), XPC and XPG (NER) at the ERE and PolyA chromatin regions after E2 induction.

ChIP analysis shows a rapid OGG1 recruitment with two peaks (15 and 45-60 min) suggesting that also DNA oxidation and repair at the ERE and PolyA sites, undergo the same cycle observed in histone demethylation and loop formation. In addition, we notice important and selective differences in the recruitment of XPC and XPG: XPC is recruited earlier at the ERE than XPG (15 min versus 45 min), while at the PolyA both XPC and XPG are recruited with the same timing (Figure 23).

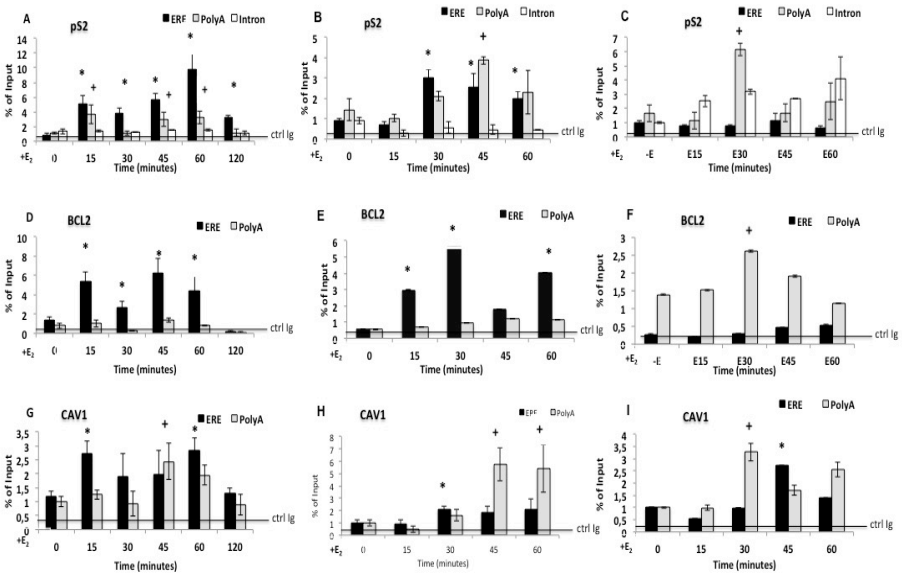

Figure 23: **Estrogen induced BER and NER cycles on genes target.** MCF7 cells were serum starved and exposed to 50 nM E_2 at the indicated times (0, 15, 30, 45 and 60 min). qChIP was carried out using specific antibodies recognizing OGG1, XPC and XPG. **A, D, G.** OGG1 occupancy at ERE and PolyA. **B, E, H.** XPC occupancy at ERE and PolyA. **C, F, I.** XPG occupancy at ERE and PolyA. The statistical analysis derived from at least 3 experiments in triplicate (n ≥9; Mean±SD). *p <0.01 (matched pairs t test) compared to E_2-unstimulated sample.

These data suggest a hierarchy in the recruitment of BER and NER and between different types of NER enzymes. In fact, we find cyclic OGG1 recruitment at ERE region at 15 and 45 – 60 min, whereas XPC and XPG increase only at 30 min. Also, at the ERE, XPC is recruited before XPG (30 min), which is recruited mainly at the PolyA at 30 min. This information is relevant, because XPC is part of the Global Genome NER that recognizes lesions caused by the distortion of the double helix. This suggests that the oxidative or apurinic site is recognized by XPC independently of the presence of stalled PolII in the transcription coupled repair (TCR) recognized by XPG. E2 and presumably other nuclear hormones induce

DNA oxidation, loop formation assisted by BER and NER enzymes, which are essential for the proper repair and looping of DNA.

4.7. Estrogen induces strand specific oxidation and repair

The data shown above, indicate that E2 induces a burst of DNA oxidation and selective and ordered recruitment of BER and NER enzymes to the ERE and PolyA sites of target genes. To directly document the DNA oxidative lesions and to monitor site-specific repair, we mapped precisely oxodGs by using the Ligation Proximity Amplification (LPA) technique. Briefly: ligation and amplification of contiguous oligonucleotides terminating at the specific G under study, are inhibited if this G is oxidized and eliminated by glycosylase. Inhibition of PCR, before or after the G-glycosylase treatment, provides the information on the oxidation state of the specific G. The cells were treated with E2 50nM for various periods of time, the genomic DNA was extracted and treated with the 8-oxoGuanine DNA Glycosylase from E.coli (FpG) to generate apurinic sites from 8-oxoG. We have measured 4 CpG at the ERE, TATA, Intron regions of pS2 gene (- 399, - 20 from TSS).

Figure 24 shows the sensitivity of the technique. Control cells were treated with and without hydrogen peroxide (H_2O_2), which is a strong oxidant. DNA was extracted, treated with or without FpG, and, after ligation, was amplified with strand specific probes. We find that without FpG treatment, there are small differences in the efficiency of PCR between the genomic DNA extracted from control and H_2O_2-treated cells, whereas FpG treatment increases this difference by 4 fold. Note that H_2O_2 oxidizes both strand (- and + strand, template and non-template strand, respectively) with the same efficiency.

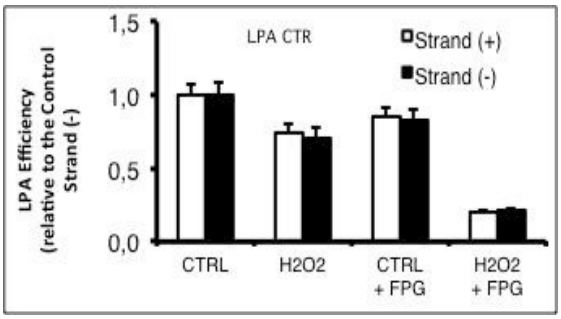

Figure 24: **LPA assay control.**
MCF7 cells were treated with 1mM of H2O2. DNA was extracted, treated with the DNA glycosylase from E.coli (FPG) to generate apurinic sites, where 8-oxoG was present. The nick generated by FPG cannot support ligation and PCR of contiguous primers. The statistical analysis derived from at least 3 experiments in triplicate (n ≥9; Mean±SD).

Figure 25 shows the results of LPA on 2 Gs located at the ERE, TATA and intron of pS2 gene in cells exposed for various times at E2. At the ERE region, we find that 2 Gs are selectively repaired on the (-) and (+) strands: the first (top panels) shows oxidation at 5min and repair at 15 min at the (+) strand and oxidation at 15 min and repair at 30 min at the (-) strand. The C (indicated as ERE II) is oxidized with perfect complementary timing at the (+) and (-) strands, respectively. The C at the TATAA, instead is oxidized at 0 (when PolII is inefficiently active), repaired at 30 min on the (+) strand and at 15 min on the (-) strand. In all cases, the oxidation of Gs measured with LPA mirrors the H3 histone methylation–demethylation cycles and the timing of loop formation induced by E2.

These data indicate a precise order in timing and space of oxidation and repair induced by E2 and highlight the symmetry of cycles of methylation and oxidation that govern the assembly of the transcription machine induced by the hormones.

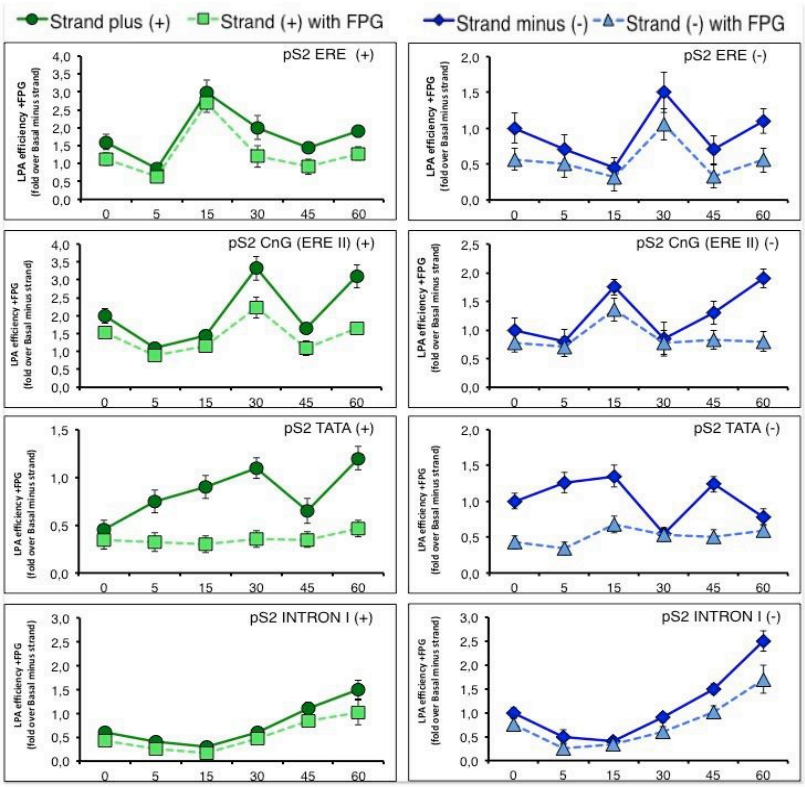

Figure 25: **Strand specific DNA oxidation induced by Estrogen.**
MCF7 cells were treated with 50nM of E_2 at the indicated times (0, 15, 30, 45 and 60 min). DNA was extracted, treated with the DNA glycosylase from E.coli (FPG) to generate apurinic sites, where 8-oxoG was present. We have measured 4 CpG at the ERE, TATA, Intron regions of pS2 gene (- 399, - 20 from TSS). The statistical analysis derived from at least 3 experiments in triplicate (n ≥9; Mean±SD).

4.8.Recruitment of DNMT3a to the ERE-PolyA chromatin regions induced by Estrogen regulates the DNA oxidation levels

DNA oxidation involves not only G but also C. In fact C can be oxidized only when methylated *in vivo*. It has been reported that estrogens induce cycles of the CpG methylation within the pS2 promoter through recruitment of DNMTs enzymes (Metivier et al.2003). The DNA

methyltransferase enzyme, DNMT3a, cooperates with Tymidine DNA Glycosilase that recognizes G/T mismatches in DNA (Ya-Qiang Li et al. 2007).

To dissect the role of DNMT3a in oxidation and more general, transcription induced by estrogen, we determined the recruitment of DNMT3a at ERE and PolyA of pS2 gene. ChIP analysis shows that DNMT3a recruitment peaks at 30min and its cycle at the ERE appears complementary to that of OGG1 (Figure 26).

To define a possible role of DNMT3a in DNA oxidation induced by E2, we silenced DNMT3a and measured OGG1 recruitment at regulatory regions of pS2 gene. Figure 24 shows that depletion of DNMT3a increases OGG1 density at the ERE region basally and in E2-induced cells.

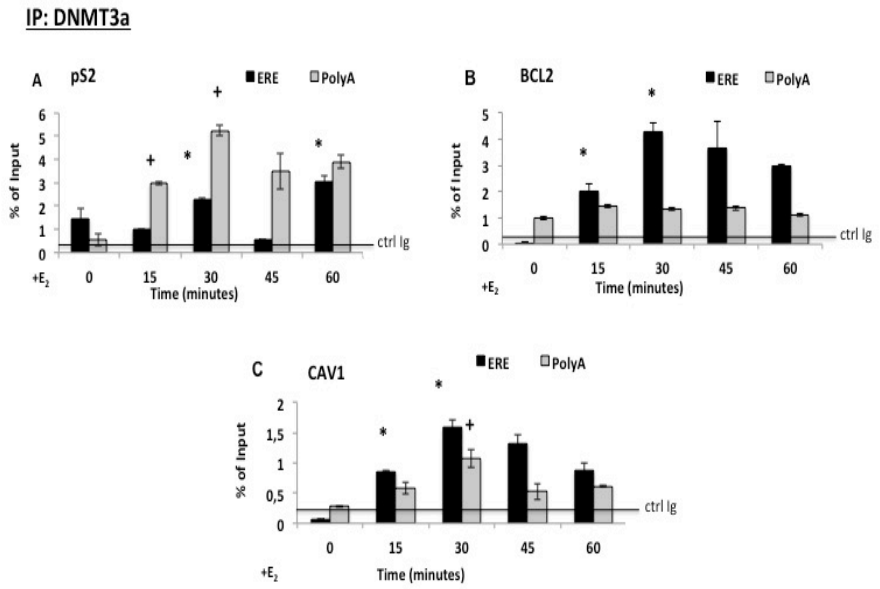

Figure 26: **Estrogen induces recruitment of DNMT3a at the ERE and PolyA sites of target genes.**
MCF7 cells were serum starved and exposed to 50 nM E_2 at the indicated times (0, 15, 30, 45 and 60 min). qChIP was carried out using specific antibodies recognizing DNMT3a. **A.**DNMt3a occupancy at ERE and PolyA of pS2. **B.**DNMT3a occupancy at ERE and PolyA of BCL2. **C.** DNMT3a occupancy at ERE and PolyA of CAV1. The statistical analysis derived from at least 3 experiments in triplicate (n ≥9; Mean±SD). *p <0.01 (matched pairs t test) compared to E_2-unstimulated sample.

Strikingly, the recruitment of OGG1 was reduced at the PolyA site, suggesting that the ERE and PolyA sites were not physically contiguous in the absence of DNMT3a. This corresponds to inhibition of E2-induced mRNA accumulation in DNMT3a- depleted cells.

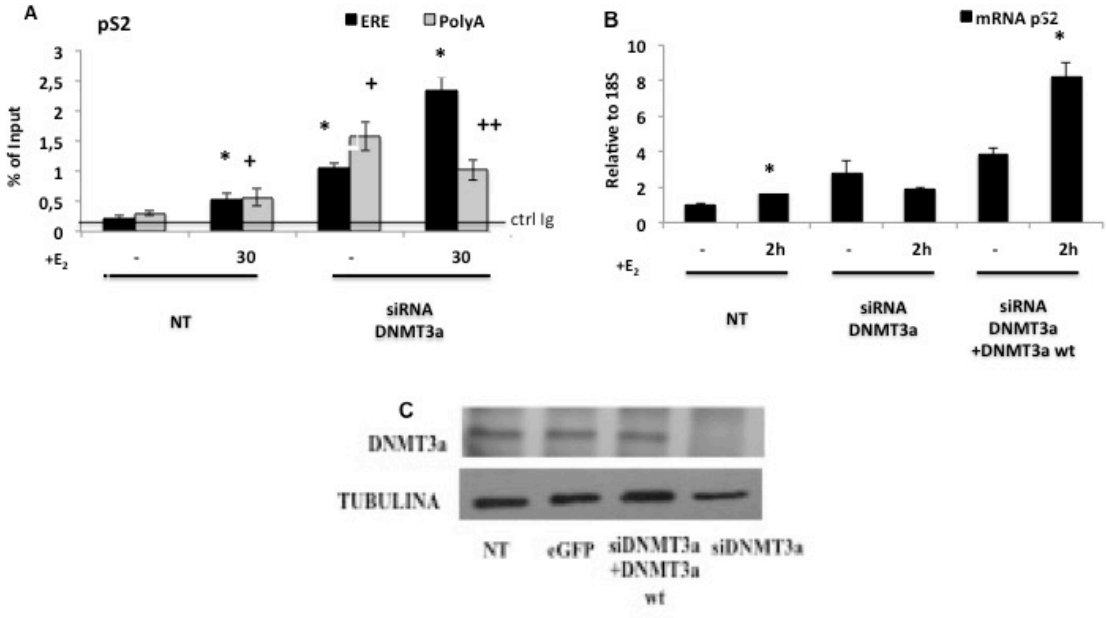

Figure 27: **DNMT3a silencing enhances OGG1 recruitment at ERE region and reduces pS2 transcription.**
MCF7 cells were transfected with siRNA DNMT3a, serum starved and exposed to 50 nM E_2 at the indicated times (0 and 30). **A.** qChIP analysis shows OGG1 occupancy at ERE of pS2. **B.**DNMT3a silencing inhibits transcription induced by estrogen. **C.** Western blot analysis shows silencing of DNMT3a.
The statistical analysis derived from at least 3 experiments in triplicate (n ≥9; Mean±SD). *p <0.01 (matched pairs t test) compared to E_2-unstimulated sample, ++ p<0.01 (matched pairs t test) comparing 0 to 30 min. of E_2 exposure.

We conclude that DNMT3a is important for productive transcription induced by estrogens and its activity is necessary to control oxidation and OGG1 recruitment. The loss of OGG1 at the 3' end is compatible with the absence of 5'-3' loop connecting the ERE to the PolyA sites. Increase of

OGG1 in DNMT3a depleted cells may indicate that repair of the oxidative lesions is not efficient (Ya-Qiang Li, et al. 2007).

We also analyzed the recruitment of TDG and TET1 enzymes.

TET1 can induce oxidation of methyl-cytosine in hydroxyl-methyl-Cytosine, Formyl-Cytosine and Carboxy-Cytosine that can also be directly excised by TDG (Rahul M. Kohli & Yi Zhang, 2013).

ChIP analysis shows that estrogen induced TDG recruitment at 15 and 45 min at the PolyA site of pS2, CAV1 and BCL2 gene, whereas TDG was recruited 15 min at ERE of BCL2. Instead, TET1 increased at 15 – 30 - 45 min at all the analyzed regions (Figure 28).

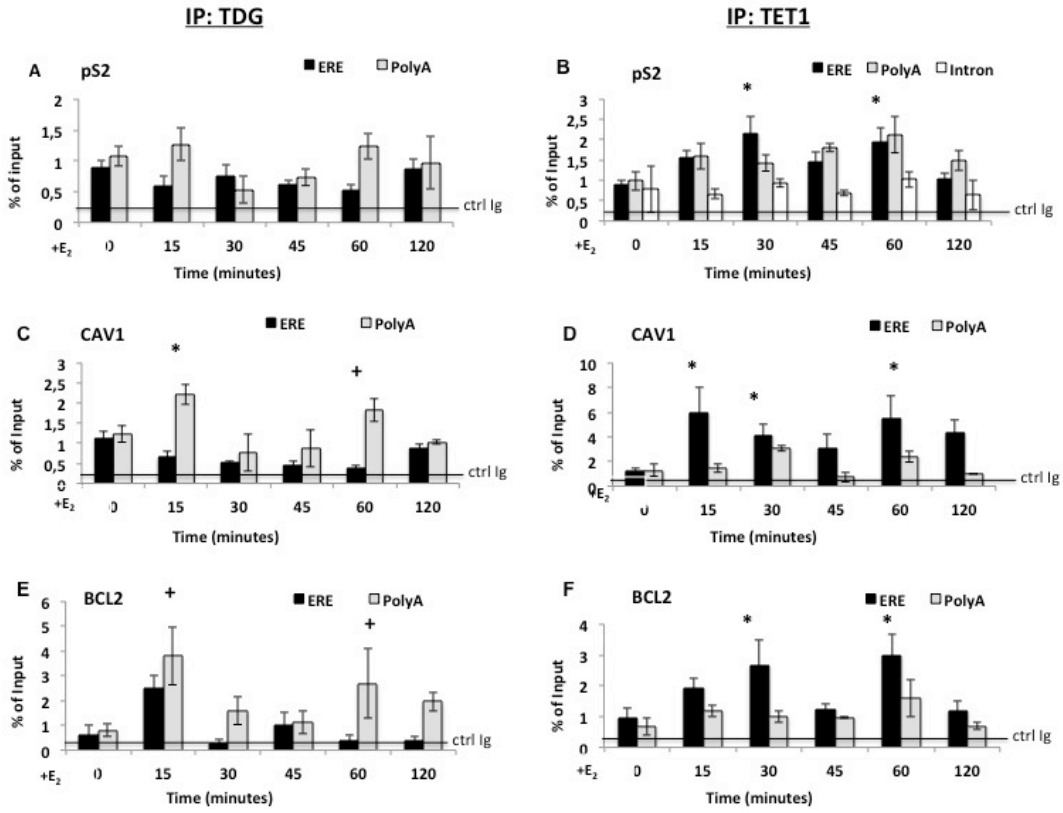

Figure 28: **Estrogen induces recruitment of TDG and TET1 at the ERE and PolyA sites of target genes.**

MCF7 cells were serum starved and exposed to 50 nM E_2 at the indicated times (0, 15, 30, 45, 60and 120 min). qChIP was carried out using specific antibodies recognizing TDG and TET1. **A, C, E.**TDG occupancy at ERE and PolyA of pS2. **B, D, F.**TET1 occupancy at ERE and PolyA of BCL2. The statistical analysis derived from at least 3 experiments in triplicate (n ≥9; Mean±SD). *p <0.01 (matched pairs t test) compared to E_2-unstimulated sample.

4.9. Coordination of C and G oxidation induced by estrogens

Estrogen induces recruitment of DNMT3a and TET1 to regulate the wave of DNA methylation and oxidation. This coordinated recruitment of methylation (DNMT3a) and hydroxymethylation (TET1) of cytosine may be crucial for repair. In addition, the presence of the TET1 oxidation products (5-hmC and 5-formylC) marks active transcription (You, et al. 2014; Neri et al. 2015).

To determine the methylation and oxidation of C induced by estrogens, we performed a modified bisulfite assay on ERE region of pS2.

The use potassium perruthenate (KRuO4) selectively oxidizes 5hmC into 5-formyl-cytosine (5fC), which after bisulfite conversion is read as uracil in the sequence. Therefore, in genomic DNA from estrogen-treated cells, we have measured methyl and hydroxyl-Cat the ERE of pS2 gene.

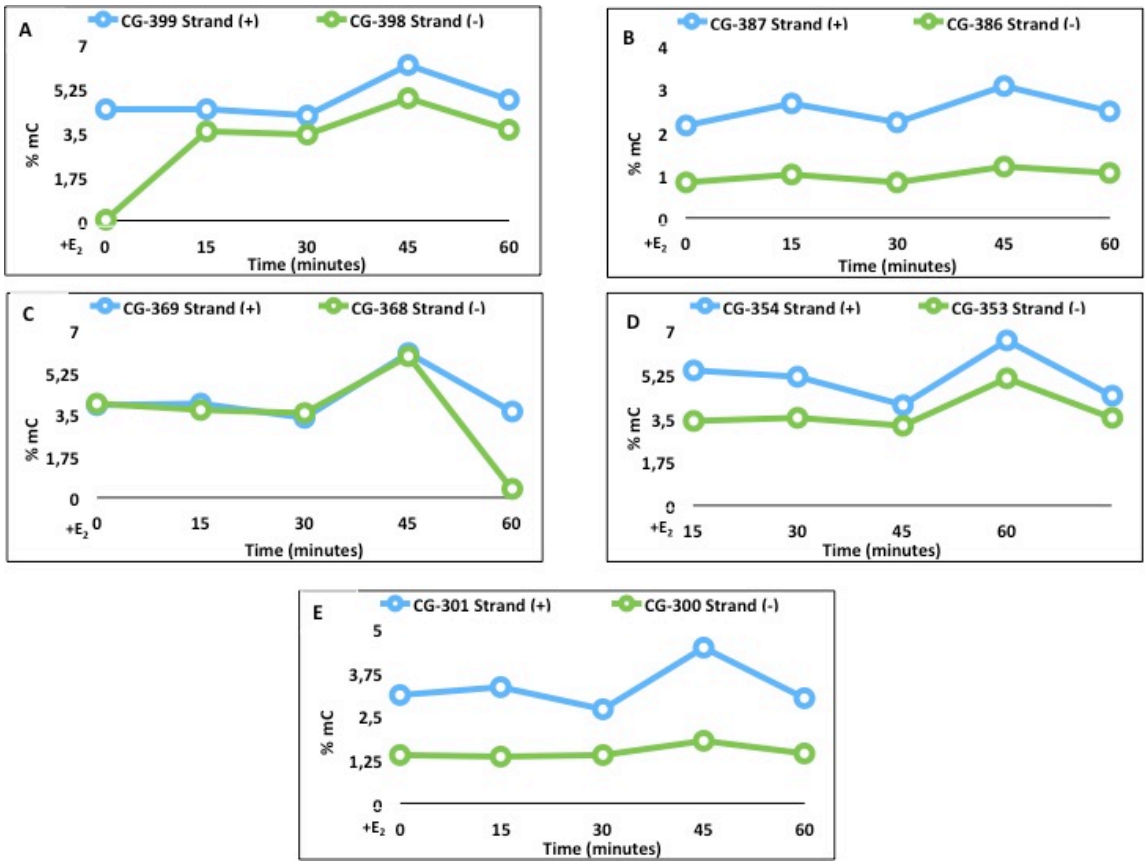

Figure 29: Estrogen induced specific CpG methylation
MCF7 cells were treated with 50nM of E_2 at the indicated times (0, 15, 30, 45 and 60 min). DNA was extracted, treated with sodium bisulfite. We analyzed 5 CG in position: - 399, - 387, - 369, - 354, - 301 from TSS of pS2 gene. The statistical analysis derived from at least 2 experiments in duplicate.

We analyzed a fragment of 200 bp on ERE containing 5 CpG.

Figure 29 shows that 4 of 5 CpG display a difference in methylation, which appears to be strand specific: the non-template (+) strand is more methylated. In addition, all 5 CpG analyzed display a methylation peak at 45 min, which overlaps with the peak of histone H3K9 methylation (Figure 16).

Note a sharp methylation peak of CG -399 on template (-) strand at 15 min (Figure 29a), and demethylation of CG - 369 at the same strand at 60 min (figure 29c). Figure 30 shows that the 5 CpG have a different levels of C

hydroxylmethylation. In fact, CG - 399 has a peak of C hydroxylmethylation at 15 and 30 min on template (-) strand and then returns to baseline at 45-60 min.

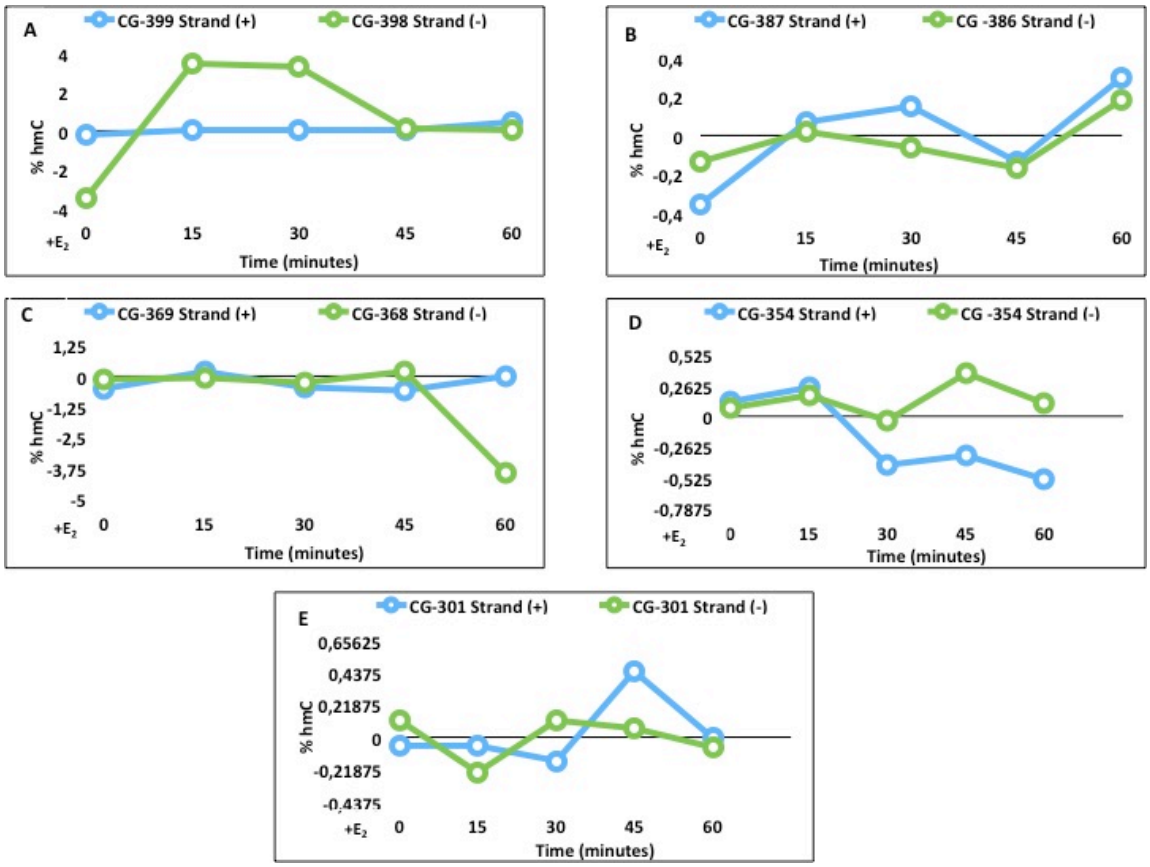

Figure 30: **specific C hydroxymethylation induced by estrogen at the *pS2* ERE.**
MCF7 cells were treated with 50nM of E_2 at the indicated times (0, 15, 30, 45 and 60 min). DNA was extracted, treated with the Potassium Perruthenate ($KRuO_4$) to generate difference between methyl-cytosine and hydroxymethyl-cytosine, where was present. Then, the samples were treated with sodium bisulfite. We analyzed 5 CG in position: - 399, - 387, - 369, -354, -301 from TSS of pS2 gene. The statistical analysis derived from at least 2 experiments in duplicate.

We conclude that estrogens induce a sharp C hydroxyl-methylation peak at specific Cs in a strand-specific manner. It is worth mention that CpG hydroxymethylation timing is dissociated from the DNA methylation.

5. DISCUSSION

Transcription induced by estrogen is associated with chromatin modification dependent from histone methylation-demethylation cycles. It has been already found that Estrogen induced transcription is driven by H3K9me2 demethylation (Perillo et al. 2008). Our data show that estrogens induce a common change of the histone code at target genes. In particular, we observe demethylation of histone H3K9 in the first 30 min, followed by a peak of methylation at 45 min and demethylation at 60 min. Also, H3K4 is characterized by a cyclical methylation (15 and 45 min) (Figure 15 – 16 - 17). Both methylation the lysines 9 and 4 are stabilized after the first hour of induced-transcription, when the transcription become productive. Interestingly, this common histone code may change slightly depending on the location of the enhancer (intra or inter-gene)) and the status of the basal transcription (see ERE BCL2 and PolyA regions in Figure 17). LSD1 and JMJD2a are the major histone demethylases responsible for histone modification induced by estrogen. We find a different timing of the recruitment of LSD1 and JMJD2a at the gene locations examined (data not shown). LSD1 dominant negative expression in MCF7 inhibits H3K9 demethylation, mRNA expression and chromatin domains induced by estrogen (Figure 21).

Transcription induced by estrogen is associated also with the formation of chromatin loops that display a precise synchronization to permit an accurate definition of the 5' and 3' borders of the transcription unit.

Pretreatment of cells with NAC inhibits gene transcription, the formation of the loop and the receptor binding to enhancer (Figure 20) suggesting that oxidation is important for transcription. It is worth noting that treatment of chromatin with RNaseH prevents the formation of the late (45 min) loop but not of the early (15 min) loop, between ERE and

PolyA regions. This suggests that hybrid DNA / RNA (R-Loop) may hold together the 5' and 3' ends of the genes carrying the receptor only after 45' of continuous stimulation with estrogens (Figure 19).

Histone demethylation generates a burst of oxidation (Perillo et al. 2008) that recruits DNA repair enzymes: BER and NER enzymes (Figure 22 and 25). The initial lesions are recognized by OGG1 and APE1, which display the same oscillations of demethylation-methylation cycles (15 and 45-60). Following OGG1, NER are recruited at 30 min. Interestingly, XPC is recruited to the enhancer, whereas XPG to the PolyA (Figure 22). XPC is part of the Global Genomic NER, which recognizes helix distortions regardless of the presence of Pol II. On the other hand, XPG is part of Transcription-Coupled NER, which assists the RNA Pol II during recognition of the lesion (Gros L. et al., 2002). These data suggest that the ERE and PolyA lesions are differently recognized and repaired. OGG1 recognizes the 8-oxo Gs detecting a distortion of the helix (Kuznetsova A.A. et al. 2014). This can represent a signal for recruitment of XPC (GG-NER) at enhancer and can determine a stall of RNA Pol II at the PolyA, which recruits XPG (TC-NER). We have evaluated in detail the specific Gs oxidized and repaired.

We have measured the formation of 8-oxo-guanine (8-oxogG) by LPA technique. The data show that estrogens induce oxidation and repair differentially at the (-) and (+) strands of the ERE region. In fact, the non-template strand is oxidized-repaired mainly 5-15min while the template strand is oxidized-repaired essentially 15 and 45 min after estrogen stimulation (Figure 26). This ordered sequence of oxidation and repair probably reflects the structure of the helix across the 25 bp spanning the Gs analyzed.

Our data shed light also on DNMT3a, which is recruited at the enhancer and PolyA sites at 30 min. DNMT3a is essential for productive transcription induced by estrogens. We find that DNMT3a silencing increases OGG1 recruitment at the ERE in the basal and in the sample stimulated with estrogens, while it reduces the OGG1 recruitment at PolyA site. This

suggests that the 5' and 3' ends are not juxtaposed as in control cells. The changes in methylation and hydroxymethylation of CpG are also associated with the recruitment of TET1 and TDG at enhancer and PolyA sites. TET1 recognizes and modifies the methylcytosine, while TDG recognizes and removes a variety of oxydized and deaminated cytosines. TET1 is recruited 15 – 30 min to the enhancer and 60 min after estrogen stimulation to the PolyA. TDG is recruited to the PolyA and enhancer of *BCL2* but not to *CAV1* and *pS2* enhancers.

Finally, we analyzed the methylation and hydroxylation status of DNA at single strand resolution. Bisulfite analysis shows that template and non-template strands have a different levels and timing of methylation. Also, hydroxymethylation of specific Cs was induced by estrogens. We note that the changes of hydroxymethylation are associated with the timing and the location of oxidized Gs, suggesting that the 2 events (G and C methylation-oxidation) are tightly associated.

6.CONCLUSION

We show periodic oscillations of histone H3 methylation, G oxidation, C methylation and hydroxyl-methylation at the enhancer and PolyA addition sites after induction of transcription in prototypic estrogen-induced genes. These oscillations correlate with formation of chromatin loops that juxtapose the 5' and 3' ends of the induced genes. BER followed by NER enzymes are recruited to the 5' and 3' end sites to repair the DNA oxidative lesions and to stabilize the 5' and 3' borders of the transcriptional units included in the loops. At the 5' and 3' end sites of the loops, repair of oxidized Gs and hydroxymethylated Cs proceeds in a strand specific fashion. DNA methylation by DNMT3a is associated to G and C oxidation and reduces the G oxidation levels. This ordered series of localized DNA oxidation and repair are essential for productive transcription induced by estrogens.

We suggest that coupling transcription with methylation and repair enzymes is the evolutionary strategy to reduce the mutational burden induced by DNA oxidation at the borders of chromatin loops.

7. ACKNOWLEDGEMENTS

At the end of my PhD program, I would like to thank...

My Supervisor and PhD Coordinator, professor Vittorio Enrico Avvedimento, for conveying to me the profound passion for research.

Professor Antonio Porcellini, for suggestions and its availability.

Dr. Giusi Russo, for her patience and encouragement, thanks to which I was able to face any obstacle encountered during my PhD.

Dr. Rosaria Landi, for the friendship that derives from an active collaboration. All students and colleague of my laboratory for their patience, availability and friendship.

My parents, Vincenzo and Giuseppina, my brother Gianluca and my sister Teresa, for their love and for conveying to me the perseverance to achieve the targets set.

My husband's parents, Raffaele and Anna, and my brother in law Fernando, for their love and for sharing with me every moment of my training path.

8. REFERENCES

Ambrosio R., Damiano V., Sibilio A., De Stefano M.A., Avvedimento V.E., Salvatore D.,Dentice M. *Epigenetic control of type 2 and 3 deiodinases in myogenesis: role of Lysine-specific Demethylase enzyme and FoxO3.* (2013). *Nucleic Acids Res.* ***41***:3551-3562.

Amente S., Bertoni A., Morano A., Lania L., Avvedimento E.V., Majello B. *LSD1-mediated demethylation of histone H3 lysine 4 triggers Myc-induced transcription.* (2010). *Oncogene* ***29*** (25): 3691-3702.

Anand R. & Marmorstein R. *Structure and mechanism of lysine-specific demethylase enzymes*. (2007). *J Biol Chem* ***282*** (49): 35425-35429.

Andrew J Bannister and Tony Kouzarides. *Regulation of chromatin by histone modifications.* (2011). *Cell Research . 21*:381–395.

Baylin S. B. & Ohm J. E. *Epigenetic gene silencing in cancer – a mechanism for early oncogenic pathway addiction?* (2006). *Nat Rev Cancer* ***6***, 107–116.

Berger S.L. "*Review Article The complex language of chromatin regulation*
during transcription". (2007). *Nature* ***447***, 407–412.

Bird A. P. & Wolffe A. P. *Methylation-induced repression–belts, braces, and chromatin.* (1999). *Cell* ***99***, 451–454.

Changjun You, Debin Ji, Xiaoxia Dai & Yinsheng Wang. *Effects of Tet-mediated Oxidation Products of 5-Methylcytosine on DNA Transcription in vitro and in Mammalian Cells.* (2014). *Sci Rep.* ***4***:7052.

Cho Y. H., Yazici H., Wu H. C., Terry M. B., Gonzalez K., Qu M., Dalay N.
& Santella R. M. *Aberrant promoter hypermethylation and genomic hypomethylation in tumor, adjacent normal tissues and blood from breast cancer patients.* (2010). *Anticancer Res.* ***30***, 2489-2496.

Choy M.K., Movassagh M., Goh H.G., Bennett M.R., Down T.A., Foo R.S. *Genome-wide conserved consensus transcription factor binding motifs are hyper-methylated*. (2010). *BMC Genomics.* ***27***;11:519.

Cuozzo C., Porcellini A., Angrisano T., Morano A., Lee B., Di Pardo A.,Messina S., Iuliano R., Fusco A., Santillo M. R., Muller M. T., Chiariotti L., Gottesman M. E. & Avvedimento E. V. *DNA damage, homology-directed repair, and DNA methylation.* (2007). *PLoS Genet.* ***3***, e110.

Dekker J., Rippe K., Dekker M., Kleckner N. *Capturing chromosome conformation*. (2002). *Science.* ***295***(5558):1306-11.

Fischle W., Franz H., Jacobs S. A., Allis C. D. & Khorasanizadeh S. *Specificity of the chromodomain Y chromosome family of chromodomains for lysinemethylated ARK(S/T) motifs.* (2008). *J. Biol. Chem.* ***283***, 19626–19635.

Fortini P., Pascucci B., Parlanti E., Sobol R. W., Wilson S. H. & Dogliotti E. *Different DNA polymerases are involved in the short- and long-patch base excision repair in mammalian cells.* (1998). *Biochemistry* ***37***, 3575-3580.

Goll M. G. & Bestor T. H. *Eukaryotic cytosine methyltransferases.* (2005).
Annu. Rev. Biochem. ***74***, 481–
514.

Grønbaek K., Treppendahl M., Asmar F., Guldberg P. *Epigenetic changes in cancer as potential targets for prophylaxis and maintenance therapy.* (2008). *Basic Clin Pharmacol Toxicol*. ***103***(5):389-96.

Gött P., Zöller L., Darai G., Bautz E.K. *A major antigenic domain of hantaviruses is located on the aminoproximal site of the viral nucleocapsid protein.* (1997). *Virus Genes.****14***(1):31-40.

Gros L., Saparbaev M. K. & Laval J. *Enzymology of the repair of free radicals-induced DNA damage.* (2002). *Oncogene* ***21***, 8905-8925.

Heldring N., Pike A., Andersson S., Matthews J., Cheng G., Hartman J., Tujague M., Ström A., Treuter E., Warner M., Gustafsson J.A. *Estrogen receptors: how do they signal and what are their targets.*
(2007). *Physiol Rev* ***87***(3):905-
31.

James D. Yager, Ph.D., and Nancy E. Davidson, M.D. *Estrogen*
Carcinogenesis in Breast Cancer. (2006). *N Engl J Med.* ***354***:270-
282.

Kirsten Grønbæk, Marianne Treppendahl, Fazila Asmar and Per Guldberg. *Epigenetic Changes in Cancer as Potential Targets for Prophylaxis and Maintenance Therapy.* (2008). *Basic Clin Pharmacol Toxicol.* ***103***(5):389-96.

Klungland A. & Lindahl T. (1997). Second pathway for completion of human DNA base excision-repair: reconstitution with purified proteins and requirement for DNase IV (FEN1). *EMBO J.* 16, 3341-3348.

Laird P. W., Jackson-Grusby L., Fazeli A., Dickinson S. L., Jung W. E., Li E., Weinberg R. A. & Jaenisch R. (1995). Suppression of intestinal neoplasia by DNA hypomethylation. *Cell* 81, 197–205

Law J. A. & Jacobsen S. E. (2010). Establishing, maintaining and modifying DNA methylation patterns in plants and animals. *Nature Rev. Genet.* 11, 204–220.

Le May N., Fradin D., Iltis I., Bougneres P. and Egly J.M. *XPG and XPF endonucleases trigger chromatin looping and DNA demethylation for accurate expression of activated genes.* (2012). *Mol Cell.* ***47***, 622-632.

Li E., Bestor T. H. & Jaenisch R. *Targeted mutation of the DNA methyltransferase gene results in embryonic lethality.* (1992). *Cell* ***69***, 915–926.

Li E., Beard C. & Jaenisch R. *Role for DNA methylation in genomic imprinting.* (1993). *Nature* ***366***, 362–365.

Lindahl T. & Wood R. D. *Quality control by DNA repair.* (1999). *Science* ***286***, 1897-1905.

Li Y.Q., Zhou P.Z., Zheng X.D., Walsh C.P., Xu G.L. *Association of Dnmt3a and thymine DNA glycosylase links DNA methylation with base-excision repair.* (2007). *Nucleic Acids Res.* ***35***(2):390-400.

Liu Y., Prasad R., Beard W.A., Kedar P.S., Hou E.W., Shock D.D., Wilson S.H., *Coordination of Steps in Single-nucleotide Base Excision Repair Mediated by Apurinic/Apyrimidinic Endonuclease 1 and DNA Polymerase β.*(2007). *Journal of Biological Chemistry* ***282*** (18): 13532–13541.

Métivier R., Penot G., Hübner M.R., Reid G., Brand H., Kos M., Gannon F. *Estrogen receptor-alpha directs ordered, cyclical, and combinatorial*

recruitment of cofactors on a natural target promoter. (2003). *Cell*. **115**(6):751-63.

Morano A., Angrisano T., Russo G., Landi R., Pezone A., Bartollino S., Zuchegna C., Babbio F., Bonapace I. M., Allen B., Muller M. T., Chiariotti L., Gottesman M. E., Porcellini A. & Avvedimento E. V. *Targeted DNA methylation by homology-directed repair in mammalian cells. Transcription reshapes methylation on the repaired gene.* (2014). *Nucleic Acids Res.* ***42***, 804-821.

Neri F., Incarnato D., Krepelova A., Rapelli S., Anselmi F., Parlato C., Medana C., Dal Bello F., Oliviero S. *Single-Base Resolution Analysis of 5- Formyl and 5- Carboxyl Cytosine Reveals Promoter DNA MethylationDynamics.(*2015). *Cell Rep.* pii: S2211-1247(**15**)00009-1.

Nilsson S**.**, Mäkelä S**.**, Treuter E., Tujague M., Thomsen J., Andersson G., Enmark E., Pettersson K., Warner M., Gustafsson J.A. *Mechanisms of estrogen action.* (2001). *Physiol Rev.* ***81***(4):1535-65.

Panning B. & Jaenisch R. *RNA and the epigenetic regulation of X chromosome inactivation.* (1998). *Cell* ***93,*** 305–308.

Perillo B., Ombra M.N., Bertoni A., Cuozzo C., Sacchetti S., Sasso A., Chiariotti L., Malorni A., Abbondanza C., Avvedimento E.V. *DNA oxidation as triggered by H3K9me2 demethylation drives estrogen-induced gene expression.* (2008). *Science* ***319***(5860): 202-206.

Rahul M. Kohl & Yi Zhang. *TET enzymes, TDG and the dynamics of DNA demethylation.* (2013). *Nature* ***502***, 472–479.

Sengupta S., Jordan V.C. *Selective estrogen modulators as an anticancer tool:mechanisms of efficiency and resistance*. (2008). *Adv Exp Med Biol.* ***630,***206-19.

Shang Y. *Molecular mechanisms of oestrogen and SERMs in endometrial carcinogenesis.* (2006). *Nat Rev Cancer.* ***6,*** 360-368.

Shang Y. *Hormones and cancer*. (2007). *Cell Research* ***17***: 277–279

Shi Y., Lan F., Matson C., Mulligan P., Whetstine J. R., Cole P. A., Casero R.A. & Shi Y. *Histone demethylation mediated by the nuclear amine oxidase homologue LSD1*. (2004). *Cell* ***119***, 941–953.
Sung J. S. & Demple B. *Roles of base excision repair subpathways in correcting oxidized abasic sites in DNA*. (2006). *FEBS J.* ***273***, 1620-

1629.

Tsukada Y., Fang J., Erdjument-Bromage H., Warren M. E., Borchers C. H., Tempst P. & Zhang Y. *Histone demethylation by a family of JmjC domain-containing proteins.* (2006). *Nature* ***439***, 811–816.

Tsujimoto Y., Finger L.R., Yunis J., Nowell P.C., Croce C.M. *Cloning of the chromosome breakpoint of neoplastic B cells with the t(14;18) chromosome translocation*.(1984). *Science* ***226*** (4678): 1097–99.

Zuchegna C., Aceto F., Bertoni A., Romano A., Perillo B., Laccetti P., Gottesman M.E., Avvedimento E.V., Porcellini A. *Mechanism of retinoic acid- induced transcription: histone code, DNA oxidation and formation of chromatin loops.* (2014). *Nucleic Acids Res.* ***42***, 11040-11055.

LIST OF PUBLICATIONS

This dissertation is based upon the following publications:

1. Morano A, Angrisano T, Russo G, Landi R, **Pezone A**, Bartollino S, Zuchegna C, Babbio F, Bonapace IM, Allen B, Muller MT, Chiariotti L, Gottesman ME, Porcellini A, Avvedimento EV. **"Targeted DNA methylation by homology-directed repair in mammalian cells. Transcription reshapes methylation on the repaired gene"**.
Nucleic Acids Res. 2014 Jan;42(2):804-21. doi: 10.1093/nar/gkt920. Epub 2013 Oct 16.
PMID: 24137009 [PubMed - indexed for MEDLINE] PMCID: PMC3902918

2. Svegliati S*, Marrone G*, **Pezone A***, Spadoni T, Grieco A, Moroncini G, Grieco D, Vinciguerra M, Agnese S, Jüngel A, Distler O, Musti AM, Gabrielli A, Avvedimento EV. "**Oxidative DNA damage induces the ATM-mediated transcriptional suppression of the Wnt inhibitor WIF-1 in systemic sclerosis and fibrosis**".
Sci Signal. 2014 Sep 2;7(341):ra84. doi: 10.1126/scisignal.2004592.

*= equal contribution

PMID: 25185156 [PubMed - in process]

Curriculum Vitae

Dr. Antonio Pezone
Via Carlo Pisacane, 2
81030 Parete (CE), Italy
(0039) 3204164075
antoniopezone@gmail.com

Date of Preparation: March 2, 2015

Personal Data

Name	Antonio Pezone
Date of Birth	April 21TH, 1984
Birthplace	Villaricca (CE)
Citizenship	Italy

Training

03/2012 – 02/2015	**Department of Molecular Medicine and Biotechnology,** University of Naples Federico II *PhD student in Molecular Pathology and Physiopathology, 27°cycle*	*Naples, Italy*
07/2013 – 09/2013	**Institute for Cancer Genetics, Irving Cancer Research Center**, Columbia University Medical Center. *Visiting researcher*	*New York, NY*
03/2008 – 02/2012	**Department of Molecular and Cellular Biology and Pathology** University of Naples Federico II *Internship*	*Naples, Italy*

Education

09/2008 – 09/2010	**Degree in Medical Biotechnology, University of Naples Federico II** *Score: summa cum laude (110/110 lode).*	*Naples, Italy*
09/2003 – 09/2008	**Degree in Biotechnological Sciences, University of Naples Federico II**	*Naples, Italy*

Honors

3/2012 – 3/2015	**Fellowship in the program " Excellence networks linking University --- Research Centers – Enterprises"** *POR Campania FSE 2007-2013*	*Naples, Italy*

Publications

09/2014	Svegliati S*, Marrone G*, **Pezone A***, Spadoni T, Grieco A, Moroncini G, Grieco D, Vinciguerra M, Agnese S, Jüngel A, Distler O, Musti AM, Gabrielli A, Avvedimento EV. **"Oxidative DNA damage induces the ATM-mediated transcriptional suppression of the Wnt inhibitor WIF-1 in systemic sclerosis and fibrosis."** **(* equally contributed)** Sci Signal. 2014 Sep 2;7(341):ra84. doi: 10.1126/scisignal.2004592.
05/2014	Di Francia R. , Catapano O. , **Pezone A**. , Lus G. , Berretta M. , Del Pup L. , Tommaselli P. A. , De Lucia D. **"Molecular diagnostics in the clinical practice – "Research Centre CETAC" Caserta (Italy) the 23/24 May 2014"** WCRJ 2014; 1 (2): e220
01/2014	Morano A, Angrisano T, Russo G, Landi R, **Pezone A**, Bartollino S, Zuchegna C, Babbio F, Bonapace IM, Allen B, Muller MT, Chiariotti L, Gottesman ME, Porcellini A, Avvedimento EV. **"Targeted DNA methylation by homology-directed repair in mammalian cells. Transcription reshapes methylation on the repaired gene"** . Nucleic Acids Res. 2014 Jan;42(2):804-21. doi: 10.1093/nar/gkt920. Epub 2013 Oct 16.

Abstract

9/2012	**A. Pezone**, R. Landi, G. Russo, A. Porcellini, V.E. Avvedimento. **"DNA oxidation, transcription and methylation: the same molecular machine with different facets".** *Conference: European Environmental Mutagen Society (EEMS).*	*Poland*
10/2012	**A. Pezone**, R. Landi, G. Russo, C. Zuchegna, A. Porcellini, V. E. Avvedimento. **"Local DNA oxidation and DNA methylation set chromatin loops and drive the transcription cycles induced by estrogen.** *Meeting: Joint National Ph.D. (poster presentation)*	*Rimini, Italy*

10/2012	R. Landi, **A. Pezone**, C. Zuchegna, G. Russo, A. Porcellini, V. E. Avvedimento. **"Methylation-BER cycles drive estrogen induced transcription".** *Meeting: Joint National Ph.D.*	*Rimini, Italy*
10/2012	G. Russo, C. Zuchegna, **A. Pezone**, R. Landi, A. Porcellini, V. E. Avvedimento. **"Targeted DNA methylation induced by homology-directed repair in mammalian cells".** *Meeting: Joint National Ph.D.*	*Rimini, Italy*
10/2012	C. Zuchegna, G. Russo, R. Landi, **A. Pezone**, V. E. Avvedimento, A. Porcellini. **"Mechanism of retinoic acid-induced transcription: epigenetic changes, DNA oxidation and chromatin loops".** *Meeting: Joint National Ph.D*	*Rimini, Italy*

804–821 *Nucleic Acids Research, 2014, Vol. 42, No. 2* *Published online 16 October 2013*
doi:10.1093/nar/gkt920

Targeted DNA methylation by homology-directed repair in mammalian cells. Transcription reshapes methylation on the repaired gene

Annalisa Morano[1,2], Tiziana Angrisano[1], Giusi Russo[1], Rosaria Landi[1], Antonio Pezone[1], Silvia Bartollino[3], Candida Zuchegna[4], Federica Babbio[5], Ian Marc Bonapace[5], Brittany Allen[6], Mark T. Muller[6], Lorenzo Chiariotti[1], Max E. Gottesman[7,*], Antonio Porcellini[4,*] and Enrico V. Avvedimento[1,*]

[1]Dipartimento di Medicina Molecolare e Biotecnologie mediche, Istituto di Endocrinologia ed Oncologia Sperimentale del C.N.R., Università Federico II, 80131 Napoli, Italy, [2]IRCCS CROB, Dipartimento di Oncologia Sperimentale, via Padre Pio, 1 85028 Rionero in Vulture, Italy, [3]Dipartimento di Medicina e di Scienze della Salute, Università del Molise, 86100 Campobasso, Itay, [4]Dipartimento di Biologia, Università Federico II, 80126 Napoli, Italy, [5]Dipartimento di Biologia Strutturale e Funzionale, Università dell'Insubria, Varese 21100, Italy, [6]Department of Molecular Biology and Microbiology and Biomolecular Science Center, University of Central Florida, 12722 Research Parkway, Orlando, FL 32826, USA and [7]Institute of Cancer Research, Departments of Microbiology and Biochemistry and Molecular Biophysics, Columbia University Medical Center, New York, NY 10032, USA

Received July 1, 2013; Revised August 30, 2013; Accepted September 19, 2013

ABSTRACT

We report that homology-directed repair of a DNA double-strand break within a single copy Green Fluorescent Protein (GFP) gene in HeLa cells alters the methylation pattern at the site of recombination. DNA methyl transferase (DNMT)1, DNMT3a and two proteins that regulate methylation, Np95 and GADD45A, are recruited to the site of repair and are responsible for selective methylation of the promoter-distal segment of the repaired DNA. The initial methylation pattern of the locus is modified in a transcription-dependent fashion during the 15–20 days following repair, at which time no further changes in the methylation pattern occur. The variation in DNA modification generates stable clones with wide ranges of GFP expression. Collectively, our data indicate that somatic DNA methylation follows homologous repair and is subjected to remodeling by local transcription in a discrete time window during and after the damage. We propose that DNA methylation of repaired genes represents a DNA damage code and is source of variation of gene expression.

INTRODUCTION

DNA methylation is a feature of higher eukaryote genomes. It is thought to help organize large segments of noncoding DNA in heterochromatin and to contribute to genome stability (1). DNA methylation is critical during development in plants and mammals. In somatic cells, patterns of methylated CpGs are transmitted to daughter cells with high fidelity (2,3). Aberrant methylation, both hyper- and hypo-methylation, has been found in cancer cells (4).

There are two patterns of DNA methylation: (i) Stable methylation, which is the basis of imprinting, is inherited in a sex-specific fashion and is invariant among individuals and cell types. Loss or modification of stable methylation results in significant phenotypic and genetic alterations. (ii) Unstable or metastable methylation, which is variable among individuals and cell types.

Despite numerous analyses of the methylation profiles of single chromosomes, the regulation of DNA methylation is largely unknown. Somatic DNA methylation is associated with gene silencing and heterochromatin formation and is neither sequence- nor cell-specific.

We are investigating the nature of somatic DNA methylation and its link to gene silencing during neoplastic progression (5,6). Since formation of DNA double-strand

*To whom correspondence should be addressed. Tel: +39081679047; Fax: +39081679233; Email: antonio.porcellini@unina.it
Correspondence may also be addressed to Max E. Gottesman. Tel: +1 212 305 6900; Fax: +1 212 305 1741; Email: meg8@columbia.edu
Correspondence may also be addressed to Enrico V. Avvedimento. Tel: +390817463251; Fax: +390817463308; Email: avvedim@unina.it

breaks (DSBs) and activation of DNA damage checkpoints may precede genomic instability (7) and DNA methylation and gene instability appear to be linked in cancer (8), we speculated that DNA methylation was associated with DNA damage and repair.

We previously reported that homology-directed repair (HDR) modifies the methylation pattern of the repaired DNA (9). This was demonstrated using a system pioneered by Jasin (10,11), in which recombination between partial duplications of a chromosomal Green Fluorescent Protein (GFP) gene is initiated by a specific DSB in one copy. The unique DSB is generated by cleavage with the meganuclease I-SceI, which does not cleave the eukaryotic genome. The DSB is repeatedly formed and repaired, until the *I-SceI* site is lost by homologous or nonhomologous repair or depletion of I-SceI enzyme. Recombination products can be detected by direct analysis of the DNA flanking the DSB or by the appearance of functional GFP (9).

Two cell types are generated after recombination: clones expressing high levels of GFP and clones expressing low levels of GFP, referred to as H and L clones, respectively. Relative to the parental gene, the repaired GFP is hypomethylated in H clones and hypermethylated in L clones. The altered methylation pattern is largely restricted to a segment just 3′ to the DSB. Hypermethylation of this tract significantly reduces transcription, although it is 2000 bp distant from the strong cytomegalovirus (CMV) promoter that drives GFP expression (9,12). The ratio between L and H clones is ~1–2 or 1–4, depending on the insertion site of the GFP reporter. These experiments were performed in mouse embryonic (ES) or human cancer (Hela) cells. HDR-induced methylation was dependent on DNA methyl transferase I (DNMT1). Furthermore, methylation induced by HDR was independent of the methylation status of the converting template (9). These data, taken together, argue for a cause–effect relationship between DNA damage-repair and DNA methylation.

The link between DNA damage, repair and de novo methylation has been confirmed by other studies (13–15). We also note that genome wide surveys show that imprinted sites are historical recombination hot spots, reinforcing our conclusion and that of other workers, that DNA methylation marks the site of DNA recombination (16,17).

We report here that methylation induced by HDR is influenced by recruitment of Np95 and GADD45a to the DSB and that DNMT3a is also active at the DSB. We also show that methylation is reduced by transcription of the repaired region.

MATERIALS AND METHODS

Cell culture, transfections and plasmids

HeLa cells lines were cultured at 37°C in 5% CO_2 in RPMI medium supplemented with 10% fetal bovine serum (Invitrogen), 1% penicillin-streptomycin, and 2 mM glutamine.

HeLa-pDRGFP cells were obtained by transfection of HeLa cells with the pDRGFP plasmid. Briefly: 5×10^6 cells were seeded in a 100 mm dish and transfected with lipofectamine as recommended by the manufacturer (Invitrogen) with 2 μg of linearized pDRGFP plasmid and selected in the presence of puromycin (2 micrograms/ml). Four clones were isolated and expanded, the remaining clones were screened for single pDRGFP insertion by quantitative Polymerase Chain Reaction (qPCR) [supporting information in (9)] and pooled (~200 clones with a pDRGFP copy number ranging from 0.8 to 1,2 copies/genome). Clone 3 is the same clone 3 described in (9); clone 4 is a subclone of the clone 2 assayed also by Southern Blot (9). 10^6 puromycin-resistant cells were transient transfected by electroporation with 2.5 μg of plasmid DNAs and/or small interfering RNA (siRNA) (200 nM) as indicated in the Figures. After transfection cells were seeded at 3×10^5 cells per 60 mm dish, 24 h post-transfection, cells were treated and harvested as described in figures. Pools of clones were generated in three independent transfections and frozen in aliquots. Transient transfections with I-SceI were carried at different times of culture after the primary transfection. Transfection efficiency was measured by assaying β-galactosidase activity of an included pSVβGal vector (Promega). Normalization by fluorescent-activated cell sorter (FACS) was performed using antibodies to β-gal or pCMV-DsRed-Express (Clontech). pEGFP (Clontech) was used as GFP control vector. The structure of the pDRGFP and other plasmids are described in the supplementary data (Suplementary Methods and Supplementary Figure S12).

Nucleic acid extraction and quantitative reverse Transcription Polymerase Chain Reaction, qPCR and PCR

Total RNA was extracted using Triazol (Gibco/Invitrogen). Genomic DNA extraction was performed as described in (9). cDNA was synthesized in a 20 μl reaction volume containing 2 μg of total RNA, four units of Omniscript Reverse Transcriptase (Qiagen), and 1 μl random hexamer (20 ng/μl) (Invitrogen). mRNA was reverse-transcribed for 1 h at 37°C, and the reaction was heat inactivated for 10 min at 70°C. The products were stored at −20°C until use. Amplifications were performed in 20 μl reaction mixture containing 2 μl of synthesized cDNA product or 0.1 μg of genomic DNA, 2 μl of 10X PCR buffer, 1.5 mM $MgCl_2$, 0.5 mM dNTP, 1.25 unit of Taq polymerase (Roche), and 0.2 μM of each primer on a TC3000G thermocycler (Bibby Scientific Italia). The number of cycles was selected and validated by running several control reactions and determining the linear range of the reaction. 15 μl of the PCR products were applied to a 1.2% agarose gel and visualized by ethidium bromide staining. Densitometric analysis was performed using a phosphoimager. Each point was determined in at least three independent reactions. Quantitative reverse Transcription Polymerase Chain Reaction (qRT-PCR) and qPCR were performed three times in six replicates on a 7500 Real Time-PCR on DNA template (RT-PCR) System (Applied Biosystems) using the SYBR Green-detection system (FS Universal SYBR Green MasterRox/Roche Applied Science). The complete list of oligonucleotides is reported in Supplementary Table S1.

FACS analysis

HeLa-DRGFP cells were harvested and resuspended in 500 µl of phosphate buffered saline (PBS) at density of 10^6 cells/ml. Cell viability was assessed by propidium iodide (PI) staining. Cytofluorimetric analysis was performed on a 9600 Cyan System (Dako Cytometrix) or FACScan Flow Cytometer (Becton Dickinson, Franklin Lakes, NJ, USA). PI positive cells were excluded from the analysis by gating the PI-negative cells on a FSC-Linear versus FL2H-Log plot. GFP^+ cells were identified by using a gate (R1 in Supplementary Figure S3A) on a FL1H-Log versus Fl2H-Log plot after sample compensation for FL1 versus FL2 channels. L and H cells were identified on FL1H Histogram of the R1-gated cells with two range-gate, as shown in Figure 1. The same gate was used for all cytofluorimetric determinations.

Cell cycle analysis was carried out by FACS: 1×10^6 cells were resuspended in 1 ml of PBS and fixed 10 ml of ice-cold 70% ethanol. Afther 3 h, the cells were washed and stained for 30 min at room temperature with 0.1% Triton X100, 0.2 mg/ml Dnase-free RnaseA, 20 µg/ml PI. Fluorescence was evalued by FACS and analyzed by ModFit LT 2.0 (Verity Software House, Topsham, ME, USA).

Population comparison was performed using the Population Comparison module of the FlowJo software (Tree Star, Inc., Ashland, OR). Difference in fluorescence intensity (mean) was determined using the matched pairs Student's *t* test.

Bisulfite DNA preparation, PCR and sequence analysis

Sodium bisulfite analysis was carried out on purified genomic DNA and on 'chromatinized' DNA. The full list of the buffer formulation is reported in the Supplementary Methods (Buffers Formulation). Chromatinized DNA was obtained as follows: 10^7 cells were fixed at 4°C temperature with 1% formaldehyde for 3 min. The reaction was stopped with glycine to a final concentration of 125 mM. Nuclei were isolated and permeabilized by incubating cells for 20 min in Buffer A, 20 min in Buffer B and then resuspended in Buffer C (see Buffers Formulation in Supplementary Methods). Nuclei or purified genomic DNA was heat denaturated (96°C for 10 min) incubated in a fresh solution containing 5 M sodium bisulfite and 20 mM hydroquinone and incubated at 37°C for 18 h. The cross-link was reversed, and proteins were digested with proteinase K (50 µg/ml at 55°C for 2 h, and then at 65°C overnight). DNA was purified using a Wizard genomic purification kit (Promega), and then disulphonated by incubation for 15 min with NaOH to a final concentration of 0.3 M, neutralized with ammonium acetate to a final concentration of 3 M, and purified by ethanol precipitation. DNA was amplified by PCR using primers, listed in the Supplementary Table S1, using Taq polymerase, which is able to copy deoxyuridine, cloned in TOPO TA vector (Invitrogen), and sequenced with the M13 reverse primers.

Chromatin Immunoprecipitation

Cells were transfected and/or treated as indicated in the legends of the figures. The cells ($\sim 1 \times 10^6$) were fixed by adding formaldehyde directly in the culture medium to a final concentration of 1% for 10 min at room temperature and washed twice using ice cold PBS containing 1× protease inhibitor cocktail (Roche Applied Science) and 1 mM Phenylmethylsulfonyl Fluoride (PMSF). Fixed cells were harvested and the pellet was resuspended in 200 µl of sodium dodecyl sulphate Lysis Buffer (ChIP Assay Kit/ Upstate). After 10 min incubation on ice, the lysates were sonicated to shear DNA to 300-and 1000-bp fragments. Sonicated samples were centrifuged and supernatants duluted 10-fold in the ChIP Dilution Buffer (ChIP Assay Kit/Upstate). An aliquot (1/50) of sheared chromatin was further treated with proteinase K, phenol/chloroform extracted and precipitated to determine DNA concentration and shearing efficiency (input DNA). The chromatin immunoprecipitation (ChIP) reaction was set up according to the manufacturer's instructions. Briefly, the sheared chromatin was precleard for 2 h with 20 µl of protein-A or protein-G agarose (Upstate) and 2 µg of nonimmune IgG (New England Biolabs). Precleared chromatin was divided in two aliquots and incubated at 4°C for 16 h with 20 µl of protein-A/G agarose and 2 µg of the specific antibody (Np95, generated and characterizated by IM Bonapace; RNA Pol II from Upstate cat. # 05-623; DNMT1, DNMT3a and DNMT3b from Abcam, cat. # ab-13537, ab-2850 and ab-2851, respectively) and nonimmune IgG respectively. Agarose beads were washed with wash buffers according to the manufacturer's instructions and immunoprecipitated DNA was recovered and subjected to qPCR using the primers indicated in the legend of the specific figures and in Supplementary Table S1.

Methylated DNA immunoprecipitation

Cells were transfected and/or treated as indicated in the legend of the figures. The cells ($\sim 5 \times 10^6$) were harvested and genomic DNA extracted as described above. Ten micrograms of total genomic DNA were digested in 200 µl for 16 h with restriction endonuclease mix containing 30 U each of Eco RI, Bam HI, Hind III, XbaI, Sal I (Roche Applied Science), phenol/chloroform extracted, ethanol precipitated and resuspended in 50 µl of Tris-HCl/EDTA buffer (10 mM Tris-HCl pH 7.8, 1 mM EDTA) (TE) buffer. An aliquot (1/10) of digested DNA was used as input to determine the DNA concentration and digestion efficiency. Methylated DNA immunoprecipitation (MEDIP) was performed essentially as described (18) except that 2 µg of antibody specific for 5mC (Abcam cat. # ab-124936) were used to precipitate methylated DNA from 5 µg of total genomic DNA. H19 and UE2B were used to control in each experiment the efficiency of 5mC immunoprecipitation; the CpG island located to 5′ end of human beta-actin was used as undamaged transcribed DNA gene control.

Statistical analysis

All data are presented as mean ± standard deviation in at least three experiments in triplicate ($n \geq 9$). Statistical significance between groups was determined using Student's *t* test (matched pairs test or unmatched test were used as indicated in figure legends). Hierarchical clustering

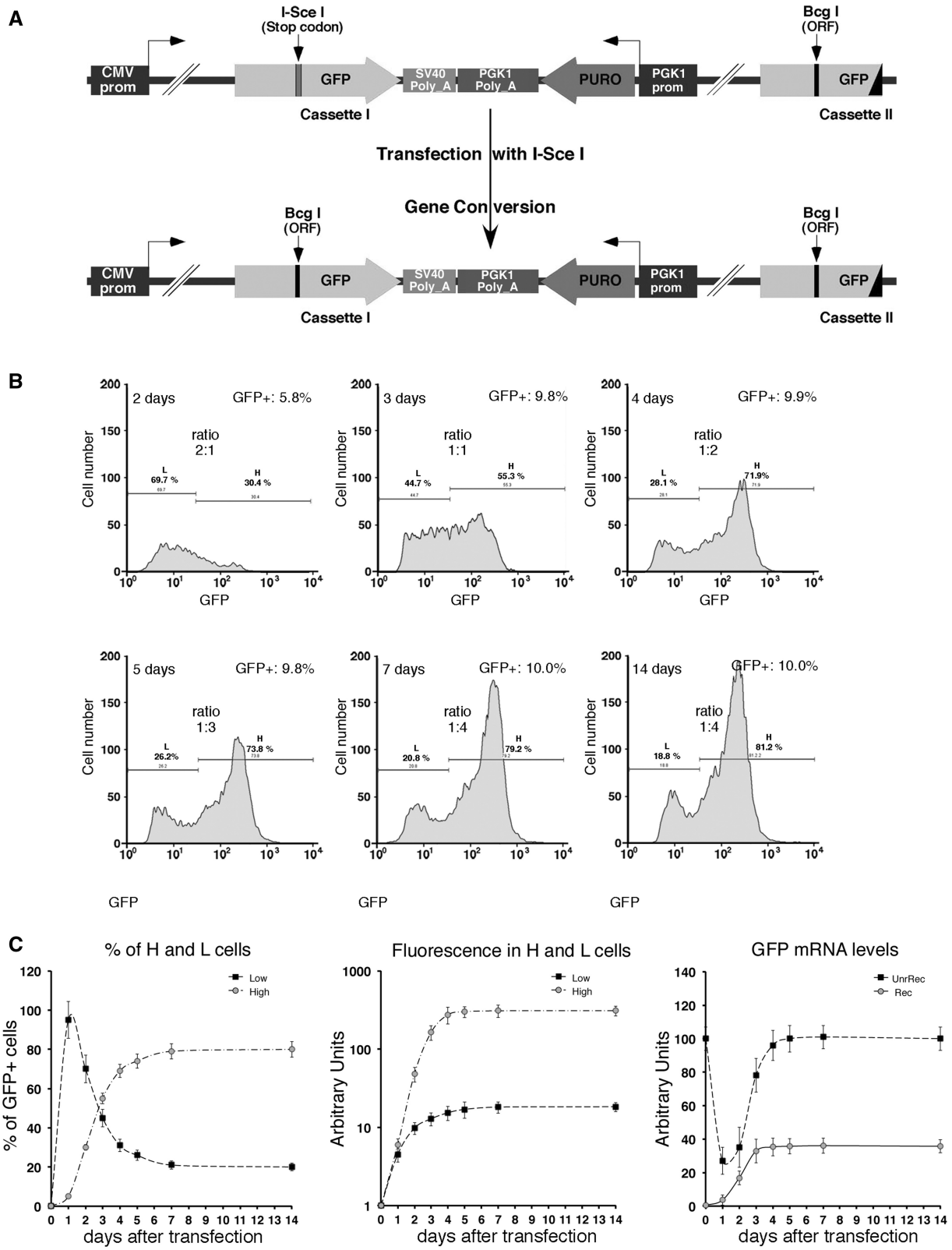

Figure 1. HDR generates high and low GFP-expressing clones. (**A**) Structure of the integrated tester DRGFP plasmid before and after repair. The structure of the plasmid (10,11) has been verified by sequence analysis. The boxes and arrows with different grayscales represent the structural elements of the integrated nonrecombinant (upper) and recombinant (lower) plasmid. The conversion of the *I-SceI* to *BcgI* restriction site marks the gene conversion event driven by the copy of GFP gene located at the 3′ end of DRGFP (cassette II). (**B**) Generation and accumulation of high (H) and low (L) expressor cells following homologous repair. Kinetics of L and H clones accumulation. Cells containing a single copy of DRGFP (clones 3 and 4, see 'Materials and Methods' section) or pool of clones (shown here), characterized as described in 'Materials and Methods' section, were transfected with I-SceI and subjected to FACS analysis at the times indicated. GFP positive (GFP^+) cells were identified by the R1 gate

(continued)

(Ward's criterion) analysis was performed using the *JMP Statistical Discovery*^{TM} software by SAS, Statistical Analysis Software. Sequence analysis and alignments were performed using MegAlign software (a module of the Lasergene Software Suite for sequence analysis by DNASTAR) for MacOSX.

RESULTS

Repair-induced methylation at the 3′ end of a DSB

The system we use to study DNA methylation induced by damage and repair relies on a single-copy integrated plasmid (DRGFP), which contains two inactive versions of GFP. Introduction of a DSB in one copy of the gene (cassette I) by expressing the nuclease I-SceI, generates a functional GFP only in cells in which the second copy of GFP (cassette II) provides the template to repair the DSB (10,11) (Figure 1A). Homologous repair both in pools and single clones generates cells expressing low (L clones) or high levels (H clones) of GFP. These clones can be tracked by FACS analysis, using bivariate plots and gating strategies.

The integrated DRGFP undergoes several cycles of cutting and resealing until the *I-SceI* site is lost by nonhomologous end joining (NHEJ) or homology-dependent repair (HDR). We defined the time window of HDR by monitoring the appearance of recombinant GFP DNA in the population of cells transiently expressing I-SceI. We also measured the levels of I-SceI protein in transfected cells to estimate the period of enzymatic cleavage. Supplementary Figure S1A shows that the levels of recombinant GFP reached a plateau 3 days after transfection with I-SceI. The enzyme accumulated between 12 and 24 h and progressively disappeared 48–72 h after transfection. The estimated half-life of I-SceI protein was between 12 and 24 h (Supplementary Figure S1B).

Having established that the bulk of repair activity occurred in 3 days, we monitored the appearance and stabilization of L and H clones during and after HDR (9). Figure 1B shows the accumulation of L and H cells after exposure to I-SceI in a pool of HeLa clones as well as in single insertion clones carrying DRGFP inserts at different loci (see the legend of Figure 1B). Three days after I-SceI transfection, when HDR was almost complete, L and H cells accumulated in a 1:1 ratio (Figure 1B). We have used time-lapse microscopy to monitor GFP appearance during 30 h after I-SceI induction. The Supplementary Movie shows the I and II/III cycles (relative to GFP expression) during repair and the appearance of H and L cells from single repair events. In the I cycle, H and L cells are generated; in the II/III cycle (H-H and L-L), the phenotypes are stably propagated. Eventually, the ratio L/H cells changes as a function of time, until day 7 when the L to H ratio stabilized at 1:4 (Figure 1B). No further change was detected after numerous subsequent passages, and no new GFP clones appeared (data not shown). Note that this shift to high GFP-expressing cells occured after DSB repair, and therefore represents an inherited epigenetic process.

The drift toward H clones is detailed in Figure 1C. This figure also shows the levels of GFP mRNA as a function of time after transfection with the I-SceI plasmid. The changes in GFP mRNA concentrations correlate well with the fluorescence measurements that reflect GFP expression. We wondered if the time-dependent epigenetic changes were related to transcription of the GFP gene. This notion was tested by adding α-amanitin during repair and following the appearance of L and H clones. α-Amanitin inhibits translocation of elongating RNA polymerase II (Pol II) and increases the concentration of the polymerase on transcribed genes (19).

The pool of DRGFP clones, as well as one clone (Cl4), was transfected with I-SceI, and after 24 h, exposed to α-amanitin for 24 h. Five days later (day 7 after I-SceI transfection), GFP expression was analyzed by cytofluorimetry. Exposure of the cells to the drug did not influence the rate of recombination (Supplementary Figure S2A). As expected, it significantly enriched GFP chromatin with Pol II molecules (Supplementary Figure S2B). Figure 2A and Supplementary Figure S3 show that α-amanitin treatment of pooled cells (or clone 4) shifted the populations of L and H classes in opposite directions (see arrows AMA): L and H cells displayed on the average, lower or higher fluorescence intensity, respectively. Exposure to α-amanitin 6 days before transfection with I-SceI or 6 days after did not affect the distribution of L and H clones (Figure 2A and Supplementary Figure S3A). Statistical analysis of the data of 28 independent experiments in which α-amanitin was added during recombination to pools or single clones indicates that the results are reproducible (Figure 2B and Supplementary Figure S3B). Quantitative analysis of GFP fluorescence in H and L cells exposed to α-amanitin during repair reveals that the fraction of L cells increased and that the GFP expression in these cells was markedly reduced. Conversely, the H cell fraction decreased, but the intensity of the fluorescent signal in these cells was enhanced (Figure 2B). We hypothesize that transient stalling of Pol II induced by α-amanitin during repair, increased GFP methylation, yielding higher numbers of L clones and reducing the fraction of H clones.

We therefore asked if α-amanitin altered the DNA methylation profile of the repaired GFP gene. Clones 3 and 4 were

Figure 1. Continued
(see Supplementary Figure S3A) on a bivariate plot (FL1H versus FL2H) after I-SceI transfection. A representative experiment, displaying the L and H cells is shown. Each panel shows (i) the days after I-SceI transfection; (ii) total GFP positive cells (%); (iii) the range gates used to discriminate H and L cells; (iv) the ratio L/H, which reached a plateau 7–14 days after I-SceI transfection. Panel (**C**): the number (percent of total GFP^+ cells, left) and the fluorescence intensity (mean, center) of H and L cells derived from clones (not shown here) or pool of clones, based on at least five independent experiments. After 7–14 days, the L/H ratio and the intensity of L and H peaks stabilize. CMV–EGFP transfected cells, as control lines, display a single fluorescence peak (9). The right panel shows the relative levels, normalized to 18 S RNA, of nonrecombinant (UnRec) and recombinant (Rec) GFP mRNA after I-SceI transfection (see 'Materials and Methods' section).

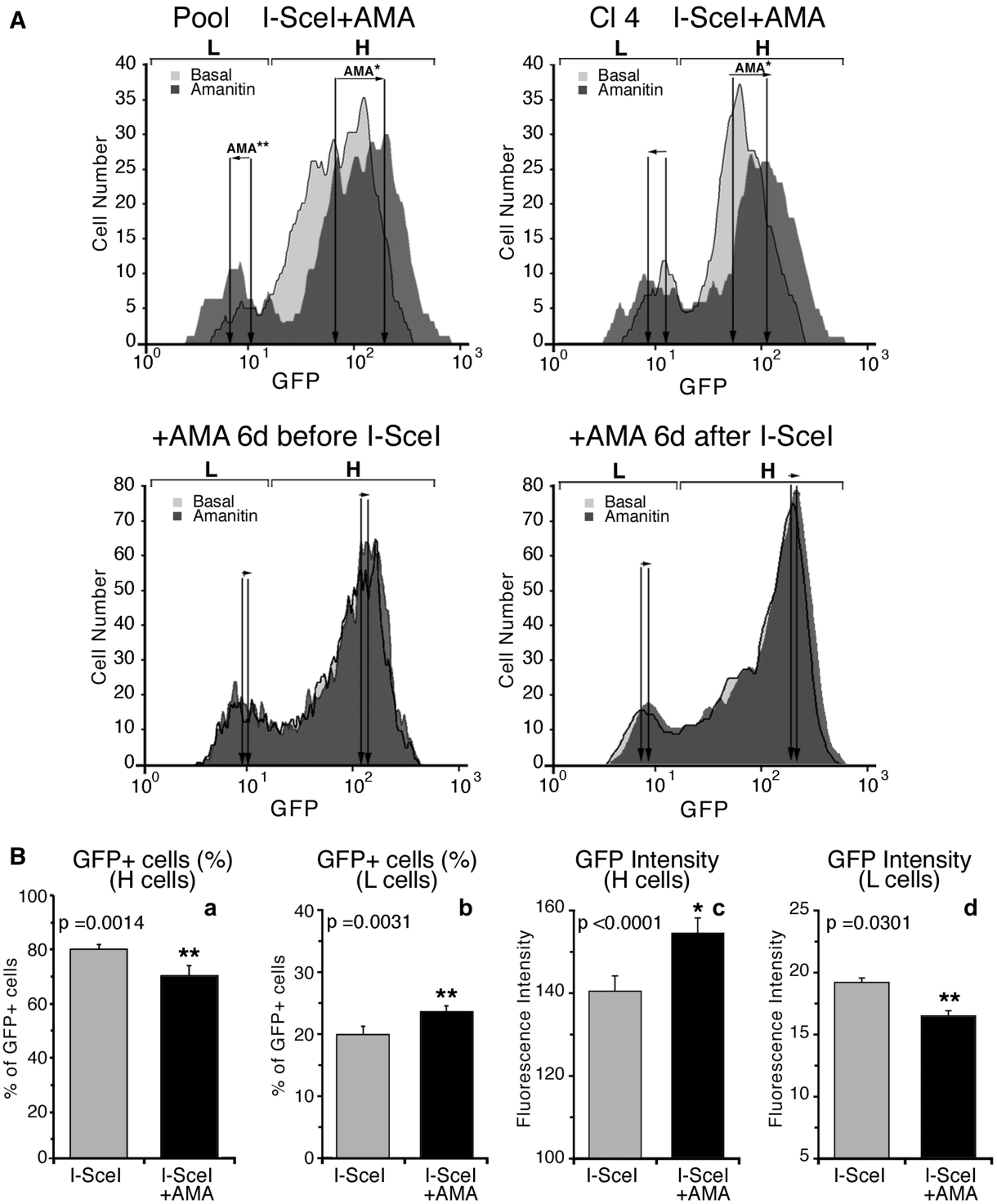

Figure 2. Synchronization of transcription by α-amanitin during repair amplifies and consolidates L and H clones. (**A**) Cytofluorimetric analysis. Cells were exposed to α-amanitin before, during or after I-SceI transfection as indicated on the top of each panel. A pool of HeLa DRGFP cells or a clone carrying a single insert were transfected with I-SceI expression vector, and 24 h later, an aliquot was exposed for 24 h to 2.5 μM α-amanitin. The cells were washed and cultured in normal medium for 5 days, when FACS analysis was carried out (day 7 after I-SceI transfection). The fluorescence plots of GFP positive cells (overlay of the histograms of RI gates, see Supplementary Figure S3) are shown. L and H represent the range gates to identify high and low expressors, respectively. The arrows, indicated by AMA, represent the shift of the mean fluorescence after α-amanitin treatment. Differences between treatments were tested for statistical significance using Student's matched pairs *t* test: $*P < 0.001$, $**P < 0.05$. Under these conditions, α-amanitin did not affect cell survival or growth rate. Five days after 24-h 2.5-μM α-amanitin treatment, transcription of several housekeeping genes was similar to untreated controls. The changes of GFP expression following the short treatment(s) with the drug during repair (24 h after I-SceI transfection) were stable for up 3 months in culture. (**B**) Statistical analysis derived from 28 independent experiments, in which DRGFP cells were exposed to α-amanitin during repair as indicated above. The panel shows the statistical significance of the means (± SD). Differences between treatments were tested for statistical significance using Student's matched pairs *t* test: $*P < 0.001$, $**P < 0.05$.

treated with α-amanitin (6–24 h), sorted 5 days later into H and L clones and analyzed by MEDIP assay with specific antibodies against 5-methylcytidine (anti-5mC) with primers indicated in Figure 3A. Figure 3B shows that anti-5mC recognizes the region 3′ to the *I-SceI* site in the repaired GFP. As predicted, the frequency of 5mC was higher in L clones than in H clones. Consistent with GFP expression profiles shown in Figure 2, α-amanitin increased the levels of 5mC in the L clones. The changes in 5mC levels were specific to the recombinant GFP segment, since the methylation status of the β-actin 5′ CpG island did not change (data not shown). Additionally, the methylation status of H19-DMR (Differentially Methylated Region), or UBE2B gene (NC_000005.9), used as positive and negative controls of MEDIP immunoprecipitation, did not change after α-amanitin (Figure 3C). To visualize directly the methylation status of the repaired segment of GFP in α-amanitin-exposed cells, we performed bisulfite analysis of the GFP gene in treated cells (Supplementary Figure S4). The repaired GFP gene just 3′ to the DSB was selectively hypermethylated or hypomethylated in L and H cells, respectively. Treatment with α-amanitin for 6 or 24 h accentuated these alterations of methylation: L clones became more methylated and H clones less methylated than untreated cells. Longer exposure (48 h) to α-amanitin did not significantly alter the methylation pattern seen at 6 or 24 h (see the legend of Supplementary Figure S4).

To explore further the local chromatin changes induced by methylation and the effects of α-amanitin on this process, we analyzed sites on the GFP gene that were protected from bisulfite conversion. Briefly, chromatin of L and H cells was fixed with formaldehyde, heat denatured and exposed to bisulfite. By probing GFP DNA, we can detect specific DNA segments protected, most likely by bound proteins, that block C to T conversion by bisulfite or by structures preventing single-strand formation (Figure 3D). The protected segment of GFP corresponds to the region containing the methylated sites at the 3′ end of *I-SceI*, as shown in Supplementary Figure S4. We found no protected areas in the H clones, whether or not they were treated with α-amanitin. Exposure to α-amanitin enhanced protection against bisulfite in most of the regions found to have increased DNA methylation after repair (compare Figures 3 and Supplementary Figure S4).

We propose that stalled RNA polymerase during repair favors the recruitment of enzymes that methylate the repaired DNA, consolidating the methylation of L clones. This event occurs only during repair because stalling Pol II before or after DSB repair does not modify GFP methylation and expression.

Transcription modifies methylation of the repaired gene

The α-amanitin experiments suggest that the transcription machinery plays a major role in repair-induced methylation. We chose to inhibit transcription in a different fashion, by treating the cells with actinomycin-D (Act-D) for 6 h after repair. In contrast to α-amanitin, Act-D depletes RNA polymerase II from chromatin (20).

We were unable to use Act-D during repair, owing to inhibition of HR by the drug (data not shown). After repair, 6 h exposure to Act-D did not alter DNA replication or HDR (legend of Figure 4). Under these conditions, the treatment with Act-D prevented the accumulation of H clones at 2 and 4 days later (5 and 7 days after I-SceI transfection), although the number of GFP^+ cells was similar in all samples (~9.5%), and the recombination frequency was unaltered (Figure 4B and data not shown). This finding suggests that the conversion of L to H cells after repair requires transcription (Figure 4B). To confirm the effectiveness of Act-D and to explore the mechanism of inhibition of H cell formation, we measured mRNA levels of several genes. Specifically, we analyzed the accumulation of stable and unstable RNAs: (i) recombinant (Rec) and nonrecombinant (UnRec) GFP; (ii) c-Myc (0.5–1 h half-life) (21); (iii) β-actin (8–12 h half-life; data not shown) (22); and (iv) 18 S ribosomal RNA, 10 and 96 h after Act-D treatment. Figure 4C (left panel) shows the expected reduction in c-Myc, unRec and Rec mRNA levels 10 h after Act-D treatment (day 3). Rec mRNA was more stable than unRec mRNA. However, 96 h after Act-D exposure (day 7), UnRec and c-Myc mRNA concentrations returned to control values, whereas Rec mRNA levels remained lower than controls (Figure 4C, middle panel). Depletion of Pol II after Act-D exposure and the restauration of GFP-bound Pol II were confirmed by ChIP analysis of Un-Rec and Rec DNA (Figure 4C, rightmost panel). After 12–15 days, the increase of methylation and the inhibition of transcription of the GFP gene, induced by Act-D, progressively disappeared. Resumption of transcription promoted methylation loss during this period and accumulation of H cells from L cells (Figure 4B). These changes occurred only 2–3 weeks after the repair and were specific to repaired DNA because Act-D did not change the expression of undamaged GFP and, when administered 27–30 days after repair, did not modify GFP methylation (Supplementary Figure S5). We note that the time window of Act-D responsiveness (3–15 days after exposure to I-SceI) corresponds to the time required to stabilize the L/H cell ratio (Figure 1), suggesting that stabilization of the DNA–chromatin domain induced by HDR occurs in this interval. Collectively, these data indicate that after repair transcription converts a fraction of L to H cells by favoring loss of methylation.

Hierarchical clustering analysis of GFP methylation in repaired clones links discrete methylation states to gene expression variation

The data shown above indicate that the original methylation profiles induced by HDR are remodeled in a transcription-dependent fashion during the first 15 days after repair. The pattern eventually stabilizes, locking the epigenetic status of the repaired DNA in each cell (see Supplementary Movie, cycles I and II/III). By using hierarchical clustering analysis of bisulfite-treated GFP molecules before and after HDR, we were able to track and identify the original methylation profiles (epialleles) induced by HDR and modified during transcription. We

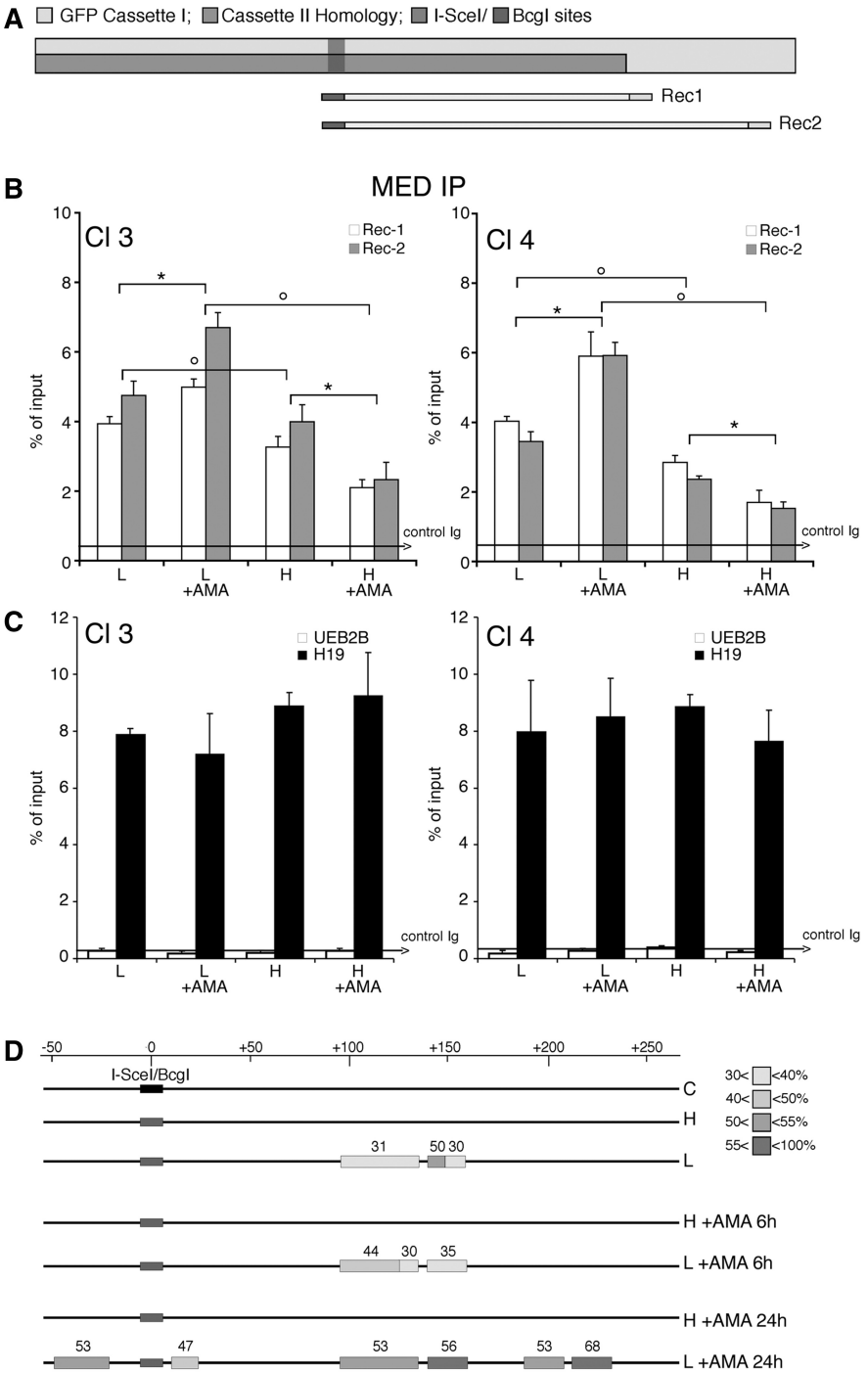

Figure 3. DNA methylation and chromatin modifications of the DSB region in cells exposed to α-amanitin during repair. (**A**) Location of Bcg, Rec1 and Rec2 primers, which recognize selectively recombinant GFP. Cassette I and II refer to Figure 1. (**B**) MEDIP with anti-5mC antibodies of recombinant GFP gene. Clones 3 and 4 were treated with α-amanitin for 24 h as described in Figure 2 and sorted 5 days after I-SceI as described in 'Materials and Methods' section. Content of 5mC is higher in L cells compared with H cells, α-amanitin also increases the levels of 5mC in L cells and lowers them in H cells. The results are similar for both amplicons (REC1 and REC2). All data derive from three independent experiments performed in triplicate (mean ± SD; n = 9). Differences between treatments were tested for statistical significance using Student's matched pairs *t* test: $*P < 0.01$ as compared with the each control (α-amanitin treated versus untreated cells). Differences between cells (H versus L) were tested for statistical significance using Student's *t* test: $P < 0.01$. (**C**) MEDIP analysis of the methylated H19 DMR (differentially methylated region) and the hypomethylated UBE2B genes in clone 3 and 4, treated with α-amanitin, as indicated in B. Longer exposure (48 h) to α-amanitin did not significantly alter the methylation pattern seen at 6 or 24 h assayed by bisulfite analysis (Supplementary Figure S4). (**D**) Bisulfite protection of GFP chromatin in L and H cells. Clone 4 cells were treated with α-amanitin for 6 or 24 h after transfection and sorted as indicated in 'Materials and Methods' section. Chromatin was purified as described in 'Materials and Methods' section, denatured and treated with sodium bisulfite. DNA was extracted, amplified, cloned in TOPO TA vector and sequenced. The amplified segment corresponds to the Rec1 region and primers were designed for the bisulfite-converted (+) strand. The boxes represent stretches of nonconverted dCs present in the GFP sequence. At least 15 independent GFP molecules were analyzed for each treatment, including cells not exposed to I-SceI (C). The numbers with the grayscale boxes represent the percentage of the molecules protected from bisulfite conversion in the regions indicated by boxes. The scale shows the coordinates of the GFP sequence relative to the DSB (indicated as 0 or *I-SceI*/*BcgI* site).

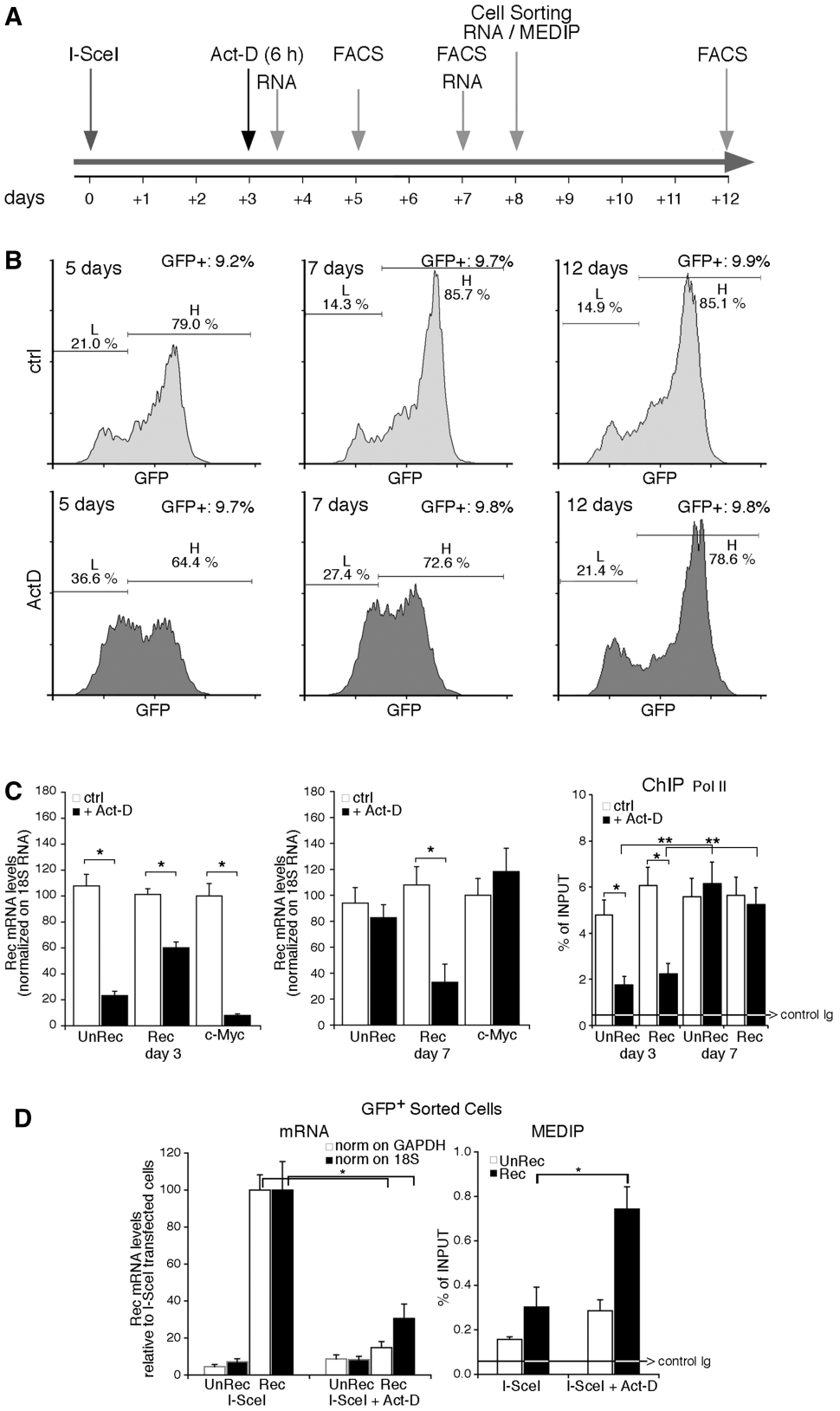

Figure 4. Transient exposure of recombinant cells to Actinomycin D increases methylation of the repaired gene. Panel (**A**) shows the time frame of actinomycin-D (Act-D) treatment and the assays performed. The cells were transfected with I-SceI expression vector and 72 h later were exposed to Act-D (0.05 mg/ml) for 6 h. Act-D did not induce detectable modifications of the cell cycle by PI analysis (G1 50 ± 2 versus 50 ± 3; S 23 ± 1.2 versus 25 ± 1.6; G2/M 27 ± 1.6 versus 25 ± 1.8 in the presence of 6 h Act-D); the cells were viable and RNA polymerase II was depleted from the chromatin. Five days after the treatment, the recombination frequency, measured by qPCR and GFP transcription were comparable between treated and untreated cells. The arrows indicate the time window of RNA analysis, MEDIP, FACS and cell sorting, relative to I-SceI transfection.

(continued)

also were able to link the methylation states of epialleles to GFP expression levels, since the bisulfite analysis was carried out on fluorescent-sorted cells. Clones expressing intermediate levels of GFP (L2 and H2) contain a set of GFP epialleles originating from a common GFP precursor segregating in the L fraction. This epiallele precursor in L cells generates many similar epialleles as a result of losing methyl groups (Supplementary Figures S6 and S7). These sites are shared by L2 and H2 clones and are located in 2 symmetric domains downstream of the DSB, spanning the length of a nucleosome (150 bp) (Supplementary Figure S7C and D). The sites are demethylated by 5-AzadC and methylated by Act-D treatments (Supplementary Figure S7C and D or data not shown). These data definitely link gene expression to specific methylation states and explain the stochastic expression of GFP after HDR (see Supplementary Movie).

DNMT3a is transiently recruited to repaired GFP and stimulates DNA methylation

We previously reported that the hypermethylated L cell population was not found in a mutant lacking the maintenance DNMT1. In contrast, hypermethylation of the repaired gene was seen in both DNMT3a$^{-/-}$ and DNMT3b$^{-/-}$ mutants (9). However, loss of methylation induced by repair in stable DNMT1 mutant cells may be the indirect consequence of lack of propagation of methylation in daughter cells by DNMT1. Since large stretches of DNA are resynthesized during homologous recombination and are devoid of methylation marks, it is possible that de novo DNMTs such as DNMT3a and 3 b have a role during or early after repair, and that DNMT1 may propagate the methylation marks set by DNMT3a and/or 3 b during replication. To investigate this possibility, we analyzed the recruitment of DNMT3a and 3 b to the I-SceI–cleaved chromatin. Figure 5A and B show that both DNMT3a and DNMT3b were recruited to the *I-SceI* site 24 h after the onset of DSB formation and rapidly disappeared (48 h). We then selectively silenced DNMT3a and 3 b during repair and analyzed the distribution of L and H cells. Figure 5C shows that the yield of L cells was significantly reduced and both the number and GFP fluorescence intensity of H cells increased when DNMT3a expression was silenced. In contrast, depletion of DNMT3b did not alter the ratio of L and H cells (Figure 5C). Expression of wild-type enzyme in DNMT3a-silenced cells prevented the loss of L cells. The changes of GFP expression levels were caused by DNA methylation, since the rescue of L cells by DNMT3a was prevented by treatment with 5azadC (Figure 5C).

In conclusion, we propose that DNMT3a helps the formation of hypermethylated clones and DNMT1 propagates these methylation patterns through at least several generations. This finding reinforces the notion that maintenance and de novo methyl transferases cooperate (23).

Np95 is recruited to repaired GFP and stimulates DNA methylation

We reported that DNMT1 was required for hypermethylation of repaired GFP. We now ask if proteins that modify DNMT1 activity influence DNA methylation at the repaired DSB. We probed for Np95 (also known as UHRF1 or ICBP90), a protein that binds to DNMT1, DNMT3a, DNMT3b and PCNA and stimulates methylation of hemi-methylated DNA (24–26). ChIP analysis of GFP chromatin from clones 3 and 4 showed that Np95 preferentially accumulated on the repaired chromatin of the L clones. Treatment with α-amanitin during repair significantly amplified or decreased Np95 recruitment to GFP chromatin in L or H cells, respectively (Figure 6A). Note that the binding of Np95 to H19, UEB2B or β-actin CpG island chromatin was unaffected by α-amanitin (Figure 6B and data not shown). Thus, the association of Np95 with the DSB of GFP DNA appears to be linked to hypermethylation and reduced GFP expression in the L cell population.

To test whether Np95 recruitment to recombinant chromatin was relevant to repair-induced methylation, we selectively silenced Np95 expression during recombination.

Figure 4. Continued
(**B**) FACS analysis (a representative of five independent experiments) was performed as described in Figure 1 at 5, 7 and 12 days after I-SceI transfection (2, 4 and 9 days after Act-D treatment, respectively). Panel (**C**) Left. GFP mRNA accumulation assayed by qPCR after Act-D treatment (3 days after I-SceI transfection and 10 h after Act-D, or 7 days after I-SceI and 96 h after Act-D) normalized to 18 S RNA. Recombinant (Rec) and nonrecombinant (UnRec) mRNA levels are expressed as percent of untreated levels ± SD because the absolute mRNA levels cannot be compared because of the differences of the efficiency of the primers. The same results were obtained normalizing GFP RNA to GAPDH mRNA. Differences between treatments were tested for statistical significance using Student's matched pairs *t* test: $*P < 0.01$ as compared with the each untreated control. Right. RNA polymerase II recruitment on recombinant and nonrecombinant GFP chromatin after Act-D treatment. ChIP with anti-Pol II large fragment antibodies of chromatin extracted from Act-D–treated cells 3 days after I-SceI transfection (10 h after Act-D) or 7 days after I-SceI (96 h after Act-D). $*P < 0.01$ compared with the each untreated control; $**P < 0.01$, 3 days compared to 7 days time point; the average of immunoprecipitated DNA with a control Ig is reported on the bar graph. (**D**) GFP mRNA levels and MEDIP assay at day 8 on sorted GFP$^+$ cells. Left: Recombinant (Rec) and nonrecombinant (UnRec) primers were used to quantify GFP mRNA by qPCR and to measure the contamination of nonrecombinant GFP negative cells. The values were normalized to GAPDH (white columns) or 18 S (black columns) RNAs. Rec mRNA levels are shown as percent of the levels found in control cells (I-SceI transfected/Act-D untreated cells); UnRec mRNA levels are expressed as percent of control (untransfected DRGFP cells) (mean of three experiments in triplicate ± SD). $*P < 0.01$ as compared with untreated control. Right: 5mC content was carried out on sorted GFP$^+$ cells (H and L) as indicated in panel A. Specifically, we analyzed the 5mC content of (i) a segment of the GFP promoter, 1 kb upstream the DSB (oligo b and c, see Supplementary Table S1); (ii) the region 3′ to the DSB, which was methylated by HDR; and (iii) H19 and UE2B genes, as controls of hypermethylated and undermethylated genes, respectively, and to monitor the efficiency of MEDIP assays. The 5mC levels in these regions, except the segment 3′ to the DSB, were not modified by 6 h Act-D treatment (data not shown). 5mC levels are expressed as percentage of input (mean ± SD of three experiments in triplicate); the average of immunoprecipitated DNA with a control Ig is reported on the bar graph. $*P < 0.01$ as compared with the each untreated control. Act-D, administered 27, 30 and 35 days after I-SceI for 6 h, transiently inhibited transcription, but did not change GFP gene methylation.

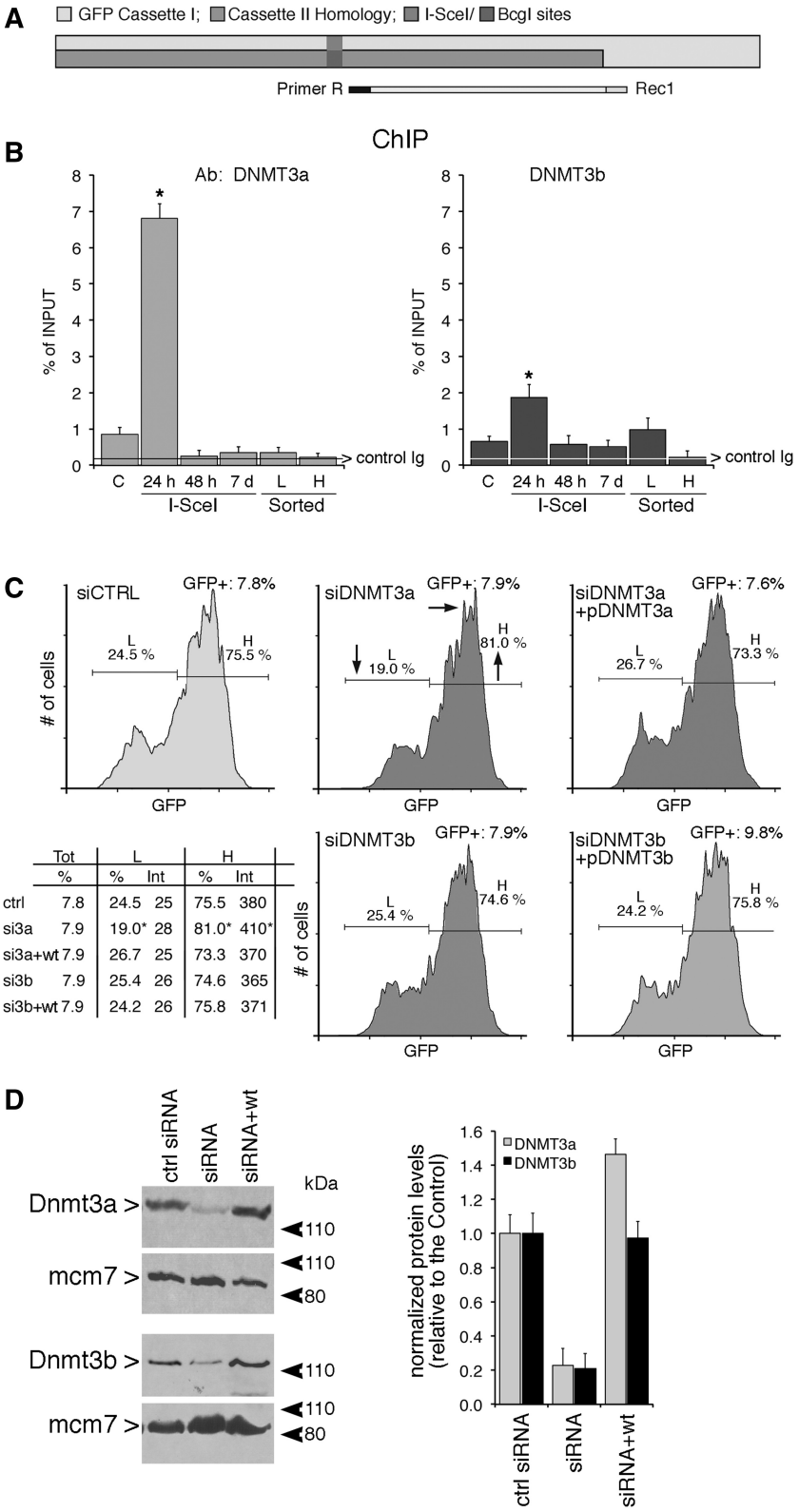

Figure 5. DNMT3a and 3b are recruited to the DSB early during repair, but only DNMT3a is necessary for generation of L cells (**A** and **B**) Recruitment of DNMT3a, DNMT3b to the *I-SceI* chromatin. Cells were transfected with I-SceI and 24 h, 48 h or 7 days later, were fixed, collected, chromatin-extracted and subjected to ChIP analysis with specific anti-DNMT3a and DNMT3b antibodies. The specific primers used to amplify the GFP cassette I are indicated in (A). Data represent the fraction of immunoprecipitated DNA relative to the input chromatin-DNA present in the reactions (% of input; mean ± SD; $n \geq 9$); the average of immunoprecipitated DNA with a control Ig is reported on each bar graph. $^*P < 0.01$, paired *t* test. (**C**) Silencing the expression of DNMT3a reduces L cells. Cells were electroporated with the siRNA targeting DNMT3a and DNMT3b (see 'Materials and Methods' section and protocol S1) and analyzed 7 days later, when L and H cells were clearly separated. On the bottom left

(continued)

We measured GFP expression, DNA methylation in the repaired segment and the frequency of recombination. Figures 6C (left panel) and Supplementary Figure S8 show that silencing of Np95 expression significantly enhanced fluorescence intensity in both the L and H cell fractions. Np95 depletion did not affect recombination frequency (Supplementary Figure S8A) but induced loss of methylation at the 3′ end of the repaired GFP gene (Figure 6C, right panel). Under the same conditions, Np95 depletion did not modify the methylation status of β-actin CpG island, or stably methylated gene, H19 (DMR) (see the legend of Figure 6C). Overexpression of mouse wild-type Np95 reversed the effects of the silencing and reduced GFP expression (Supplementary Figure S8B).

Np95 interacts with several proteins involved in chromatin remodeling, specifically those that set repressive marks on histones, such as SUV39 and EZH2 (27,28). Indeed, 24 h after DSB induction, the I-SceI chromatin shows an accumulation of histone repressive (H3K9 m2-m3) and a reduction of positive H3K4 (m2 and m3) marks, respectively [(13) and data not shown]. To test if SUV39 and EZH2, which also interact with DNMT1 (27,28), play a role on DNA methylation induced by damage and repair, we silenced their expression during repair and determined the distribution of L and H cells. Knockdown of these proteins did not significantly modify the intensity of the GFP signal in either L or H cells (Supplementary Figure S9A). Although a modest decrease in GFP expression in SUV39-depleted cells was caused by inhibition of recombination (Supplementary Figure S9C), the levels of GFP methylation were not modified in cells in which SUV39 and EZH2 were silenced (Supplementary Figure S9D).

GADD45a binds DSB and inhibits de novo methylation induced by HDR

To identify a DNMT1 partner that inhibits DNA methylation during repair and generates H cells, we monitored GADD45a (G45a) expression and localization after DSB formation. We recently found that GADD45A binds hemi-methylated DNA, inhibits DNMT1 *in vitro* and *in vivo* and reduces the fraction of L cells (18), suggesting that GADD45A promotes loss of methylation on the repaired DNA (29,30).

We first measured GADD45A mRNA levels in cells exposed to I-SceI or to the DNA-damaging agent, etoposide. GADD45A mRNA was induced by I-SceI and decreased to pre-induced levels 48 h after I-SceI transfection (Supplementary Figure S10). We next asked if GADD45A accumulated on DNA during HDR. ChIP analysis shows that GADD45A was recruited to GFP chromatin 48 h after I-SceI expression, confirming a previous observation (18). Recruitment of GADD45A, as well as DNMT1 and Pol II, was further stimulated by α-amanitin (Figure 7A and B). Note that DNMT1 accumulation on MGMT and p16, genes normally methylated in Hela cells, was not stimulated by I-SceI expression or α-amanitin (Figure 7A, lower panel).

We next tested the effects of silencing GADD45A on recombinant DNA methylation. Figure 6C shows that GADD45A knockdown (Supplementary Figure S11) inhibited GFP expression at 2 and 4 days after the damage. However, although reproducible, this effect, which was not noted previously (18), was transient; it was statistically significant at day 2 and progressively disappeared at 4 and 7 days after I-SceI expression (Figure 7C and Supplementary Figure S11 panels A and C). The consequences on GFP expression of GADD45A silencing at 2 days were reversed by co-transfection with a mouse GADD45A expression vector (Figure 7D, left panel). GADD45A silencing did not alter the frequency of recombination (Supplementary Figure S11D) but methylation of GFP was significantly stimulated, as shown by MEDIP analysis (Figure 7D, right panel). Under the same conditions, GADD45A depletion did not modify the methylation status of β-actin CpG island or of stably methylated genes, such as H19 (DMR) (Figure 7D).

The transient effects of GADD45A depletion on GFP expression may be dependent on the transient rise of the protein (18) and mRNA levels during damage and repair (Supplementary Figure S10). To address this issue, we overexpressed the wild-type protein, 2 days after I-SceI transfection, when endogenous protein levels were already low. Under these conditions, Ga45a stimulated GFP fluorescence intensity in H cells for longer periods (4–7 days after I-SceI), but at day 10 from the DSB, the effects disappeared (Supplementary Figure S11E and data not shown). However, 1 month after the DSB or in cells expressing CMV-EGFP, forced expression or induction of GADD45A by etoposide did not modify GFP levels (see the legend of Figure 7).

Taken together, these results indicate that Np95 and GADD45A favor the generation of L and H cells, respectively, during HDR.

DISCUSSION

Mechanism of DNA repair-induced methylation

The results shown here argue for a link between HDR and DNA methylation at the site of a repaired DSB. Without DNA damage and repair, the expression of GFP is stable and uniform (Supplementary Figure S6, the red peak). DSB formation within GFP and repair by HDR

Figure 5. Continued
panel, statistical analysis derived from three independent experiments is shown. $*P < 0.01$, paired *t*-test comparing GFP intensity, Chi Square ($\chi 2$) comparing the percentage of L/H cells. The horizontal and vertical arrows in the central inset indicate the shift in fluorescence intensity and in the distribution of L and H cells, respectively. Treatment with 5azadC (10 μM for 2 days, 48 h after I-SceI transfection) rescued completely the loss of L cells (intensity and % GFP^+ cells) induced by DNMT3a overexpression in siDNMT3a-silenced cells (data not shown). (**D**) Western blot analysis of DNMT3a and 3 b in silenced cells. Total cell extracts were prepared 48 h after electroporation and analyzed by immunoblot with the specific antibodies indicated. On the right is shown quantitative analysis derived from three immunoblots (mean ± SD).

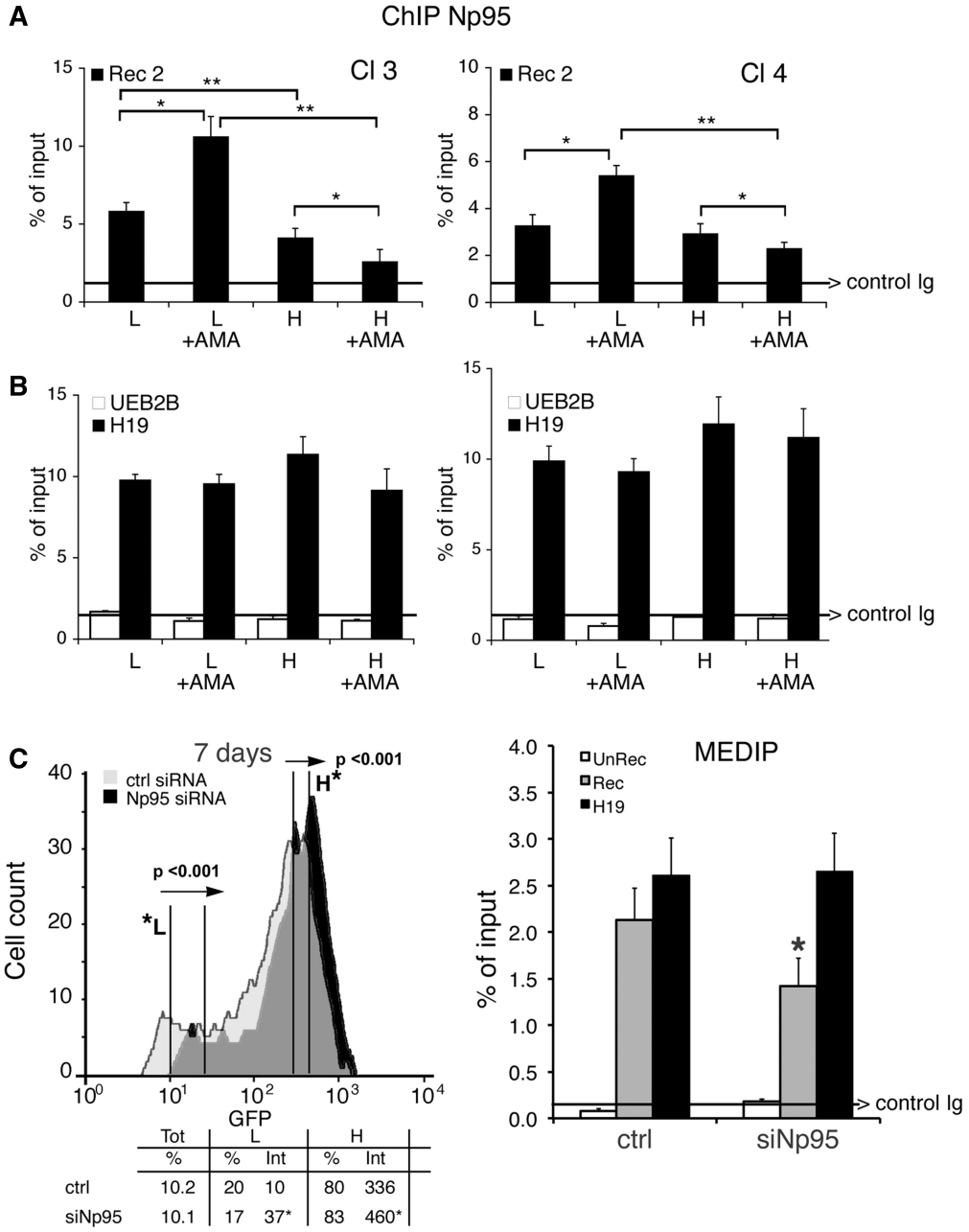

Figure 6. Np95 (UHRF1) is recruited to repaired GFP and stimulates DNA methylation. (**A**) ChIP with anti-Np95 antibodies of sorted cells exposed to α-amanitin during repair. Clones 3 and 4 were transfected with I-SceI and treated with α-amanitin for 24 h as described in Figure 2. The cells were sorted 5 days after I-SceI transfection and chromatin was collected from formaldehyde-fixed cells and subjected to ChIP analysis with specific antibodies to Np95. Primers Bcg and Rec2 were used to amplify recombinant GFP DNA. The data derive from three independent experiments performed in triplicate (mean ± SD; n = 9). Differences between treatments were tested for statistical significance using Student's matched pair *t*-test: $*P < 0.01$ as compared with the each control (α-amanitin treated versus untreated cells). Differences between cells (H versus L) were tested for statistical significance using Student's *t*-test: $**P < 0.01$. (**B**) ChIP analysis of Np95 on H19 DMR and UBE2B genes. qPCR was carried out with specific H19 DMR and UBE2B primers on the same samples indicated above. The fraction of immunoprecipitated DNA by control Ig is reported on each bar graph. (**C**) DRGFP cells (pool of clones; clone 3 and 4 are not shown here) were transiently transfected with a mixture of siRNAs targeting specifically human NP95 or control scrambled siRNA (ctrl) and the mouse I-SceI expression vector (see 'Materials and Methods' section). Six days later, the cells were subjected to FACS analysis and MEDIP. The left panel shows a representative experiment: arrows indicate the shift in silenced cells of GFP fluorescence intensity. The columns below the fluorescence plot show (i) the number of GFP^+ cells (Tot, expressed as percentage of cells); (ii) the mean fluorescence intensity (Int.); and (iii) Percentage of L and H cells on GFP^+ cells. Mean fluorescence intensity at day 7 increased from 10 to 37 in L cells and from 336 to 460 in H cells (left panel). FACS analysis was performed in triplicate in at least three experiments. Differences between treatments were tested for statistical significance using Student's matched pair *t*-test: $*P < 0.001$ as compared with the each control (siRNA-treated versus untreated cells). Samples expressing NP95 wild-type and control cells were treated with 1 μM 5azadC for 1 day (48 h after I-SceI), and the differences in fluorescence intensity was used to quantify methylation-dependent changes of GFP expression. The panel on the right shows the results of MEDIP immunoprecipitation with anti-5mC antibodies in control and siRNA-treated samples. Np95 depletion by siRNA did not modify the methylation status of stably methylated genes, such as H19 (DMR) and β-actin CpG island. $*P < 0.01$ for *t*-value (matched pair test) relative to the cells treated with control scramble siRNA (CTRL). Data are expressed as mean ± SD, $n = 9$; the average of immunoprecipitated DNA with a control Ig is reported on the bar graph.

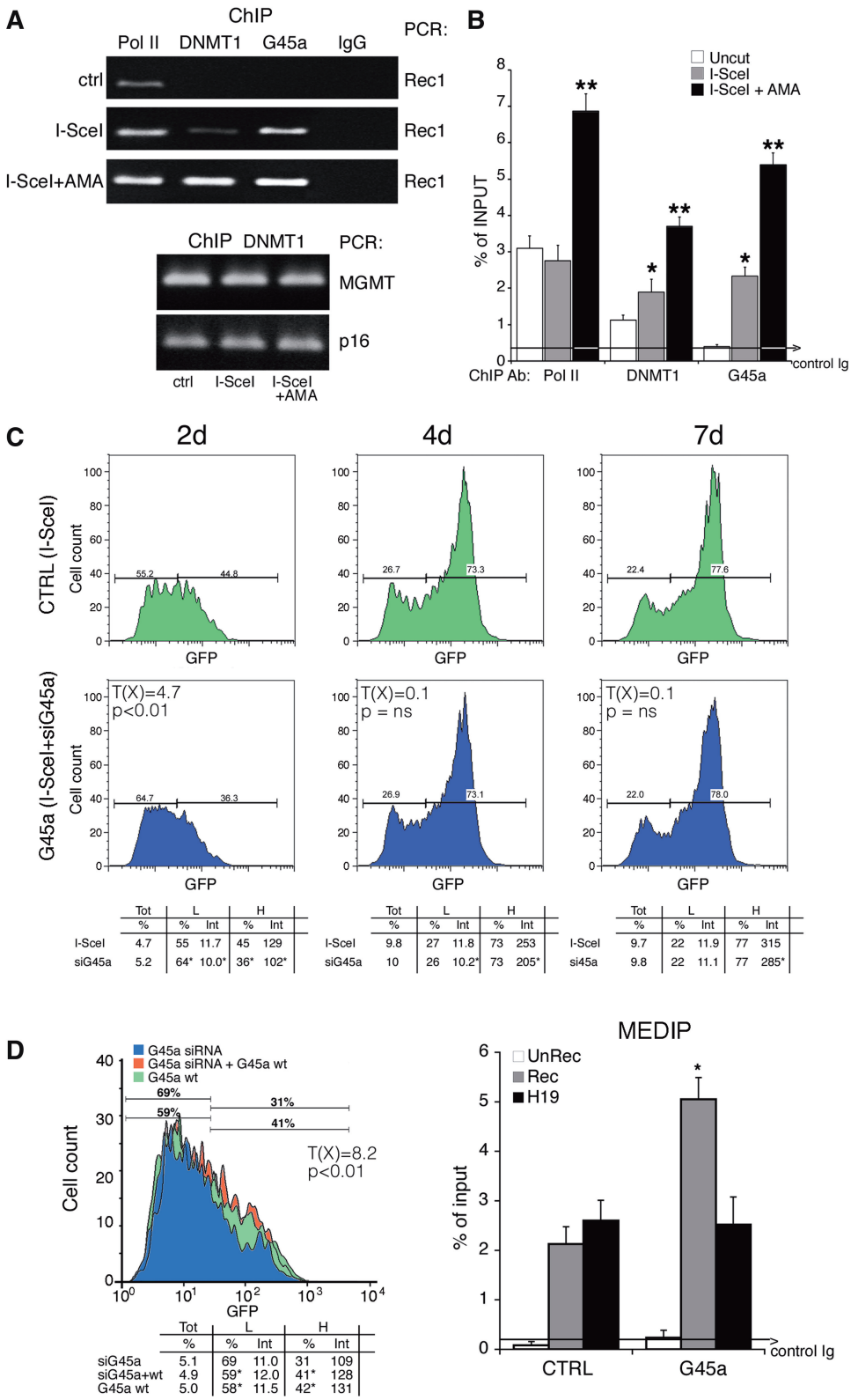

Figure 7. GADD45 is recruited to the DSB and transiently inhibits de novo methylation induced by HDR. (**A**) ChIP analysis with anti-GADD45A, DNMT1 and RNA polymerase II large fragment antibodies in HeLa cells, transfected (36 h) with I-SceI. Twelve hours after transfection, an aliquot of cells was treated for 24 h with α-amanitin and processed as described in 'Materials and Methods' section. Bcg and Rec1 primers were used for semiquantitative PCR. Two methylated genes, MGM and p16, were used as controls for DNMT1 ChIP. Control IgG represents an average of nonimmune immunoglobulins used in ChIP. (**B**) Quantitative analysis by qPCR of at least three ChIP experiments in triplicate ($n \geq 9$). Differences between treatments were tested for statistical significance using Student's matched pairs *t*-test: $*P < 0.01$ as compared with uncleaved control; $**P < 0.01$ compared with I-SceI. The average of immunoprecipitated DNA with a nonimmune Ig is reported on the bar graph. (**C**) DRGFP cells (pool of clones) were transiently transfected with siRNA pools targeting specifically GADD45A or control scrambled siRNA (ctrl) and

(continued)

significantly alter the methylation pattern of GFP in two steps. We propose that some actors at this phase are DNMT1/3 a, Np95 and GADD45A, which transiently maintain the processed DSB 3′ segment hemi-methylated, until replication generates methylated and hypomethylated daughter molecules. Figure 8 shows a simplified scheme describing the main events during and after DSB repair: (i) DNMT1 and DNMT3a are recruited to the DSB with Ga45a and NP95. DNMT3a is recruited in the first 24 h after damage and transiently cooperates with DNMT1 to methylate repaired DNA. At 48 h, Np95 and Ga45a amplify or limit transiently, respectively, DNMT1 activity on the hemi-methylated DNA, until replication duplicates the methylated and unmethylated DNA strands. This is better shown in the video presented in the Supplementary Movie, in which time lapse microscopy offers a unique snapshot into homologous repair. The appareance of the GFP signal in I-SceI synchronized cells can be monitored in the first and second cycle after recombination, relative to the GFP signal, generated by HDR. In the first cycle, H and L cells are formed from the same cell (square in the Supplementary Movie); in subsequent cycles, H and L cells stably propagate in culture the H or L phenotype (circle in the Supplementary Movie); (ii) After repair, transcription resumes at day 2–3 after DSB and progressively modifies local methylation profiles until the local domains of the *I-SceI* chromatin (loop A in H cells and loop C in L cells) are stabilize. We believe that this strand-selection mechanism accounts for the ∼1:1 L/H ratio early after repair (Figures. 1 and 4). In fact, GADD45A exerts its action early during repair (2–4 days), when the L/H ratio is close to 1 and before significant remodeling of methylation occurs (Figures 1, 4 and 7). Stalled RNA Pol II by α-amanitin during repair may facilitate targeting DNMT1/3 a complex to the 3′ end (−) transcribed strand, thus promoting hyper-methylation of the 300 bp repaired DNA segment that lies 3′ to the DSB relative to transcription orientation (Figure 3D and Supplementary Figure S4). The 3′ end (+) strand, free from transcription proteins, probably is more prone to invade and find the homologous region to direct the annealing, the synthesis and ultimately the repair of the DSB (Synthesis Directed Strand Annealing, SDSA) (31). This mechanism may account for the relatively high efficient HDR in our system.

Remodeling of methylation by transcription after repair

The second step of methylation induced by HDR begins ∼48 h after formation of the DSB. At this point, repair is terminated, but chromatin and DNA continue to undergo epigenetic changes (9,13). H cells progressively increase and are similar in terms of methylation profile to a subpopulation of L cells (L2 in Supplementary Figure S6). Accumulation of these L2/H cells is favored by continuous transcription of GFP because transient inhibition of transcription after repair shifts the L/H ratio and favors accumulation of methylated clones (L2 in Figure 4D). We obtained essentially the same results shown in Figure 4 by transiently blocking transcription after repair with a dominant negative cdk9-expression vector, which inhibits phosphorylation of elongating RNA polymerase II (G.R., unpublished observations). However, 27, 30 and 35 days after DNA damage, inhibition of transcription by exposure to Act-D or expression of the dominant negative cdk9 did not alter methylation or expression of GFP (Supplementary Figure S5). These data indicate that inhibition of transcription per se does not trigger de novo methylation (33–35) and suggest that transcription may favor active demethylation. In fact, depletion of base excision repair (BER) enzymes (OGG1; APE1) or TDG increased methylation of repaired GFP similarly to Act-D treatment (data not shown), in agreement with the notion that transcription is associated with DNA methylation-demethylation (32,36) and DNA oxidation cycles (37). We note that the different effects of α-amanitin and Act-D are related to the ability of these drugs to increase (α-amanitin, Supplementary Figure S2B) or deplete (Figure 4D) RNA polymerase II from chromatin: (i) Stalled pol II during repair increases targeting and recruitment of DNMT1-Np95 on the DSB and favors accumulation of L clones; (ii) depletion or loss of pol II by slow resolution of Act-D/DNA inhibit transcription and active demethylation.

We suggest that transcription of damaged-repaired DNA is associated with stochastic replacement of methylated C by BER or nucleotide excision repair

Figure 7. Continued
the I-SceI expression vector (see 'Materials and Methods' section). After 2, 4 and 7 days, the cells were subjected to FACS analysis as described in Figure 1. FACS analysis was performed in triplicate in at least three experiments. Differences in GFP expression between control and GADD45A-silenced cells were tested for statistical significance using the Chi Square test, T(X) (Population Comparison module of the FlowJo software from Tree Star). Differences of L and H (percentage and intensity) were tested for statistical significance using Student's t test: $^*P < 0.01$ (see Supplementary Figure S10). $\chi 2$ value (4.7), 2 days after I-SceI (control and GADD45A-silenced cells) ($P < 0.01$); at day 4 and 7, $\chi 2$ value was not discriminant as day 2, although differences in fluorescence intensity of L an H cells between the control and GADD45A-silenced cells were significant ($P < 0.02$). All samples were treated with 1 μM 5azadC for 1 day (48 h after I-SceI) to quantify methylation-dependent changes. (**D**) Left panel. Forced expression of GADD45A increases GFP expression. Cells were exposed to siRNA targeting the 3′ UTR human GADD45A alone or in combination with vector expressing GADD45A. GFP fluorescence and Rec mRNA were analyzed 4 days later. The levels of specific GADD45A mRNA, the frequency of recombination in GADD45A-depleted cells and the statistical analysis of GFP expression are shown in Supplementary Figure S8. Differences between populations (control and GADD45A-silenced cells) were tested for statistical significance using the Chi Square test (Population Comparison module of the FlowJo software). Cells expressing CMV-EGFP–treated with etoposide or transfected with Ga45a expressing vector did not change GFP expression. Right panel. 5mC content of recombinant GFP in cells silenced for GADD45A. Four days after transfection, the cells were subjected to MEDIP assay. GADD45A depletion by siRNA did not modify the methylation status of stably methylated genes, such as H19 (DMR) and β-actin CpG island. $^*P < 0.01$ for t value (matched pair test) relative to cells treated with control scramble siRNA (CTRL). All the samples in independent experiments were treated with 1 μM 5azadC for 1 day (48 h after I-SceI) to quantify methylation-dependent changes. The average of immunoprecipitated DNA with a control Ig is reported.

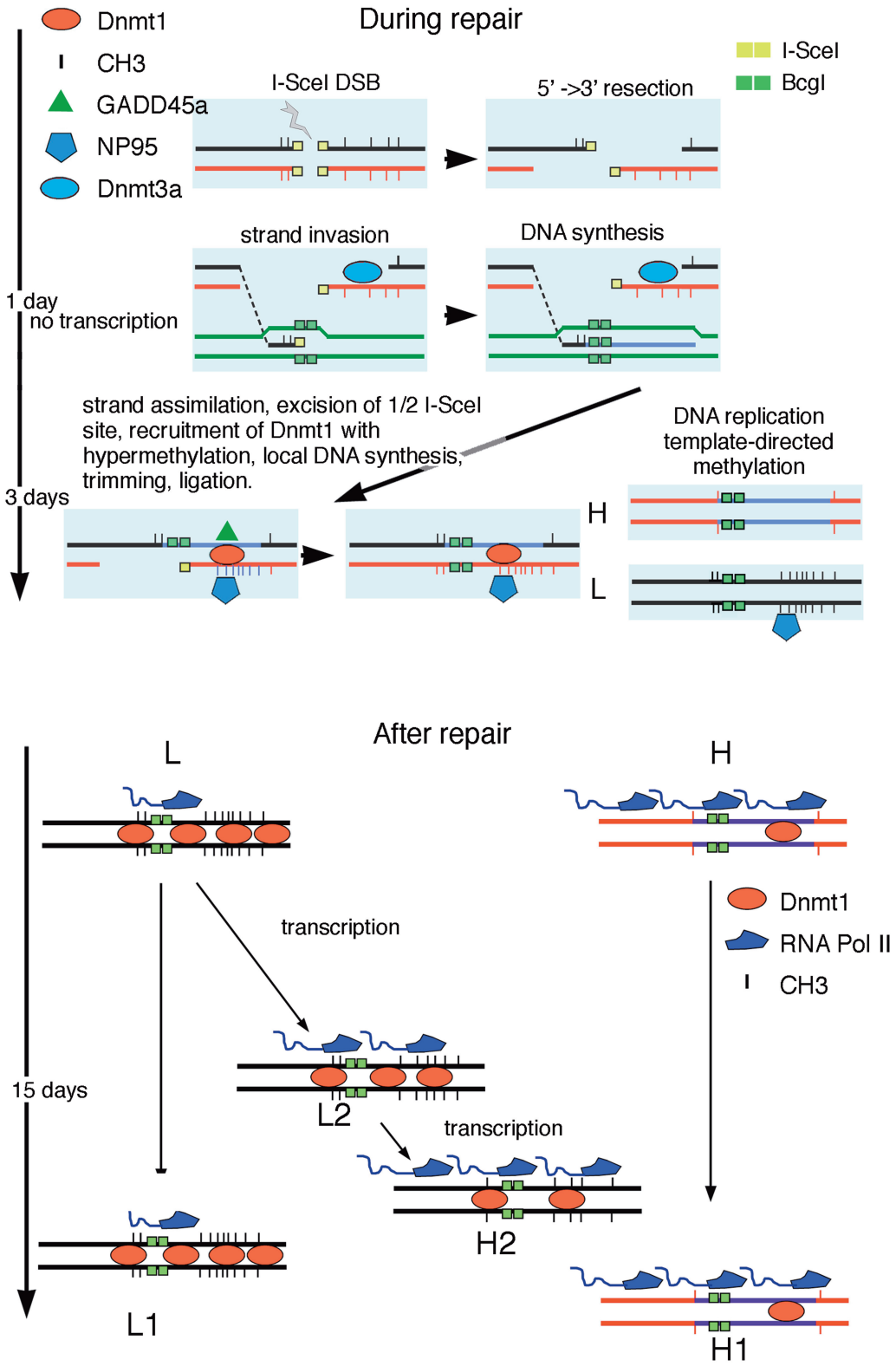

Figure 8. Targeted methylation during and after homologous repair. The cartoon represents a schematic model illustrating the events during and after repair. The DSB undergoes 5′ –> 3′ end resection and one of the 3′ free single strand end invades the DNA of the GFP cassette II. The half *I-SceI* site is removed (flap removal) and new DNA is synthesized. Eventually, the invading strand returns to the original configuration and directs the synthesis of new DNA at the *BcgI* site corresponding to the DSB, according to the SDSA model (Synthesis Directed Strand Annealing) (31). We propose that the asymmetric distribution of methylated CpGs in repaired GFP is caused by selective invasion of the (+) strand. The (−) strand, blocked by stalled RNA Pol II (DNMT1 and 3a), becomes a preferential target of DNMT1-Np95. The hemi-methylated DNA is replicated and generates H and L cells. After repair, transcription resumes and RNA Pol II-DNMT1 is associated with methylation/demethylation cycles (32) that in 15 days may remove some methyl groups in a subpopulation of L cells, leading to the conversion of L2 to H 2 cells.

(NER) followed by repair synthesis (38,39). The events in this phase are distinct from those leading to the generation of H and L cells during repair, which are amplified by stalled RNA polymerase II and are dependent on Np95 and Ga45a. Under our conditions, GADD45A, transiently induced by DSB, recruited to the DSB, enhanced accumulation of hypomethylated clones (H) by inhibiting DNMT1 [Figure 7, Supplementary Figure S11 and (18)] and disappeared in 3–4 days. This inhibition may represent a barrier to spreading of repair-induced methylation. The opposing role of Np95 and GADD45A on DNMT1 activity is not new because DNMT1 stimulation and inhibition by Np95 and Ga45a, respectively, are required to maintain progenitor function in self-renewing somatic tissue (40).

Evolution and stability of epialleles: qualitative analysis of methylation

Our data show that the repaired DSB in the GFP gene is marked locally by de novo methylation. Unlike the GFP system, in which we induced a site-specific DSB, DSBs in genomic DNA are essentially random in terms of sequence specificity, although the overall distribution is nonrandom, due to chromatin organization (41). Assuming that methylation marks these DSBs after homologous repair, the overall distribution of methylated sites in genomic DNA will appear random in the absence of selective pressure. We have extended our analysis to homologous targeting of GFP in ES cells and we find that genetically identical clones express variable GFP levels, due to de novo methylation or targeted gene (data not shown).

In our system, qualitative analysis of the methylation profiles, i.e. the location of methylated CpG in the various GFP molecules, 3′ end to the DSB, is able to distinguish repaired GFP molecules from nonrecombinant or uncleaved molecules (Supplementary Figures S6 and S7). This discrimination is based on the relatedness of methylation profiles, not on the total methyl CpG content. GFP DNA molecules, shown in Supplementary Figures S4 and S6, can be considered epigenetic alleles because their methylation profiles are stable and are inherited in human and mouse cells over several generations. We have applied the same type of analysis shown in Supplementary Figures S6 and S7 to several somatically methylated genes and we find that the epialleles are stable, evolve rapidly following DNA damage and can be individually tracked in a complex mixtures of cells. HDR-induced specific methylation states may be ultimately responsible for stochastic gene expression in populations of mammalian cells.

In conclusion, we propose that DNA methylation represents a damage-repair code that modifies the expression of genes in cell populations and drives adaptation to environmental challenges. Selection of methylated alleles in each cell may be relevant for the rapid evolution of cancer cell phenotypes.

SUPPLEMENTARY DATA

Supplementary Data are available at NAR Online, including [42].

ACKNOWLEDGMENTS

The authors thank A. Simeone and D. Acampora for providing us the ES clones with EGFP gene targeted to the rosa 26 locus; G. Tell, G. Scholes and G. Diez Roux for helpful comments and F. Porcellini for video editing.

FUNDING

AIRC IG [11364 to V.E.A.]; Epigenomics Flagship Project—EPIGEN (to C.N.R.) and Fondazione Medicina Molecolare e Terapia Cellulare, Universita' Politecnica delle Marche. Funding for open access charge: Epigenomics Flagship Project—EPIGEN (to C.N.R.).

Conflict of interest statement. None declared.

REFERENCES

1. Rizwana,R. and Hahn,P. (1999) CpG methylation reduces genomic instability. *J. Cell Sci.*, **112**, 4513–4519.
2. Fu,A.Q., Genereux,D.P., Stöger,R., Laird,C.D. and Stephens,M. (2010) Statistical inference of transmission fidelity of DNA methylation patterns over somatic cell divisions in mammals. *Ann. Appl. Stat.*, **4**, 871–892.
3. Probst,A.V., Dunleavy,E. and Almouzni,G. (2009) Epigenetic inheritance during the cell cycle. *Nat. Rev. Mol. Cell Biol.*, **10**, 192–206.
4. Cho,Y.H., Yazici,H., Wu,H.C., Terry,M.B., Gonzalez,K., Qu,M., Dalay,N. and Santella,R.M. (2010) Aberrant promoter hypermethylation and genomic hypomethylation in tumor adjacent normal tissues and blood from breast cancer patients. *Anticancer Res.*, **30**, 2489–2496.
5. Avvedimento,E.V., Obici,S., Sanchez,M., Gallo,A., Musti,A. and Gottesman,M.E. (1989) Reactivation of thyroglobulin gene expression in transformed thyroid cells by 5-azacytidine. *Cell*, **58**, 1135–1142.
6. Angrisano,T., Sacchetti,S., Natale,F., Cerrato,A., Pero,R., Keller,S., Peluso,S., Perillo,B., Avvedimento,V.E., Fusco,A. *et al.* (2011) Chromatin and DNA methylation dynamics during retinoic acid-induced RET gene transcriptional activation in neuroblastoma cells. *Nucleic Acids Res.*, **39**, 1993–2006.
7. Halazonetis,T.D., Gorgoulis,V.G. and Bartek,J. (2008) An oncogene-induced DNA damage model for cancer development. *Science*, **319**, 1352–1355.
8. Lengauer,C., Kinzler,K.W. and Vogelstein,B. (1997) DNA methylation and genetic instability in colorectal cancer cells. *Proc. Natl Acad. Sci. USA*, **94**, 2545–2450.
9. Cuozzo,C., Porcellini,A., Angrisano,T., Morano,A., Lee,B., Di Pardo,A., Messina,S., Iuliano,R., Fusco,A., Santillo,M.R. *et al.* (2007) DNA damage homology-directed repair and DNA methylation. *PLoS Genet.*, **3**, e110.
10. Jasin,M. (1996) Genetic manipulation of genomes with rare-cutting endonucleases. *Trends Genet.*, **12**, 224–228.
11. Pierce,A.J., Johnson,R.D., Thompson,L.H. and Jasin,M. (1999) XRCC3 promotes homology-directed repair of DNA damage in mammalian cells. *Genes Dev.*, **13**, 2633–2638.
12. Rountree,M.R. and Selker,E.U. (1997) DNA methylation inhibits elongation but not initiation of transcription in Neurospora crassa. *Genes Dev.*, **11**, 2383–2395.
13. O'Hagan,H.M., Mohammad,H.P. and Baylin,S.B. (2008) Double strand breaks can initiate gene silencing and SIRT1-dependent onset of DNA methylation in an exogenous promoter CpG island. *PLoS Genet.*, **4**, e1000155.
14. Lee,G.E., Kim,J.H., Taylor,M. and Muller,M.T. (2010) DNA methyltransferase 1-associated protein (DMAP1) is a co-repressor that stimulates DNA methylation globally and locally at sites of double strand break repair. *J. Biol. Chem.*, **285**, 37630–37640.

15. Ha,K., Lee,G.E., Palii,S.S., Brown,K.D., Takeda,Y., Liu,K., Bhalla,K.N. and Robertson,K.D. (2011) Rapid and transient recruitment of DNMT1 to DNA double-strand breaks is mediated by its interaction with multiple components of the DNA damage response machinery. *Hum. Mol. Genet*., **20**, 126–140.
16. Sandovici,I., Kassovska-Bratinova,S., Vaughan,J.E., Stewart,R., Leppert,M. and Sapienza,C. (2006) Human imprinted chromosomal regions are historical hot-spots of recombination. *PLoS Genet*., **2**, e101.
17. Sigurdsson,M.I., Smith,A.V., Bjornsson,H.T. and Jonsson,J.J. (2009) HapMap methylation-associated SNPs markers of germline DNA methylation positively correlate with regional levels of human meiotic recombination. *Genome Res*., **19**, 581–589.
18. Lee,B., Morano,A., Porcellini,A. and Muller,M.T. (2012) GADD45α inhibition of DNMT1 dependent DNA methylation during homology directed DNA repair. *Nucleic Acids Res*., **40**, 2481–2493.
19. Gong,X.Q., Nedialkov,Y.A. and Burton,Z.F. (2004) Alpha-amanitin blocks translocation by human RNA polymerase II. *J. Biol. Chem*., **279**, 27422–27427.
20. Jones,E., Kimura,H., Vigneron,M., Wang,Z., Roeder,R.G. and Cook,P.R. (2000) Isolation and characterization of monoclonal antibodies directed against subunits of human RNA polymerases I, II, and III. *Exp. Cell Res*., **254**, 163–172.
21. Ioannidis,P., Havredaki,M., Courtis,N. and Trangas,T. (1996) *In vivo* generation of 3' and 5' truncated species in the process of c-myc mRNA decay. *Nucleic Acids Res*., **24**, 4969–4977.
22. Leclerc,G.J., Leclerc,G.M. and Barredo,J.C. (2002) Real-time RT-PCR analysis of mRNA decay: half-life of Beta-actin mRNA in human leukemia CCRF-CEM and Nalm-6 cell lines. *Cancer Cell Int*., **2**, 1.
23. Walton,E.L., Francastel,C. and Velasco,G. (2011) Maintenance of DNA methylation: Dnmt3b joins the dance. *Epigenetics*, **6**, 1373–1377.
24. Sharif,J., Muto,M., Takebayashi,S., Suetake,I., Iwamatsu,A., Endo,T.A., Shinga,J., Mizutani-Koseki,Y., Toyoda,T., Okamura,K. *et al*. (2007) The SRA protein Np95 mediates epigenetic inheritance by recruiting Dnmt1 to methylated DNA. *Nature*, **450**, 908–912.
25. Meilinger,D., Fellinger,K., Bultmann,S., Rothbauer,U., Bonapace,I.M., Klinkert,W.E., Spada,F. and Leonhardt,H. (2009) Np95 interacts with de novo DNA methyltransferases, Dnmt3a and Dnmt3b, and mediates epigenetic silencing of the viral CMV promoter in embryonic stem cells. *EMBO Rep*., **10**, 1259–1264.
26. Rottach,A., Frauer,C., Pichler,G., Bonapace,I.M., Spada,F. and Leonhardt,H. (2010) The multi-domain protein Np95 connects DNA methylation and histone modification. *Nucleic Acids Res*., **38**, 1796–1804.
27. Papait,R., Pistore,C., Negri,D., Pecoraro,D., Cantarini,L. and Bonapace,I.M. (2007) Np95 is implicated in pericentromeric heterochromatin replication and in major satellite silencing. *Mol. Biol. Cell*, **18**, 1098–1106.
28. Hervouet,E., Lalier,L., Debien,E., Cheray,M., Geairon,A., Rogniaux,H., Loussouarn,D., Martin,S.A., Vallette,F.M. and Cartron,P.F. (2010) Disruption of Dnmt1/PCNA/UHRF1 interactions promotes tumorigenesis from human and mice glial cells. *PLoS One*, **5**, e11333.
29. Barreto,G., Schäfer,A., Marhold,J., Stach,D., Swaminathan,S.K., Handa,V., Döderlein,G., Maltry,N., Wu,W., Lyko,F. *et al*. (2007) Gadd45a promotes epigenetic gene activation by repair-mediated DNA demethylation. *Nature*, **445**, 671–675.
30. Jin,S.G., Guo,C. and Pfeifer,G.P. (2008) GADD45A does not promote DNA demethylation. *PLoS Genet*., **4**, e1000013.
31. Helleday,T., Lo,J., van Gent,D.C. and Engelward,B.P. (2007) DNA double-strand break repair: from mechanistic understanding to cancer treatment. *DNA Repair (Amst)*, **6**, 923–935.
32. Métivier,R., Gallais,R., Tiffoche,C., Le Péron,C., Jurkowska,R.Z., Carmouche,R.P., Ibberson,D., Barath,P., Demay,F., Reid,G. *et al*. (2008) Cyclical DNA methylation of a transcriptionally active promoter. *Nature*, **452**, 45–50.
33. Mutskov,V. and Felsenfeld,G. (2004) Silencing of transgene transcription precedes methylation of promoter DNA and histone H3 lysine 9. *EMBO J*., **23**, 138–149.
34. Hinshelwood,R.A., Melki,J.R., Huschtscha,L.I., Paul,C., Song,J.Z., Stirzaker,C., Reddel,R.R. and Clark,S.J. (2009) Aberrant de novo methylation of the p16INK4A CpG island is initiated post gene silencing in association with chromatin remodelling and mimics nucleosome positioning. *Hum. Mol. Genet*., **18**, 3098–3109.
35. Stirzaker,C., Song,J.Z., Davidson,B. and Clark,S.J. (2004) Transcriptional gene silencing promotes DNA hypermethylation through a sequential change in chromatin modifications in cancer cells. *Cancer Res*., **64**, 3871–3877.
36. Kangaspeska,S., Stride,B., Métivier,R., Polycarpou-Schwarz,M., Ibberson,D., Carmouche,R.P., Benes,V., Gannon,F. and Reid,G. (2008) Transient cyclical methylation of promoter DNA. *Nature*, **452**, 112–115.
37. Perillo,B., Ombra,M.N., Bertoni,A., Cuozzo,C., Sacchetti,S., Sasso,A., Chiariotti,L., Malorni,A., Abbondanza,C. and Avvedimento,E.V. (2008) DNA oxidation as triggered by H3K9me2 demethylation drives estrogen-induced gene expression. *Science*, **319**, 202–206.
38. Le May,N., Fradin,D., Iltis,I., Bougnères,P. and Egly,J.M. (2012) XPG and XPF endonucleases trigger chromatin looping and DNA demethylation for accurate expression of activated genes. *Mol. Cell*, **47**, 622–632.
39. Chen,Z.X. and Riggs,A.D. (2011) DNA methylation and demethylation in mammals. *J. Biol. Chem*., **286**, 18347–18353.
40. Sen,G.L., Reuter,J.A., Webster,D.E., Zhu,L. and Khavari,P.A. (2010) DNMT1 maintains progenitor function in self-renewing somatic tissue. *Nature*, **463**, 563–567.
41. Radulescu,I., Elmroth,K. and Stenerlöw,B. (2004) Chromatin organization contributes to non-randomly distributed double-strand breaks after exposure to high-LET radiation. *Radiat. Res*., **16**, 1–8.
42. Citterio,E., Papait,R., Nicassio,F., Vecchi,M., Gomiero,P., Mantovani,R., Di Fiore,P.P. and Bonapace,I.M. (2004) Np95 is a histone-binding protein endowed with ubiquitin ligase activity. *Mol. Cell Biol*., **24**, 2526–2535.

PHYSIOLOGY

Oxidative DNA damage induces the ATM-mediated transcriptional suppression of the Wnt inhibitor WIF-1 in systemic sclerosis and fibrosis

Silvia Svegliati,[1]* Giusi Marrone,[2]* Antonio Pezone,[2]* Tatiana Spadoni,[1] Antonella Grieco,[1] Gianluca Moroncini,[1,3] Domenico Grieco,[2] Maria Vinciguerra,[4] Savina Agnese,[2] Astrid Jüngel,[5] Oliver Distler,[5] Anna Maria Musti,[6] Armando Gabrielli,[1,3]† Enrico V. Avvedimento[2]†

Systemic sclerosis (SSc) is an autoimmune disease characterized by extensive visceral organ and skin fibrosis. SSc patients have increased production of autoreactive antibodies and Wnt signaling activity. We found that expression of the gene encoding Wnt inhibitor factor 1 (WIF-1) was decreased in fibroblasts from SSc patient biopsies. WIF-1 deficiency in SSc patient cells correlated with increased abundance of the Wnt effector β-catenin and the production of collagen. Knocking down WIF-1 in normal fibroblasts increased Wnt signaling and collagen production. WIF-1 loss and DNA damage were induced in normal fibroblasts by either SSc patient immunoglobulins or oxidative DNA-damaging agents, such as ultraviolet light, hydrogen peroxide, or bleomycin. The DNA damage checkpoint kinase ataxia telangiectasia mutated (ATM) mediated WIF-1 silencing through the phosphorylation of the transcription factor c-Jun, which in turn activated the expression of the gene encoding activating transcription factor 3 (ATF3). ATF3 and c-Jun were recruited together with histone deacetylase 3 (HDAC3) to the *WIF-1* promoter and inhibited *WIF-1* expression. Preventing the accumulation of reactive oxygen species or inhibiting the activation of ATM, c-Jun, or HDACs restored *WIF-1* expression in cultured SSc patient cells. Trichostatin A, an HDAC inhibitor, prevented WIF-1 loss, β-catenin induction, and collagen accumulation in an experimental fibrosis model. Our findings suggest that oxidative DNA damage induced by SSc autoreactive antibodies enables Wnt activation that contributes to fibrosis.

INTRODUCTION

The Wnt (Wingless) family is a group of highly conserved secreted proteins that regulate cell-to-cell interactions during embryogenesis and is implicated in carcinogenesis, aging, and fibrosis (*1*). To be effective during embryogenesis and stem cell differentiation, Wnt signals need to be carefully controlled temporally and spatially (*2*). This is accomplished by a balance of Wnt-activating proteins or Wnt-inhibiting proteins [for a review, see (*3*)]. Specifically, inhibitors either bind directly to Wnt, such as Wnt inhibitory factor 1 (WIF-1), or interact with the Wnt receptor complex (*4*).

WIF-1 is a highly conserved gene containing a unique Wnt inhibitory domain and five epidermal growth factor (EGF)–like repeat domains. WIF-1 inhibits Wnt signaling during development (*5*), and it is silenced during the neoplastic progression of various human cancers (*6*, *7*). Increased Wnt signaling is also linked to mesenchymal differentiation and tissue-specific cellular aging. Unrestrained Wnt signaling decreases the pool of mesenchymal stem cells and ultimately induces fibrosis (*8*). Systemic sclerosis (SSc) is a disease characterized by extensive tissue fibrosis, and Wnt–β-catenin signaling is a key player in fibroblast activation and tissue fibrosis in SSc (*9*). We previously showed that fibroblasts derived from SSc patients undergo senescence prematurely because of extensive oxidative stress and DNA damage. This phenotype is induced in normal cells through constitutive activation of platelet-derived growth factor receptor (PDGFR) signaling by agonistic autoreactive antibodies (*10*, *11*), but the specific mechanism leading to Wnt activation in SSc cells is not yet clear. Notably, Wnt activation has different consequences on the fate of epithelial and mesenchymal cells: DNA damage promotes transformation or death in epithelial cells (*12*) but accelerates aging and increases collagen abundance in mesenchymal cells (*8*, *13*). Therefore, we investigated the mechanism linking the effects of SSc patient–derived immunoglobulins with the induction of Wnt signaling in either normal or SSc patient fibroblasts derived from skin biopsies.

RESULTS

WIF-1 is silenced in SSc patient fibroblasts by promoter histone deacetylation

Wnt signaling is increased in the skin and fibroblasts of SSc patients compared with the same samples derived from normal subjects (*9*, *13*), suggesting that either the activity of proteins that stimulate the pathway is increased or that of proteins which inhibit Wnt signaling is decreased. We found that the abundance of the secreted Wnt inhibitor, WIF-1, was decreased in skin biopsies from SSc patients compared with normal cultured fibroblasts (Fig. 1, A to C, and fig. S1A). Immunofluorescence detection of WIF-1 in SSc patient fibroblasts further confirmed significantly decreased WIF-1 abundance, as well as a concomitant increase in that of β-catenin (Fig. 1D), which is a marker of canonical Wnt signaling. Because *WIF-1* is silenced in breast cancer cells by methylation of its promoter (*14*),

[1]Dipartimento di Scienze Cliniche e Molecolari, Clinica Medica, Università Politecnica delle Marche, 60126 Ancona, Italy. [2]Dipartimento di Medicina Molecolare e Biotecnologie Mediche, Università degli Studi di napoli Federico II, 80132 Naples, Italy. [3]Dipartimento di Medicina Interna, Ospedali Riuniti, 60126 Ancona, Italy. [4]Cancer Research UK, Clare Hall, London EN6 3LD, UK. [5]Center of Experimental Rheumatology, Department of Rheumatology, University Hospital Zurich, 8091 Zurich, Switzerland. [6]Dipartimento di Farmacia e Scienze della Salute e della Nutrizione, Università della Calabria, Arcavacata di Rende (CS) 87036, Italy.
*These authors contributed equally to this work.
†Corresponding author. E-mail: avvedim@unina.it (E.V.A.); a.gabrielli@univpm.it (A.G.)

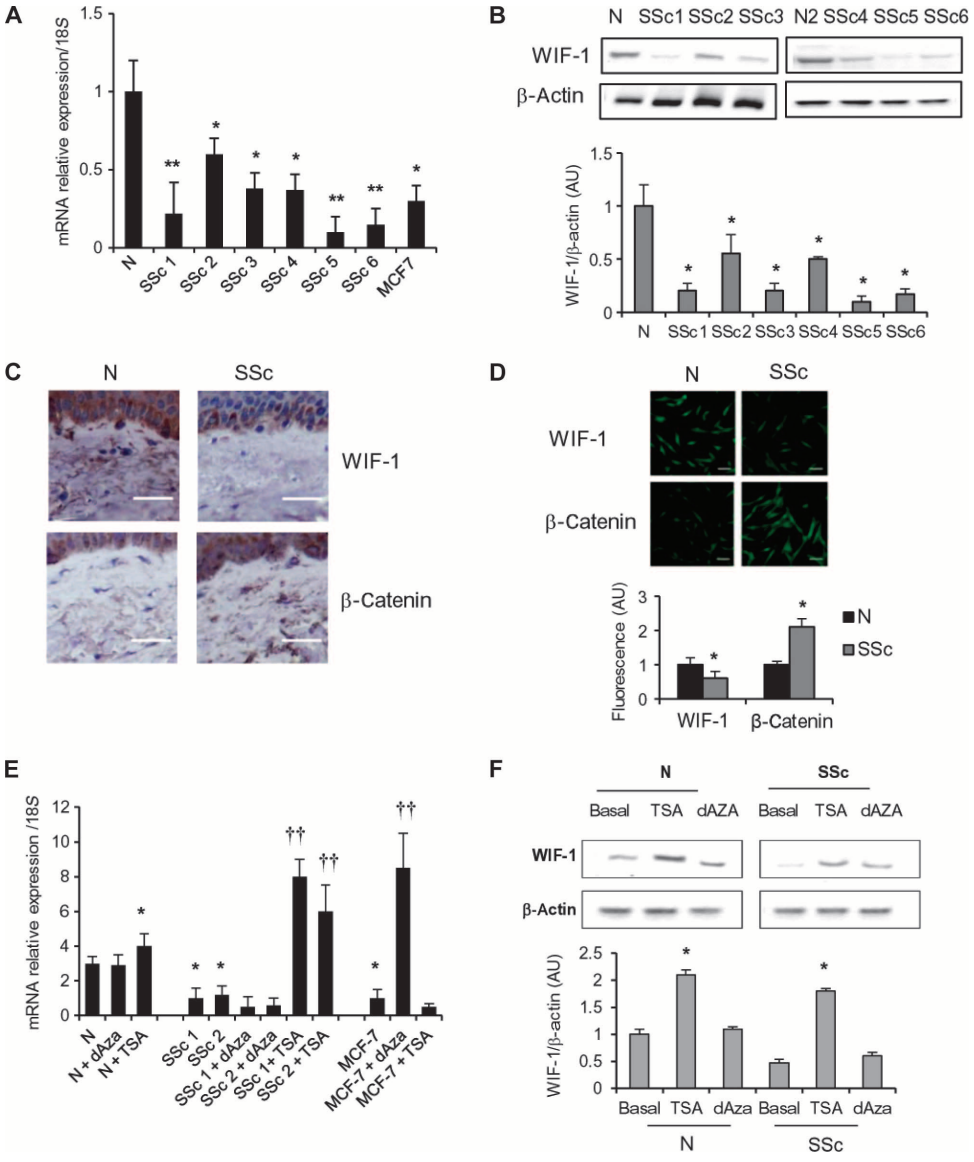

Fig. 1. Silencing of WIF-1 in fibroblasts from SSc and in breast cancer cells (MCF7). (**A**) Reverse transcription polymerase chain reaction (RT-PCR) for *WIF-1* mRNA abundance in serum-starved primary fibroblasts from six normal subjects (N, means ± SD from fig. S1A) or six SSc patients compared with MCF7 cells. Data are means ± SD from three independent experiments normalized to 18*S* RNA abundance. (**B**) Western blot for WIF-1 in whole-cell lysates from six SSc patients compared with normal samples. Data are means ± SD from three independent cultures from each patient. AU, arbitrary unit. (**C**) Representative immunohistochemistry for WIF-1 and β-catenin in skin biopsies from three SSc and three normal subjects. Scale bars, 100 μm. (**D**) Confocal microscopy for WIF-1 and β-catenin in SSc or normal fibroblasts. Data are means ± SD of at least 50 cells per field from six SSc patients and six normal subjects. Scale bars, 100 μm. (**E** and **F**) Analysis of *WIF-1* expression (E) and WIF-1 abundance (F) in normal or SSc fibroblasts (from six patients each) and MCF7 cells treated with 300 nM TSA or 4 μM 5-azacytidine for 24 hours. Data are means ± SD of three independent experiments. $^{*}P < 0.05$, $^{**}P < 0.01$ compared to normal control; $^{\dagger\dagger}P < 0.01$ compared to SSc.

and because the abundance of *WIF-1* mRNA in a culture of MCF7 breast cancer cells was similar to that in SSc patient fibroblasts (Fig. 1A), we hypothesized that the same may be true in SSc patient cells. However, in contrast to that in MCF7 cells, the *WIF-1* gene was not methylated in SSc patient fibroblasts as assessed by bisulphite sequencing (fig. S1B), and its expression was not restored by treatment with 5-azacytidine, a demethylating agent (Fig. 1E). It was, however, restored and further increased by treatment with the histone deacetylase (HDAC) inhibitor trichostatin A (TSA) at both the mRNA and protein levels (Fig. 1, E and F). In contrast, the expression of *WIF-1* was restored in MCF7 cells only by 5-azacytidine (Fig. 1E), indicating that whereas the loss of WIF-1 may be caused by DNA methylation in breast cancer epithelia, its loss is caused by histone deacetylation in SSc patient fibroblasts.

WIF-1 silencing enhances Wnt activity and induces *COL1A1* expression

To investigate the consequences of decreased *WIF-1* expression in SSc cells, we silenced *WIF-1* in normal fibroblasts using targeted silencing RNAs (siRNAs) and measured the transcript abundance of *COL1A1* (encoding collagen type 1 α 1) and *CTNNB1* (encoding β-catenin). Loss of WIF-1 initially increased the expression of *CTNNB1* (Fig. 2A). The abundance of β-catenin at both the transcriptional and translational levels was inversely correlated with WIF-1 abundance (Fig. 2A and fig. S2A), possibly because of the stabilizing effects of Wnt on β-catenin (*15*). *COL1A1* mRNA, however, increased only 96 hours after WIF-1 siRNA transfection, suggesting an indirect effect of *WIF-1* on *COL1A1* gene expression (Fig. 2A). We noticed a significant and unexpected early inhibition of *COL1A1* expression in the first 48 hours after transfection with *WIF-1* siRNA (Fig. 2A). We speculate that in the absence of certain growth factors [such as platelet-derived growth factor (PDGF), which induces collagen synthesis (*10*)], a rapid increase of β-catenin may inhibit rather than stimulate *COL1A1* expression.

To this end, we analyzed the effects of WIF-1 depletion in cells stimulated with PDGF. Loss of WIF-1 at 72 to 96 hours increased the basal expression of *COL1A1* and prevented PDGF-induced expression of *COL1A1* (Fig. 2, B and C), suggesting that cells with low abundance of WIF-1 (such as SSc cells) express increased *COL1A1* and are thus refractory to collagen-inducing signals. Decreased WIF-1 correlated with the induction of β-catenin and T cell factor (TCF)–dependent transcription in SSc patient cells, as assessed with a luciferase reporter (fig. S2B), as well as high abundance of β-catenin in idiopathic lung fibrosis cells (fig. S2C) (*16*), which is also evident in other fibrotic tissues (*17*, *18*).

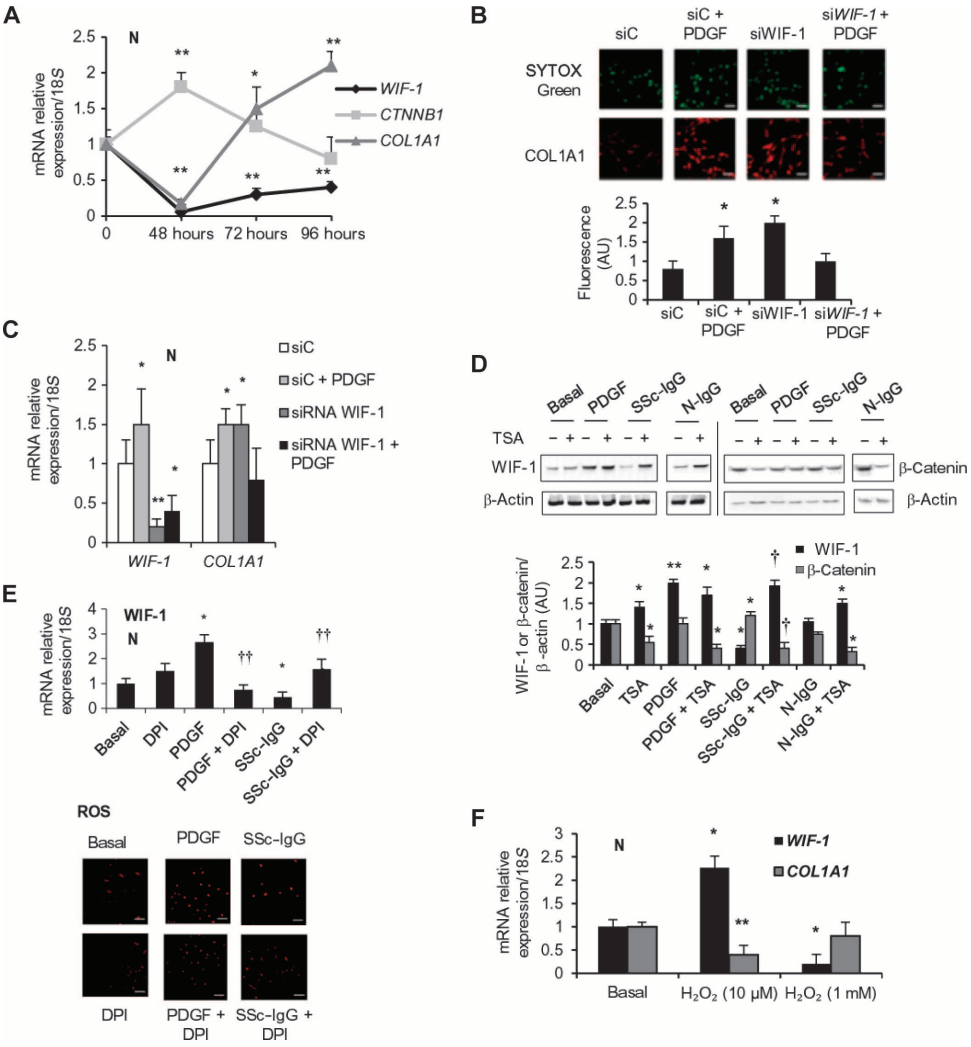

Fig. 2. WIF-1 silencing amplifies Wnt signaling and induces COL1A1 expression. (A) Normal fibroblasts were transiently transfected with scrambled or WIF-1–targeted siRNA (siWIF-1). At the indicated times, the relative expression of endogenous *WIF-1*, *CTNNB1*, and *COL1A1* was measured by RT-PCR. (B) Representative immunofluorescence staining for COL1A1 in control-transfected (siC) or WIF-1–silenced cells (siWIF-1) for 48 hours, and then stimulated with PDGF (15 ng/ml) for 24 hours. Images were captured at 72 hours after transfection. (C) RT-PCR analysis of *COL1A1* and *WIF-1* mRNA in fibroblasts treated as in (B). (D) WIF-1 and β-catenin immunoblot in serum-starved normal fibroblasts pretreated with TSA (300 nM, 1 hour) and then stimulated with PDGF (15 ng/ml, 24 hours) or IgG isolated from three SSc or normal subjects (200 μg/ml, 24 hours). (E) *WIF-1* mRNA abundance (upper panel) and ROS detection (lower panel) of fibroblasts not treated (basal) or pretreated with DPI (10 μM, 1 hour) and then stimulated with PDGF (15 ng/ml) or immunoglobulin isolated from three distinct SSc patients (SSc-IgG) (200 μg/ml) for 24 hours. (F) *WIF-1* and *COL1A1* mRNA abundance in serum-starved normal fibroblasts treated with H_2O_2 (10 μM or 1 mM for 2 hours). Data in (A) to (F) are means ± SD of three independent experiments. $^*P < 0.05$, $^{**}P < 0.01$ compared to controls; $^{\dagger}P < 0.01$ compared to SSc-IgG–treated sample (D); $^{\dagger\dagger}P < 0.01$ compared to PDGF-treated sample (E).

Persistent oxidative stress silences WIF-1

To investigate the mechanism that silenced WIF-1, the abundance of WIF-1 and β-catenin was measured in normal fibroblasts exposed to recombinant PDGF or immunoglobulins isolated from normal volunteers (N-IgG) or SSc patients (SSc-IgG). After 24 hours in PDGF, the abundance of WIF-1 increased and that of β-catenin did not change in normal fibroblasts (Fig. 2D). In contrast, exposure to SSc-IgG, but not N-IgG, decreased WIF-1 and increased β-catenin protein abundance. Fibroblasts lacking functional PDGFR showed no changes in either *WIF-1* or *COL1A1* transcript abundance in response to PDGF or SSc-IgG, whereas reconstitution of PDGFR restored the effects of both PDGF and SSc-IgG on *WIF-1* expression and increased the expression of *COL1A1* (fig. S2D). This suggested that although PDGF and SSc-IgG had opposite effects on the abundance of WIF-1, they appeared to act through the same receptor. To rule out possible artifacts caused by contaminants in SSc-IgG fractions and to demonstrate the biological activity of SSc-IgG on *WIF-1* expression, we tested a recombinant IgG (immunoglobulin G) targeting PDGF that was cloned from lymphocytes of a scleroderma patient. This IgG reduced *WIF-1* expression (fig. S2E). Because inhibition of HDAC by TSA reactivated *WIF-1* expression in SSc cells, we tested whether TSA inhibited SSc-IgG effects. TSA not only reverted the effects of SSc-IgG in normal fibroblasts but also markedly stimulated the expression of *WIF-1* and reduced β-catenin content (Fig. 2D), suggesting that HDAC is a target of the action of SSc-IgG.

To identify the targets of PDGF and SSc-IgG in altering *WIF-1* expression, we inhibited reactive oxygen species (ROS), which mediates the induction of *COL1A1* expression by PDGF or SSc-IgG (*10*). Depletion of ROS by diphenyleneiodonium (DPI), a general inhibitor of ROS-producing flavoenzymes (fig. S3) (*19*), prevented the effects of either PDGF or SSc-IgG on the expression of *WIF-1* (Fig. 2E). Normal fibroblasts exposed to increasing H_2O_2 concentrations differentially affected the expression of *WIF-1*, depending on the time and the concentrations used. Whereas addition of 10 μM H_2O_2 for 2 hours increased *WIF-1* expression, exposure to 1 mM H_2O_2 for 2 hours significantly decreased it compared to basal expression (Fig. 2F). Low H_2O_2 mimicked the effects of PDGF (induced *WIF-1* expression), whereas high H_2O_2 replicated SSc-IgG action (inhibited *WIF-1* expression). We note that ROS induced by PDGF are transient and rapid, whereas ROS induced by SSc-IgG are prolonged (*11*); this may explain why only high H_2O_2 inhibited *WIF*-1 expression in normal cells. In SSc cells, ROS persist longer even in the absence of serum or exogenous SSc-IgG because they sustain an autoamplification loop involving active extracellular signal–regulated kinase 1 and 2 (ERK1/2) and NADPH (reduced form of nicotinamide adenine dinucleotide phosphate) oxidase (*10*).

Collectively, the data suggest that WIF-1 silencing induced by high or persistent ROS exposure promotes Wnt signals to respond to oxidative stress.

DNA damage and checkpoint kinase ataxia telangiectasia mutated silence WIF-1

Persistent oxidative stress, caused by H_2O_2 or ultraviolet (UV) light, for example, can induce DNA damage and activation of ataxia telangiectasia mutated (ATM) and the DNA damage response (DDR) (*20*). SSc patient–derived fibroblasts and normal fibroblasts treated with high concentrations of H_2O_2 displayed conspicuous DNA damage, evident by the accumulation of phosphorylated ATM (Fig. 3, A and B) and phosphorylated p53 binding protein 1 (53BP1) (Fig. 3C), hallmarks of the DDR (*20*). In SSc fibroblasts, inhibiting ATM with the competitive inhibitor KU55933 (KuDOS 55933) increased *WIF-1* expression and reduced *COL1A1* expression compared to that seen in normal cells (Fig. 3D). Similarly, DNA damage induced by UV light in normal fibroblasts reduced *WIF-1* mRNA abundance (Fig. 3E). Treatment with the ATM inhibitor not only prevented UV-induced repression of *WIF-1* but also increased it basally (Fig. 3E). The expression of other genes that encode inhibitors of Wnt signaling, such as axis inhibition protein 2, secreted frizzled-related protein, and glycogen synthase kinase 3 was also inhibited by UV, but was not dependent on ATM (fig. S4), suggesting that WIF-1 might be a specific target in the ATM-induced damage response.

To examine whether *WIF-1* expression was inhibited by ROS and ATM through a single mechanism, we treated normal or A-T fibroblasts (GM05823) with 250 μM H_2O_2, which was sufficient to reduce *WIF-1* expression in wild-type fibroblasts (Fig. 3F). However, in A-T fibroblasts, the same concentration of H_2O_2 did not significantly affect *WIF-1* expression (Fig. 3F). Exposure of normal fibroblasts to higher concentrations (1 mM) of H_2O_2 silenced *WIF-1* expression and (as confirmation of the functional effects on Wnt signaling) stimulated β-catenin abundance, but not in the presence of the ATM inhibitor (fig. S5), indicating that ATM was downstream of ROS induction and mediated the repression of *WIF-1* expression. This finding agrees with evidence that ATM can be directly activated by ROS independently of the DDR-initiating MRE11-RAD50-NBS1 (MRN) complex (*20*). However, to test whether WIF-1 silencing was

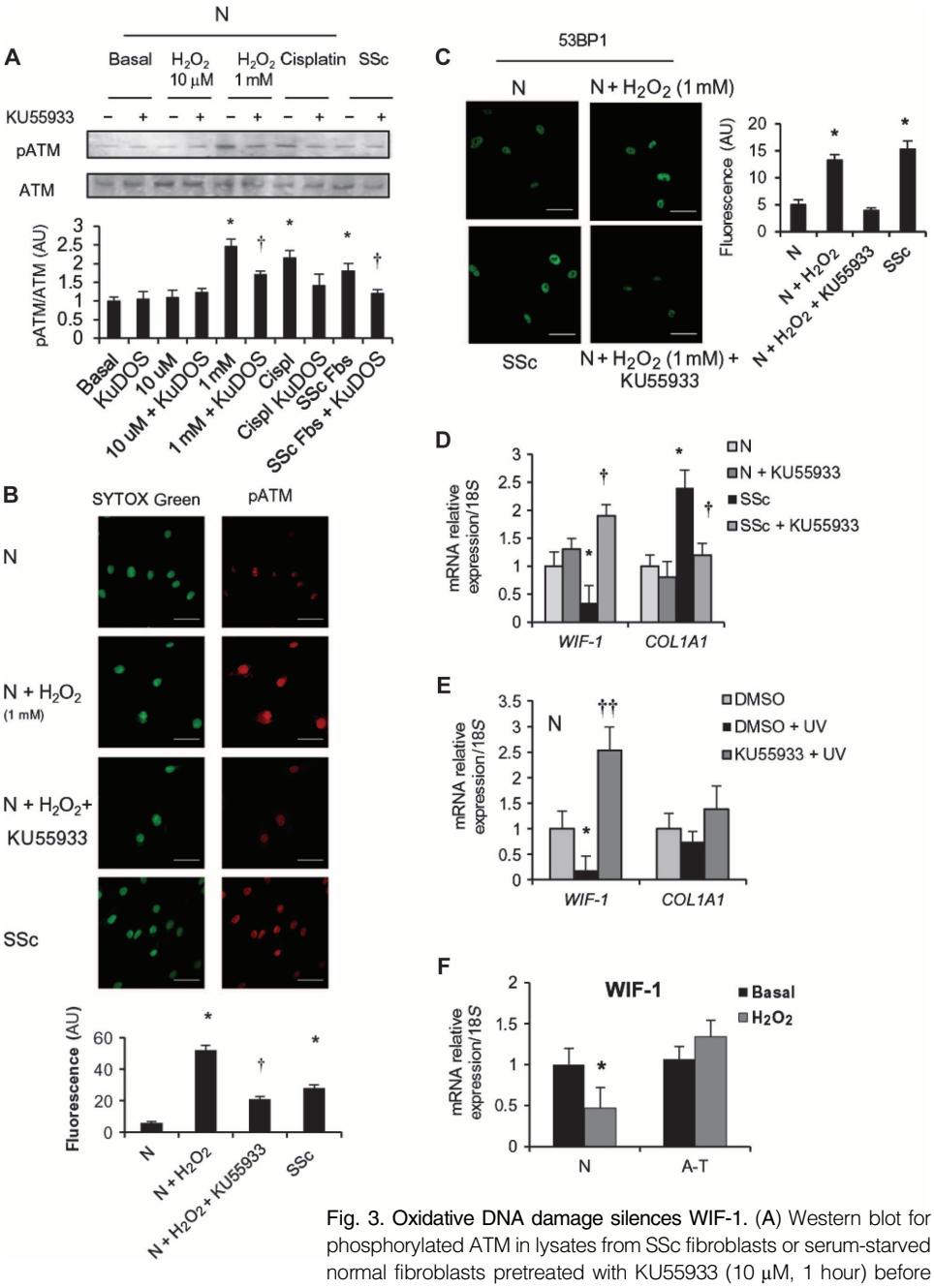

Fig. 3. Oxidative DNA damage silences WIF-1. (**A**) Western blot for phosphorylated ATM in lysates from SSc fibroblasts or serum-starved normal fibroblasts pretreated with KU55933 (10 μM, 1 hour) before H_2O_2 (10 μM and 1 mM, 2 hours) or cisplatin (5 μM, 24hours). Blots are representative of three independent experiments. (**B**) Phosphorylated ATM (Ser^{1981}; red) and DNA (SYTOX Green) in normal or SSc fibroblasts pretreated with KU55933 (10 μM, 1 hour), and then treated with H_2O_2 (1 mM, 30 min). Images are representative of four independent experiments. Scale bars, 100 μm. (**C**) Cells treated as in (A) and stained for 53BP1. Images are representative of four independent experiments. Scale bars, 100 μm. (**D**) *WIF-1* and *COL1A1* mRNA expression in normal (N) and SSc fibroblasts in the presence or absence of KU55933 (10 μM, 1 hour). (**E**) *WIF-1* and *COL1A1* mRNA abundance in normal fibroblasts pretreated with 10 μM KU55933 and then exposed to UV (80 J/m^2). DMSO, dimethyl sulfoxide. (**F**) *WIF-1* expression in serum-starved A-T or normal (N) fibroblasts after H_2O_2 treatment (250 μM, 30 min). Data in (A) to (F) are means ± SD of three independent experiments. $^*P < 0.01$ compared to basal or control; $^{\dagger}P < 0.05$ compared to H_2O_2-treated sample (A to C) or SSc cells (D); $^{\dagger\dagger}P < 0.01$ compared to UV-treated cells (E).

dependent on DDR and not ROS alone, we treated normal or A-T fibroblasts cells with bleomycin, which activates the DDR by creating DNA double-strand breaks (DSBs) and, incidentally, also induces fibrosis (*21*). Bleomycin repressed *WIF-1* and stimulated *COL1A1* expression in normal, but not in A-T, fibroblasts cells (Fig. 4, A and B, and fig. S6A); instead, *WIF-1* transcript abundance increased in the presence of bleomycin in A-T fibroblasts (Fig. 4A), further supporting a role for ATM in repressing *WIF-1* expression. We also knocked down ATM using targeted siRNA. Depletion of ATM in normal fibroblasts prevented WIF-1 silencing by bleomycin, whereas ATM knockdown increased WIF-1 abundance in SSc patient cells (fig. S6B).

The data thus far have suggested that ATM is a critical mediator of WIF-1 silencing in the presence of ROS and DNA damage. However, the question remained whether oxidative stress, in addition to DNA damage, was also involved in bleomycin-induced repression of WIF-1. Therefore, we assessed the abundance of ROS in normal fibroblasts using the ROS-sensitive fluorescent probe 2′,7′-dichlorfluorescein-diacetate (DCFH-DA) after treatment with bleomycin in the presence or absence of the various inhibitors. ROS were induced by bleomycin, but this induction was inhibited by the ATM inhibitor KU55933 or by the ROS inhibitor DPI (Fig. 4, C and D), suggesting that ATM promoted ROS abundance in normal fibroblasts after bleomycin. Furthermore, DPI or KU55933 prevented bleomycin-induced silencing of *WIF-1* and the induction of *COL1A1* expression (Fig. 4E). Finally, in SSc cells, DPI induced the expression of *WIF-1* and reduced that of *COL1A1* (fig. S7A), indicating that the conditions present in SSc fibroblasts are similar to those in normal fibroblasts exposed to oxidative stress or bleomycin. The data shown above suggest that ATM is both upstream (Fig. 4, C and D) and downstream (fig. S5) of ROS to inhibit *WIF-1* expression. However, these data do not clarify whether ATM induced by ROS is sufficient to silence *WIF-1* expression in the absence of classical DNA damage—DSBs—that selectively activates ATM (*22*). DSBs are recognized by ATM that phosphorylates γ-H2AX, the histone variant that specifically accumulates at DSBs. Cells exposed to a high concentration of H_2O_2 accumulate phosphorylated γ-H2AX, although less efficiently than bleomycin (fig. S7B), suggesting that ROS activate ATM both directly by oxidation (Fig. 3F) (*20*) and indirectly by inducing DSB.

The data thus far indicate that ROS and DNA damage silence WIF-1 and activate collagen. Therefore, we asked whether also other known profibrotic factors use the same mechanism(s). Specifically, we investigated whether transforming growth factor–β (TGF-β), which induces ROS and collagen

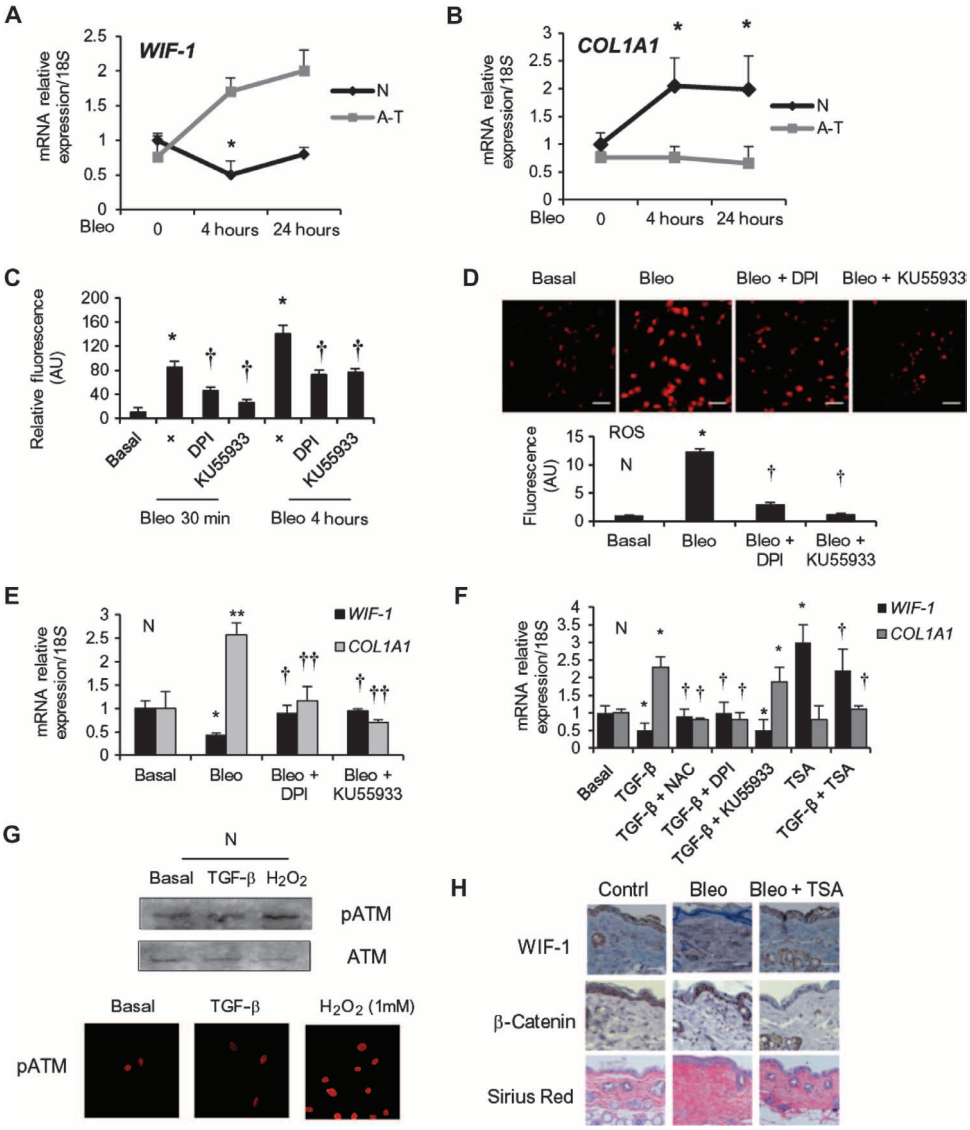

Fig. 4. ATM is essential for WIF-1 silencing by ROS and bleomycin. (A and B) *WIF-1* and *COL1A1* expression in serum-starved A-T or normal (N) fibroblasts during 24 hours of treatment with bleomycin (20 mU/ml). (C and D) Intracellular ROS after bleomycin (20 mU/ml) in normal fibroblasts pretreated with DPI or KU55933 (each 10 μM, 1 hour) assessed by fluorescence (C) and confocal microscopy (D). Images are representative of three experiments. (E) *WIF-1* and *COL1A1* expression in normal fibroblasts treated as in (C) and normalized to 18*S* RNA. (F) *WIF-1* and *COL1A1* mRNA abundance in normal fibroblasts pretreated with TSA (300 nM, 48 hours) or NAC, DPI, or KU55933 (each 10 μM, 1 hour) followed by TGF-β (10 ng/ml, 24 hours). Data in (A) to (F) are means ± SD of three independent experiments. (A, B, and F) $^{*}P < 0.01$ against basal, $^{\dagger}P < 0.05$ against TGF-β–treated samples; (C to E) $^{*}P < 0.05$ and $^{**}P < 0.01$ against basal, $^{\dagger}P < 0.05$ and $^{\dagger\dagger}P < 0.01$ against bleomycin-treated samples. (G) Immunoblot and confocal microscopy for phosphorylated ATM in fibroblasts treated with H_2O_2 (1 mM, 2 hours) or TGF-β (10 ng/ml, 24 hours). Blots and images are representative of three experiments. (H) Immunohistochemistry for WIF-1 and β-catenin in skin from mice subcutaneously injected with either phosphate-buffered saline (PBS) (Contrl) or bleomycin (Bleo) compared with mice that received intraperitoneal injection of TSA before bleomycin injection (Bleo + TSA). Images are representative of six mice each. Scale bars, 100 μm (D and H).

(*23*), had a suppressive effect on *WIF-1* expression, and whether it acted through ATM. Normal fibroblasts were preexposed to one of several inhibitors [*N*-acetyl cysteine (NAC) or DPI to reduce ROS, KU55933 to inhibit ATM, or TSA to inhibit HDAC] and treated with TGF-β for 24 hours. TGF-β reduced *WIF-1* expression in a ROS- and HDAC-dependent but ATM-independent manner, because NAC and DPI, and TSA prevented the effects of TGF-β on *COL1A1* and *WIF-1* expression, whereas KU55933 did not (Fig. 4F). TGF-β, under these conditions, did not activate ATM (Fig. 4G), suggesting that TGF-β–induced ROS can activate HDAC (*24*–*26*) and repress *WIF-1*, but do not induce DNA damage and ATM. Moreover, these data show that the effects of ATM and ROS on *WIF-1* silencing can be dissociated and suggest that ROS induced by TGF-β are neither persistent nor high enough to induce ATM.

Because inhibition of HDAC by TSA or of ATM by KU55933 individually increased *WIF-1* expression in SSc cells (Figs. 1F and 3D), we investigated whether TSA and KU55933 inhibit the same signaling pathway. The effects of TSA and KU55933 on *WIF-1* and *COL1A1* expression in SSc cells were not additive (fig. S8), suggesting that their targets, HDAC and ATM, are in the same pathway.

To test the in vivo relevance of *WIF-1* silencing, and the role of HDAC therein, we investigated its expression in a standard model of fibrosis induced by bleomycin (*27*). Briefly, repeated subcutaneous injections of bleomycin for 24 to 28 days were used to induce fibrosis in mice, confirmed by α-SMA (α–smooth muscle actin) abundance and Masson's trichrome staining (fig. S9). In subgroups of bleomycin-treated mice, pretreatment with intraperitoneal injections of TSA for 4 weeks prevented the decreased WIF-1 and increased β-catenin abundance observed after bleomycin exposure (Fig. 4H), suggesting that bleomycin-induced Wnt signaling was mediated by an HDAC-dependent mechanism in vivo. Whether ATM mediates this pathway in vivo as well remains to be investigated.

Transcription factors c-Jun and activating transcription factor 3 silence WIF-1

To identify the transcription factor (or factors) responsible for WIF-1 silencing induced by ROS and DNA damage, we used a combination of genetic and biochemical approaches to examine transcription factors induced by stress or DNA damage. In primary human fibroblasts, inhibition of nuclear factor κB (NF-κB), by expressing the dominant-inhibitor mutant form of the NF-κB inhibitor IκBα (IκBαM) (fig. S10A) (*28*), did not prevent the repression of *WIF-1* in response to H_2O_2 (fig. S10B), although it did inhibit that of NF-κB targets *IL6* and *CXCL1* in response to tumor necrosis factor, an activator of NF-κB (fig. S10C). Similarly, NF-κB inhibition did not affect *WIF-1* expression in SSc fibroblasts (fig. S10D), indicating that activation of NF-κB did not mediate transcriptional repression of WIF-1.

We then turned our attention to members of the AP1 family and inhibited several of these in SSc cells by expressing one of several dominant-negative AP1 constructs [TAM67, derived from c-Jun (*29*), or a-Fos derived from c-Fos, the human homolog of the retroviral oncogene v-Fos (*29*)] or the wild-type Fos-related antigen 1 (FRA1) to titrate possible AP1-linked repressors (*30*). Among the two dominant-negative mutants or wild-type FRA, only TAM increased *WIF-1* expression (Fig. 5A), suggesting that c-Jun inhibits *WIF-1* expression. Confirming this hypothesis, partial depletion of c-Jun with siRNA (fig. S11A) increased *WIF-1* expression but did not significantly modify *COL1A1* expression in SSc cells (Fig. 5B), suggesting that c-Jun was necessary for *WIF-1* repression, but perhaps not for induction of *COL1A1* expression. To find the missing factor regulating *COL1A1* expression, we investigated the abundance of various transcription factors that interact with c-Jun. We found that the abundance of activating transcription factor 3 (ATF3), a cAMP (adenosine 3′,5′-monophosphate)–responsive element binding (CREB) protein–like stress transcription factor (*31*), was greater in SSc cells than in normal fibroblasts (Fig. 5C and fig. S11B). In SSc cells, partial siRNA-mediated knockdown of ATF3 (fig. S11C) induced the expression of *WIF-1* and reduced that of *COL1A1* (Fig. 5D), suggesting that, whereas both c-Jun and ATF3 can silence *WIF-1* in SSc cells, only ATF3 can induce *COL1A1* expression. In normal fibroblasts, ATF3 and c-Jun were each also involved in the bleomycin-induced

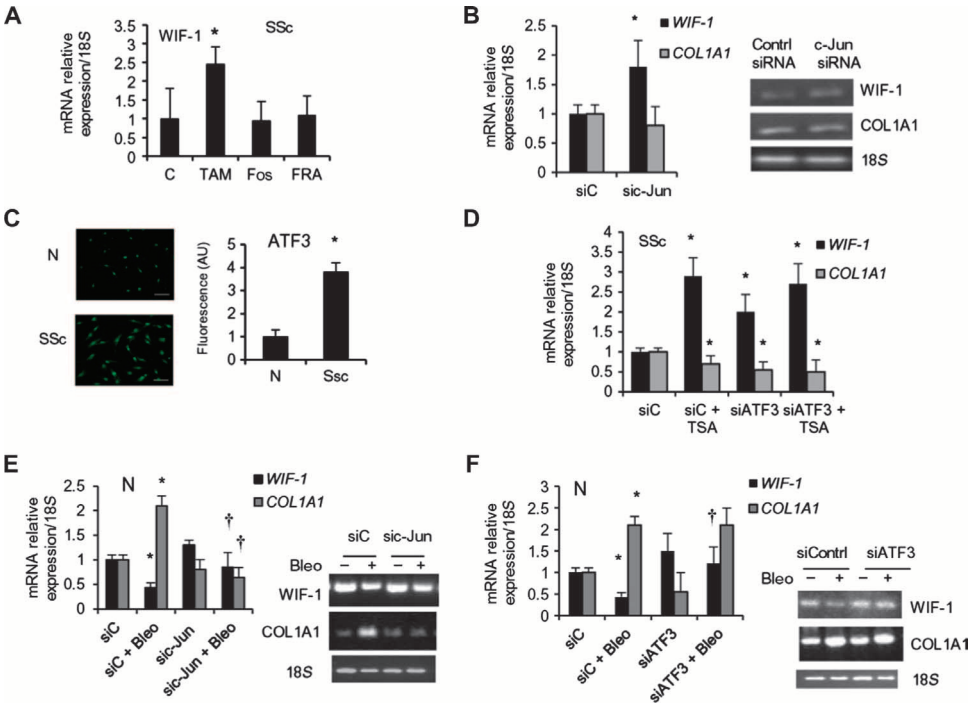

Fig. 5. The AP1 family member c-Jun and the stress-induced transcription factor ATF3 silence *WIF-1* and induce *COL1A1*. (**A**) *WIF-1* mRNA in SSc fibroblasts transfected with the control (C) or an AP1 family construct-encoding plasmid. (**B**) RT-PCR (left) or semiquantitative PCR (right) for *WIF-1* and *COL1A1* mRNA in SSc fibroblasts transfected with c-Jun siRNA (sic-Jun) or control siRNA (siC) for 48 hours. (**C**) Confocal microscopy for ATF3 in normal (N) or SSc fibroblasts. Scale bars, 100 μm. One hundred cells per field were scored. (**D**) *WIF-1* and *COL1A1* mRNA abundance in SSc fibroblasts transfected with ATF3 siRNA (siATF3) or control siRNA (siC) for 48 hours, and then treated with TSA (300 nM) for 24 hours, then lysed. (**E** and **F**) RT-PCR (left) or semiquantitative PCR (right) for *WIF-1* and *COL1A1* mRNA expression in normal fibroblasts transfected with control siRNA or siRNA against c-Jun (E) or ATF3 (F) for 48 hours and then treated with bleomycin (20 mU/ml) for 4 hours. Data in (A) to (F) are means ± SD from three independent experiments. $^{*}P < 0.05$ against basal or control, $^{\dagger}P < 0.05$ compared to bleomycin-treated cells.

repression of WIF-1; however, only c-Jun appeared to be involved in bleomycin-induced induction of *COL1A1* (Fig. 5, E and F). The different regulation of *COL1A1* in normal and SSc cells may be dependent on the abundance of other members of the AP1 family in SSc patient cells (*32*, *33*), but this is speculation and requires further investigation.

To dissect the roles of c-Jun and ATF3 on *WIF-1* expression, we monitored the recruitment of these two factors and a class I HDAC (HDAC3) to the promoter of *WIF-1*. In normal and SSc fibroblasts, ATF3, c-Jun, and HDAC3 each immunoprecipitated with the promoter of *WIF-1*, and the abundance of ATF3 and HDAC3 present on the promoter was increased in SSc patient cells (fig. S12, A to C). In SSc patient cells, partial knockdown of c-Jun with siRNA (figs. S11A and S13A) reduced the amount of ATF3 and HDAC3 that were bound to the *WIF-1* promoter (fig. S13, B and C). Partially silencing ATF3 (figs. S11C and S13D) also reduced the abundance of c-Jun that was bound to the *WIF-1* promoter (fig. S13E), whereas ATF3 knockdown had no significant effect on the recruitment of HDAC3 (fig. S13F). Together, the data suggest that although the amount of c-Jun that bound to *WIF-1* promoter in SSc and normal cells was similar (fig. S12B), recruitment of c-Jun and ATF3 to the *WIF-1* promoter in SSc cells was at least partially reciprocally dependent. We speculate that reciprocal stabilization of a complex between c-Jun and ATF3 (c-Jun/ATF3 complex) and c-Jun–mediated targeting of HDAC3 to the *WIF-1* promoter are responsible for WIF-1 silencing.

ATM activates ATF3 and c-Jun transcription factors

So far, the data indicate that ATM mediates the repression of WIF-1 after ROS or DNA damage, and that c-Jun and ATF3 have a role in silencing *WIF-1* expression in SSc patient cells. To investigate the link between ATM and the c-Jun/ATF3 complex, we analyzed this mechanism in response to DNA-damaging agents in normal cells compared with fibroblasts from ataxia telangiectasia (AT) patients, which are deficient for wild-type ATM. Unlike that in normal fibroblasts, ATF3 abundance was not induced by H_2O_2 in A-T fibroblasts (GM05823) (Fig. 6A). Because A-T fibroblasts additionally had not shown WIF-1 repression in response to H_2O_2 (Fig. 3F) or bleomycin (Fig. 4A), and we had inferred that ATF3 mediated the repression of WIF-1 in bleomycin-treated cells (Fig. 5F), we suggest that the transcriptional repression of *WIF-1* after DNA damage occurs in an ATM-dependent manner in normal fibroblasts.

Therefore, we examined the role of ATM in WIF-1 repression further by examining possible mediators between ATM and the c-Jun or ATF3 transcription factors. The phosphorylation of c-Jun at Ser^{73} and Thr^{91} by c-Jun N-terminal kinases 1 and 2 (JNK1/2) (*34*, *35*) was less in AT fibroblasts in response to H_2O_2 than in normal fibroblasts (fig. S14), suggesting that JNK may have a role downstream of ATM in repressing *WIF-1* expression. SSc cells had increased JNK-phosphorylated c-Jun, comparable to those induced by bleomycin in normal fibroblasts (Fig. 6B). Another site at the N terminus of c-Jun (Thr^{95}) is phosphorylated in stressed cells (*36*), and when mutated to a nonphosphorylatable residue (T95A) reduces JNK-mediated phosphorylation of c-Jun at Ser^{91} (*35*). In SSc cells, which also had increased ATF3 (Fig. 5C and fig. S11B), expression of the T95A c-Jun mutant induced *WIF-1* but suppressed *COL1A1* expression (Fig. 6C). In contrast, the phosphomimetic mutant c-Jun, T95D, did not significantly alter either WIF-1 or COL1A1 expression (Fig. 6C), possibly because the SSc cells are already saturated with ATM-phosphorylated c-Jun. We hypothesize that T95A c-Jun titrates the endogenous phosphorylated protein in heterodimers (with AP1 or ATF3). Conversely, in normal fibroblasts (in which c-Jun was not ATM-phosphorylated), the expression of the phosphomimetic c-Jun mutant T95D suppressed *WIF-1* and stimulated *COL1A1* expression, whereas the nonphosphorylatable mutant T95A had no significant effect (Fig. 6D). In normal fibroblasts, the phosphomimetic mutant T95D induced *ATF3* expression even in the presence of T95A because ATM-mediated phosphorylation is not active, suggesting that c-Jun phosphorylation is essential for *ATF3* induction (Fig. 6E).

To investigate whether ATM might be the kinase that phosphorylates the Thr^{95} site in c-Jun, HeLa cells (a cancer cell line of epithelial origin and amenable to transfection) and human fibroblasts were transfected with hemagglutinin (HA)–tagged wild-type or mutant c-Jun and treated with bleomycin to activate the pathway thus far investigated. In cell lysates, immunoprecipitation for the HA tag was performed followed by Western blotting with an antibody that detects phosphorylated Ser/Thr ATM/ATR substrates. Only wild-type c-Jun was detected by the antibody in HeLa

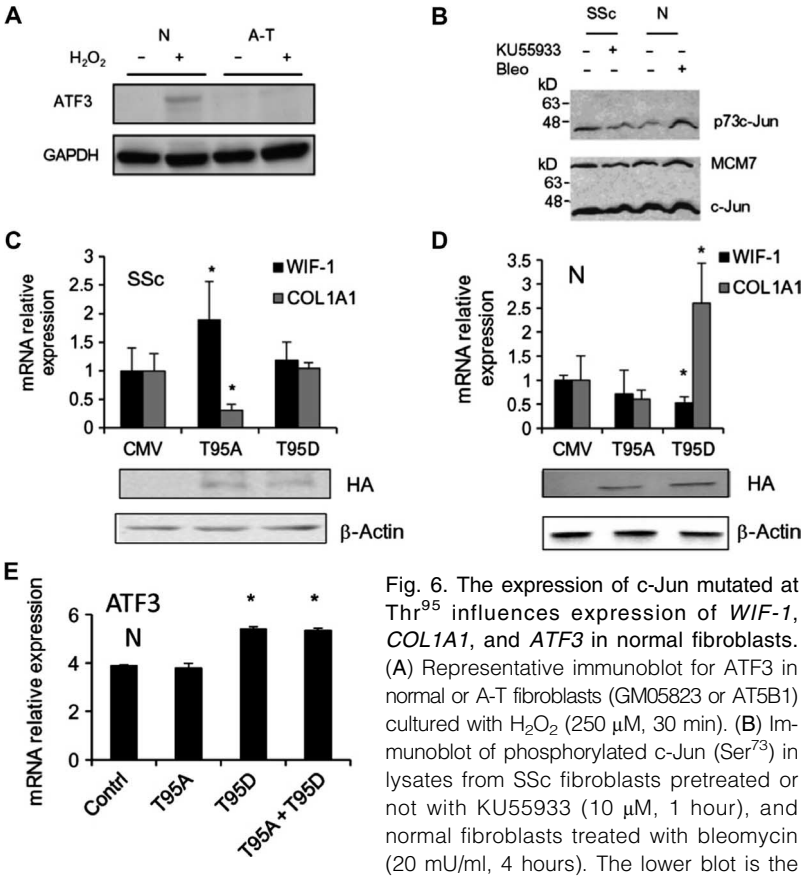

Fig. 6. The expression of c-Jun mutated at Thr^{95} influences expression of *WIF-1*, *COL1A1*, and *ATF3* in normal fibroblasts. (**A**) Representative immunoblot for ATF3 in normal or A-T fibroblasts (GM05823 or AT5B1) cultured with H_2O_2 (250 μM, 30 min). (**B**) Immunoblot of phosphorylated c-Jun (Ser^{73}) in lysates from SSc fibroblasts pretreated or not with KU55933 (10 μM, 1 hour), and normal fibroblasts treated with bleomycin (20 mU/ml, 4 hours). The lower blot is the upper gel reblotted for c-Jun and mini chromosome maintenance protein MCM7 (loading control). (**C** and **D**) RT-PCR analysis for *WIF-1* and *COL1A1* in SSc (C) and normal (D) fibroblasts transfected with empty vector [cytomegalovirus (CMV)] or vector encoding either wild-type or mutant HA-tagged c-Jun (T95A or T95D). Blots for HA below graphs confirm transfection. (**E**) RT-PCR analysis for ATF3 in normal fibroblasts transfected with T95D or T95A c-Jun–HA fusions. Blots are representative, and data in (C) to (E) are means ± SD of three independent experiments. *$P < 0.05$ compared to empty vector.

cells and fibroblasts (fig. S15, A and C). Endogenous c-Jun in HeLa cells (fig. S15B) or in normal fibroblasts (fig. S15D) exposed to bleomycin was recognized by this ATM substrate antibody, and the signal was inhibited by pharmacological inhibition (fig. S15, B and D) or siRNA-mediated knockdown of ATM (fig. S15E). These data suggest that ATM phosphorylates c-Jun at Thr^{95}. This may facilitate JNK-dependent phosphorylation of c-Jun (fig. S14) and the induction and recruitment of ATF3 (Fig. 6E) and HDAC3 (fig. S13C), and ultimately represses *WIF-1* expression, enabling Wnt signaling.

DISCUSSION

We showed that *WIF-1* expression is decreased in SSc cells through deacetylation induced by oxidative DNA damage, leading to increased Wnt signaling, associated with fibrosis. The suppression of *WIF-1* expression by oxidative DNA damage and ATM is unique among the Wnt inhibitors, and the indirect activation of ATF3 by ATM ties this mechanism to an extensive network of stress-inducible transcription factors (*37*). A schematic diagram illustrating the various components involved in WIF-1 silencing and COL1A1 induction in normal and SSc patient fibroblasts is shown in Fig. 7.

WIF-1 is a ROS marker

Our findings indicate that WIF-1 is a marker of oxidative DNA damage because ROS induced by short pulses of PDGF or low concentrations of H_2O_2 activated its expression, whereas higher ROS exposure silenced it. β-Catenin abundance asymmetrically followed WIF-1 suppression: low WIF-1 expression correlated with high total and nuclear β-catenin accumulation, leading to increased Wnt signaling, as seen in colon cells (*38*) or in mouse ectoderm (*39*). ROS can activate ATM directly (*20*, *40*) or through DNA damage (*22*), but we also propose that ROS are induced by the activity of ATM because inhibition of ATM reduced ROS. ATM seems to be a regulator of cellular ROS, and it may finely tune ROS content in stressed cells (*41*, *42*). When DNA is damaged, ATM induces ROS and transiently renders the cell refractory to exogenous signals. This ROS-adaptive response to stress is conserved in *Saccharomyces cerevisiae* (*43*), and we speculate that high levels of ROS during repair provide selection for increased fitness of stressed cells.

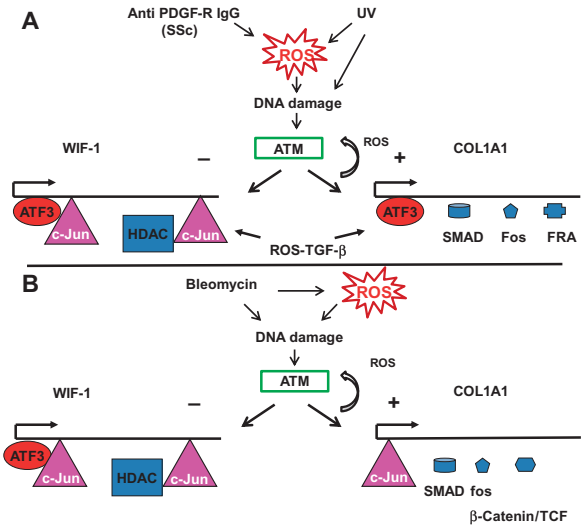

Fig. 7. Control of WIF-1 expression by stress and DNA damage. Schematic illustrating the series of events leading to WIF-1 silencing and collagen induction in SSc and normal cells. (**A**) In SSc, *COL1A1* can be induced by several members of the AP1 family (but not c-Jun), TGF-β signaling (through SMAD), and by ATF3. DNA damage or ROS activate ATM and JNK. ATM phosphorylates c-Jun and facilitates the phosphorylation of c-Jun by JNK. Phosphorylated c-Jun activates ATF3. c-Jun, ATF3, and HDAC3 bind the *WIF-1* promoter and repress its transcription. (**B**) In normal fibroblasts, bleomycin induces DNA damage, which activates ATM and ROS, which in turn activate c-Jun, JNK, and ATF3. As in SSc cells, ATF3, c-Jun, and HDAC3 are recruited to the *WIF-1* promoter and silence the gene. Unlike in SSc cells, however, c-Jun, in combination with other AP1 family members (for example, c-Fos), induces β-catenin/TCF–dependent Wnt signaling and *COL1A1* expression.

ATM is critical to the suppression of WIF-1

The transcription of *WIF-1* was regulated by ATF3 and c-Jun. ATF3 is a member of the CREB family and is induced by a variety of stress signals, including DNA damage (*31*). c-Jun is a member of the AP1 family of transcription factors and, by associating with various proteins, regulates the expression of genes involved in the cellular stress response (*44*, *45*). In our study, ATF3 was induced in normal cells only when ATM was functional, explaining why ATM-defective cells were unable to respond to bleomycin. In SSc cells, persistent oxidative stress (*10*) and DNA damage maintain a high abundance of ATF3 and phosphorylated c-Jun, which are recruited to the *WIF-1* promoter and silence the gene, resulting in increased Wnt signaling (*9*). Our data also suggest that ATM amplifies the efficacy of JNK-mediated phosphorylation of c-Jun, revealing a possible explanation for why ATM-defective livers show reduced phosphorylated c-Jun (*46*). In our study, under conditions of DNA damage, ROS-adaptive response induced by ATM stimulates JNK, c-Jun, and, eventually, ATF3 expression (*47*). Thus, ATF3 and phosphorylated c-Jun enhance Wnt signaling perhaps by two mechanisms: by reducing WIF-1–mediated inhibition of soluble Wnt, and by cooperating with β-catenin to induce transcription (*48*).

The mechanism of *WIF-1* silencing has implications for cancer and fibrosis

WIF-1 silencing is a selected phenotype both in stressed mesenchymal cells and in epithelial neoplastic cells. *WIF-1* is one of the most frequent silenced genes in cancer, and its loss is common in many tumors (*14*, *49*). Targeted disruption of WIF-1 accelerates osteosarcomagenesis, without interfering with normal bone development in mice (*50*). Our data suggest that persistent oxidative DNA damage initially silences WIF-1 by histone deacetylation in fibroblasts and possibly other cell types, whereas WIF-1 is silenced predominantly by methylation in epithelial cells (*14*). We speculate that in fibroblasts, robust stimulation of histone acetylation can reactivate the expression of the gene and repress Wnt signaling, whereas in epithelial cells, WIF-1 silencing may be permanent, irreversible, and positively selected during neoplastic progression (*49*, *51*).

If WIF-1 silencing occurs in mesenchymal cells, Wnt signaling leads to senescence and exit from the cycle (*52*); differentiated myofibroblasts (*6*) or myoblasts (*8*) exit from the cycle, synthesize collagen or α-SMA, and accumulate ROS and β-catenin, which are the hallmarks of fibrosis and wound healing (*9*, *10*, *52*, *53*). PDGF or TGF-β and other soluble factors (such as the IgG of SSc patients) cooperate efficiently with β-catenin to activate a transcription program leading to fibrosis and senescence (*54*). We propose that WIF-1 silencing is accomplished by two ROS signaling cascades: (i) low or transient ROS (TGF-β) activate HDAC (*22*–*24*), but not ATM; (ii) high or persistent ROS induce DNA damage and ATM. From this perspective, fibrosis represents an amplified secretory response of senescent fibroblasts to DNA damage associated with wound healing

(*55*). We speculate that loss of secreted WIF-1 amplifies local Wnt action and induces a proliferative burst of surrounding epithelial cells and terminal differentiation of fibroblasts. Only cells that have efficiently repaired the DNA respond to Wnt because damaged cells succumb to apoptosis through clashing signals of arrest and stimulation of growth. This provides a robust selection for fitness of epithelial cells surrounding damaged and senescent fibroblasts. Our findings in a breast cancer epithelial cell line suggests that methylation of the *WIF-1* promoter might reinforce local Wnt signaling in epithelial cells (*56*). This finding provides a mechanism linking ROS, DNA damage, fibrosis, and cancer (*57*) and may explain the higher incidence of lung cancer in SSc patients (*58*).

In conclusion, our findings exploring activated Wnt signaling in fibrosis or during neoplastic progression indicate that DNA damage and genome stability checkpoints link ROS, Wnt, and fibrosis, thus integrating many apparently heterogeneous phenotypes associated with fibrosis and cancer.

MATERIALS AND METHODS

Antibody purification

IgGs were purified from the serum of normal and SSc human subjects, after oral and written informed consent, using gravity flow columns packed with Protein A/G–agarose following the manufacturer's instructions (Pierce). The eluted IgG fractions were subjected to buffer exchange with PBS using desalting columns (limit of 5 kD) (Pierce). Purity of IgG preparations was confirmed by immunoblotting with specific cytokine antibodies [PDGF, TGF-β, and IL-1 to IL-6 (interleukin-1 to -6)]. For the recombinant antibody VH PAM-Vk16F4, the VH and VL sequences were cloned from the cDNA (complementary DNA) of peripheral lymphocytes of an SSc patient. Sequence analysis identified the VH and VL sequences, which were inserted into the Xba I–Sac I and Hind III–Eco RI restriction sites, respectively, under the control of the human cytomegalovirus (HCMV) promoter in the plasmid vector pDR12, which contains an ampicillin resistance gene for selective amplification (fig. S16). The plasmid was amplified in *E. coli* and transfected into Chinese hamster ovary cells, and the IgG was purified by immunoaffinity. The study was approved by the institutional ethics committee at the Università Politecnica delle Marche.

Cells and treatments

Human skin fibroblasts were obtained from punch biopsies taken from the forearms of normal volunteers and from the skin of patients who fulfilled the preliminary criteria of the American Rheumatism Association for the diagnosis of SSc, as described previously (*42*). Mouse embryo fibroblasts (MEFs) derived from PDGF receptor knockout embryos that do not express α and β chains of PDGFR subunits (F–/– cells) infected with PDGFR α subunit (Fα cells) were previously described (*11*). Fibroblasts, HeLa cells, and MEFs were grown in Dulbecco's modified Eagle's medium (DMEM), containing glucose (1 g/liter), supplemented with 10% fetal bovine serum (FBS), penicillin (100 U/ml), and streptomycin (100 g/ml) (Gibco). Human control (GM00024) and A-T fibroblasts (GM05823 also known as AT5B1) were obtained from Coriell Institute and maintained in EMEM (Eagle's minimum essential medium) supplemented with 15% FBS, penicillin/streptomycin (100 mU/ml), and 2 mM glutamine (Gibco). For PDGF treatments, subconfluent fibroblasts were treated with IgG (0.2 μg/μl) or recombinant PDGF-BB (15 ng/ml) (Sigma) after 4 hours of starvation (0.2% FBS) for 24 hours. In selected experiments, cells were incubated with 300 nM TSA (Sigma) for 48 hours, 4 μM 5-aza-2′-deoxycytidine (5-azacytdine; Sigma) for 24 hours, cisplatinum (5 μM; Sigma) for 24 hours, 10 μM DPI (Calbiochem) for 1 hour, KU55933 (Calbiochem) for 1 hour, and bleomycin (20 mU/ml; Sigma) for 4 or 24 hours, as indicated in the relevant legend. For UV experiments, cells were pretreated with 10 μM KU55933for 1 hour and then irradiated with UV (80 J/m^2) and incubated for a further 1 or 2 hours. Cells were transiently transfected with siRNA against *c-JUN* (Santa Cruz), *ATF-3* (Qiagen), *ATM* (Qiagen), or *WIF-1* (Santa Cruz), or transfected with the dominant-negative AP1 constructs c-Jun–derived GFP (green fluorescent protein)–TAM67 and c-Fos–derived GFP–a-Fos plasmids (*26*), or the T95A or T95D c-Jun mutant (*32*) using Lipofectamine 2000 reagent (Life Technologies) following the manufacturer's instructions. Cells were processed 48 hours after transfection, except the WIF-1 siRNA-transfected cells, which were lysed 72 hours after the transfection.

Western blotting analysis

Total cell lysates were obtained in radioimmunoprecipitation assay (RIPA) buffer (2.5 mM Na-pyrophosphate, 1 mM β-glycerophosphate, 1 mM $NaVO_4$, 1 mM NaF; Sigma) supplemented with a cocktail of protease inhibitors. The samples were stored for 30 min at 4°C and centrifuged at 10,000 rpm for 10 min at 4°C. Samples were resolved on a 4 to 12% gradient SDS–polyacrylamide gel electrophoresis (SDS-PAGE) and transferred onto a nitrocellulose membrane (Life Technologies). After blocking with 0.5% Tween for 1 hour, immunoblots were incubated with antibodies against WIF-1 (1:1000; Abcam), β-catenin (1:1000; Abcam), pATM (1:500; Abcam,), ATM (1: 500; Novus Biologicals), 53BP1 (1:500; Novus Biologicals), β-actin (1:1000; Santa Cruz Biotechnology), phospho-(Ser/Thr) ATM/ATR substrate antibody (1:1000, Cell Signaling Technology), HA (1:500; Covance), Ser^{73} c-Jun (1:1000; Cell Signaling Technology), and Thr^{91} c-Jun (1:1000; Cell Signaling Technology) overnight at 4°C. After incubation with horseradish peroxidase (HRP)–conjugated antibodies against rabbit or mouse IgG (Santa Cruz Biotechnology) for 1 hour, signals were detected with ECL Western Blotting Detection Reagents (Amersham Bioscience).

ROS detection

Fluorimetric determination of intracellular ROS was carried out using DCFH-DA (Life Technologies), as previously described (*9*), using a multiwell plate reader (Wallac 1420, PerkinElmer). For confocal microscopy experiments, cells were seeded on coverlids, loaded with 10 μM DCFH-DA or 10 μM DHE (Life Technologies) for 30 min, washed with PBS, and then visualized on a confocal microscope Eclipse C1 (Nikon).

Quantitative real-time PCR analysis

Total RNA isolation from normal, scleroderma, and *ATM*$^{-/-}$ fibroblasts was isolated with PureLink RNA Mini Kit (Life Technologies) according to the manufacturer's instructions. Total RNA (1 g) of each sample was reverse-transcribed with the iScript cDNA Synthesis Kit (Bio-Rad) according to the manufacturer's instructions. Quantitative RT-PCR was performed with SYBR Green PCR Master Mix (Bio-Rad). Primers sequences for amplification are represented in table S1. The amplification was carried out through 45 cycles of 95°C for 15 s and 60°C for 1 min in a iCycler iQ Real-Time PCR Detection System (Bio-Rad). Relative expression was calculated with the $2^{-\Delta\Delta Ct}$ method.

Methylation analysis using bisulphite genomic sequencing

The promoter region and the entire coding sequence of human *WIF-1* gene were analyzed for CG content. A CpG island was determined on the basis of a 200–base pair (bp) length of DNA with a CG content greater than 50% and a CpG/GpC ratio greater than 0.5 using CpG plot program (http://www.ebi.ac.uk/emboss/cpgplot/). Bisulphite genomic sequencing was used to analyze the methylation patterns of individual DNA molecules. Sodium

bisulphite conversion of genomic DNA (about 2 μg for each conversion) was obtained using EpiTect Bisulfite Kit (Qiagen) following the purchaser's instructions. Amplicons used for methylation analysis were obtained from about 50 ng of bisulphite threaded genomic DNA. Specific primers used for these PCRs were as follows: WifBS-Fw1: –409 –390 5′-GAGTGATGTTTTAGGGGTTT-3′, WifBS-Rv1: –16 +5 5′-CCTAAATACCAAAAAACCTAC-3′, WifBS-Fw2: 16 +5 5′-GTAGGTTTTTTGGTATTTAGG-3′, WifBS-Rv2: +242 +263 5′-TCCATAAATACAAACTCTCCTC-3′. Amplifications were carried out on 10 ng of bisulphite-treated DNA using HotStarTaq DNA Polymerase (Qiagen) for 15 min at 95°C, followed by 50 cycles of 30 s at 95°C, 40 s at 53°C, and 1 min at 72°C, then a final elongation of 10 min at 72°C before holding at 4°C in a final reaction volume of 50 μl. Confirmation of PCR product quality and freedom from contamination was established on 2% agarose gels with ethidium bromide staining. PCR products were cloned into the pGEM-T Easy Vector provided by Promega pGEM-T Easy Vector System II, following the manufacturer's procedures. Positive-screened colonies contained the unique sequence of one individual DNA molecule. Plasmid DNA from the selected positive colonies containing vectors with the insert was purified using the Qiagen Plasmid Mini Kit. Purified plasmids were sequenced in both directions using T7 and Sp6 primers. Twenty independent clones for each genomic preparation and fragment of interest were sequenced to determine the methylation pattern of individual molecules. Sequencing was performed at the CEINGE Sequencing Core Facility, Naples, Italy.

Bleomycin-induced dermal fibrosis

Skin fibrosis was induced in 6- to 8-week-old C3H/HeJ mice by subcutaneous injection in defined areas of the upper back of bleomycin for 24 to 28 days as described (*27*).

Histological analysis

Skin sections were fixed in 4% formalin and embedded in paraffin. Sections (5 μm) were stained with Sirius Red for the analysis of connective tissue, and dermal thickness was analyzed by measuring the distance between the epidermal-dermal junction and the dermal–subcutaneous fat junction at sites of induration in three consecutive skin sections from each animal. In each series of experiments, the dermal thickness was calculated as the fold increase compared with the dermal thickness in controls.

Immunohistochemistry

Skin sections were deparaffinized, rehydrated, and stained with WIF-1 and β-catenin antibodies (1:100; Abcam) overnight at 4°C, washed, and incubated with biotinylated mouse IgG antibody for 1 hour at room temperature. The peroxidase ABC method was performed for 1 hour using diaminobenzidine hydrochloride (DAB) as chromogen.

Immunofluorescence

Cells were fixed for 5 min with 4% paraformaldehyde, permeabilized with 0.2% Triton X-100, and incubated with the following primary antibodies overnight at 4°C: WIF-1 (1:100; Abcam), β-catenin (1:100; Abcam,), pATM (1:100; Abcam), and type 1 collagen (1:200; Millipore). Cells were then washed and labeled with Alexa 488– or Alexa 546–conjugated antibodies (Life Technologies) and counterstained with SYTOX Green, a DNA counterstain for fixed cells (Life Technologies). Controls were incubated with secondary antibodies alone. Cells were analyzed using the confocal microscope Eclipse C1 (Nikon).

Chromatin immunoprecipitation

Cells (1×10^6) were fixed by adding formaldehyde directly to culture medium to a final concentration of 1% for 10 min at room temperature and washed twice using ice-cold PBS containing 1× protease inhibitor cocktail (Roche Applied Science) and 1 mM PMSF (phenylmethylsulfonyl fluoride). Fixed cells were harvested, and the pellet was resuspended in 200 μl of SDS lysis buffer [Chromatin Immunoprecipitation (ChIP) Assay Kit, Upstate]. After 10 min of incubation on ice, the lysates were sonicated to shear DNA to 300- and 1000-bp fragments. Sonicated samples were centrifuged and supernatants were diluted 10-fold in the ChIP dilution buffer (ChIP Assay Kit, Upstate). An aliquot (1:50) of sheared chromatin was further treated with proteinase K, phenol/chloroform-extracted, and precipitated to determine DNA concentration and shearing efficiency (input DNA). The ChIP reaction was set up according to the manufacturer's instructions. Briefly, the sheared chromatin was precleared for 2 hours with 20 μl of Protein A– or Protein G–agarose (Upstate) and 2 μg of nonimmune IgG (Santa Cruz Biotechnology), and then was divided into two aliquots and incubated at 4°C for 16 hours with 20 μl of Protein A/G–agarose and 2 μg of the specific antibody ATF3 (Santa Cruz Biotechnology), HDAC3 (Santa Cruz Biotechnology), c-Jun (Santa Cruz Biotechnology), and nonimmune IgG, respectively. Agarose beads were washed with wash buffers according to the manufacturer's instructions, and immunoprecipitated DNA was recovered and subjected to quantitative PCR using the primers indicated in the legend of the specific figures and in table S1. Primers for *WIF-1* ChIP were (forward) 5′-CGGGTTATCAGGGAGACAGA-3′ and (reverse) 5′-CTCCCTTTCAGCCAGTAGGA-3′.

Ethical statement

Use of human material was approved by the Institutional Ethical Committee of Università Politecnica delle Marche, Ancona, Italy, and consent was obtained from all subjects who participated in this study. All assays were performed in blind fashion on coded samples.

Statistics

Data were quantified as means ± SD and were analyzed with the nonparametric Mann-Whitney test. Data were analyzed using Prism 4 (GraphPad Software Inc.). *P* values less than 0.05 were considered significant.

SUPPLEMENTARY MATERIALS

www.sciencesignaling.org/cgi/content/full/7/341/ra84/DC1

Fig. S1. *WIF-1* is methylated in MCF7 breast cancer cells, not in normal or SSc fibroblasts.
Fig. S2. *WIF-1* silencing induces β-catenin abundance.
Fig. S3. The oxidase inhibitor DPI inhibits ROS accumulation in SSc cells.
Fig. S4. Among Wnt inhibitors, only *WIF-1* is silenced by ATM.
Fig. S5. ATM mediates H_2O_2-induced silencing of *WIF-1*.
Fig. S6. Loss of ATM restores WIF-1 abundance in SSc fibroblasts and inhibits bleomycin-induced silencing of *WIF-1*.
Fig. S7. Inhibition of ROS production in SSc cells increases *WIF-1* expression and inhibits expression of the gene encoding collagen.
Fig. S8. The effects of HDAC and ATM inhibitors on *WIF-1* expression are not additive.
Fig. S9. Bleomycin-induced skin fibrosis is inhibited by an HDAC inhibitor, TSA.
Fig. S10. NF-κB does not mediate *WIF-1* silencing induced by ROS.
Fig. S11. Efficiency of c-Jun and ATF3 knockdown.
Fig. S12. ATF3, c-Jun, and HDAC3 are recruited to the *WIF-1* promoter in SSc cells.
Fig. S13. The recruitment of c-Jun to the *WIF-1* promoter in SSc cells is partially dependent on ATF3.
Fig. S14. Phosphorylation of c-Jun is induced by H_2O_2 in wild-type, but not in A-T, cells.
Fig. S15. c-Jun is a substrate of ATM in HeLa cells and human fibroblasts exposed to bleomycin.
Fig. S16. pDR12 plasmid construct.
Table S1. List of primers.

REFERENCES AND NOTES

1. J. C. Gross, V. Chaudhary, K. Bartscherer, M. Boutros, Active Wnt proteins are secreted on exosomes. *Nat. Cell Biol.* **10**, 1036–1045 (2012).
2. L. Ling, V. Nurcomb, S. M. Cool, Wnt signaling controls the fate of mesenchymal stem cells. *Gene* **433**, 1–7 (2009).

3. C. M. Cruciat, C. Niehrs, Secreted and transmembrane Wnt inhibitors and activators. *Cold Spring Harb. Perspect. Biol.* **5**, a015081 (2013).
4. Y. Kawano, R. Kypta, Secreted antagonists of the Wnt signaling pathway. *J. Cell Sci.* **1**, 2627–2634 (2003).
5. J. C. Hsieh, L. Kodjabachian, M. L. Rebbert, A. Rattner, P. M. Smallwood, C. H. Samos, R. Nusse, I. B. Dawid, J. Nathans, A new secreted protein that binds to Wnt proteins and inhibits their activities. *Nature* **398**, 431–436 (1999).
6. C. Wissmann, P. J. Wild, S. Kaiser, S. Roepcke, R. Stoehr, M. Woenckhaus, G. Kristiansen, J. Hsieh, F. Hofstaedter, A. Hartmann, R. Knuechel, A. Rosenthal, C. Pilarsky, WIF1**,** a component of the Wnt pathway, is down-regulated in prostate, breast, lung, and bladder cancer. *J. Pathol.* **201**, 204–212 (2003).
7. J. Mazieres, B. He, L. You, Z. Xu, A. Y. Lee, I. Mikami, N. Reguart, R. Rosell, F. McCormick, D. M. Jablons, Wnt inhibitory factor-1 is silenced by promoter hypermethylation in human lung cancer. *Cancer Res.* **64**, 4717–4720 (2004).
8. A. S. Brack, M. J. Conboy, S. Roy, M. Lee, C. J. Kuo, C. Keller, T. A. Rando, Increased Wnt signaling during aging alters muscle stem cell fate and increases fibrosis. *Science* **317**, 807–810 (2007).
9. C. Beyer, A. Schramm, A. Akhmetshina, C. Dees, T. Kireva, K. Gelse, S. Sonnylal, B. de Crombrugghe, M. M. Taketo, O. Distler, G. Schett, J. H. Distler, β-Catenin is a central mediator of pro-fibrotic Wnt signaling in systemic sclerosis. *Ann. Rheum. Dis.* **71**, 761–767 (2012).
10. S. Svegliati, R. Cancello, P. Sambo, M. Luchetti, P. Paroncini, G. Orlandini, G. Discepoli, R. Paternò, M. Santillo, C. Cuozzo, S. Cassano, E. V. Avvedimento, A. Gabrielli, Platelet-derived growth factor and reactive oxygen species (ROS) regulate Ras protein levels in primary human fibroblasts via ERK1/2. Amplification of ROS and Ras in systemic sclerosis fibroblasts. *J. Biol. Chem.* **280**, 36474–36482 (2005).
11. S. S. Baroni, M. Santillo, F. Bevilacqua, M. Luchetti, T. Spadoni, M. Mancini, P. Fraticelli, P. sambo, A. Funaro, A. Kazlauskas, E. V. Avvedimento, A. Gabrielli, Stimulatory auto-antibodies to the PDGF receptor in systemic sclerosis. *N. Engl. J. Med.* **354**, 2667–2676 (2006).
12. Y. Ying, Q. Tao, Epigenetic disruption of the WNT/β-catenin signaling pathway in human cancers. *Epigenetics* **4**, 307–312 (2009).
13. J. Wei, F. Fang, A. P. Lam, J. L. Sargent, E. Hamburg, M. E. Hinchcliff, C. J. Gottardi, R. Atit, M. L. Whitfield, J. Varga, Wnt/β-catenin signaling is hyperactivated in systemic sclerosis and induces Smad-dependent fibrotic responses in mesenchymal cells. *Arthritis Rheum.* **64**, 2734–2745 (2012).
14. L. Ai, Q. Tao, S. Zhong, C. R. Fields, W. Kim, M. W. Lee, Y. Cui, K. D. Brown, K. D. Robertson, Inactivation of Wnt inhibitory factor-1 (WIF1) expression by epigenetic silencing is a common event in breast cancer. *Carcinogenesis* **27**, 1341–1348 (2006).
15. R. Gherzi, M. Trabucchi, M. Ponassi, T. Ruggiero, G. Corte, C. Moroni, C. Y. Chen, K. S. Khabar, J. S. Andersen, P. Briata, The RNA-binding protein KSRP promotes decay of β-catenin mRNA and is inactivated by PI3K-AKT signaling. *PLOS Biol.* **5**, e5 (2006).
16. M. Königshoff, N. Balsara, E. M. Pfaff, M. Kramer, I. Chrobak, W. Seeger, O. Eickelberg, Functional Wnt signaling is increased in idiopathic pulmonary fibrosis. *PLOS One* **3**, e2142 (2008).
17. A. Akhmetshina, K. Palumbo, C. Dees, C. Bergmann, P. Venalis, P. Zerr, A. Horn, T. Kireva, C. Beyer, J. Zwerina, H. Schneider, A. Sadowski, M. Riener, O. A. MacDougald, O. Distler, G. Sheet, J. Distler, Activation of canonical Wnt signaling is required for TGF-β-mediated fibrosis. *Nat. Commun.* **3**, 735 (2012).
18. J. H. Cheng, H. She, Y. Han, J. Wang, S. Xiong, K. Asahina, H. Tsukamoto, Wnt antagonism inhibits hepatic stellate cell activation and liver fibrosis. *Am. J. Physiol. Gastrointest. Liver Physiol.* **294**, G39–G49 (2008).
19. S. Damiano, R. Fusco, A. Morano, M. De Mizio, R. Paternò, A. De Rosa, R. Spinelli, S. Amente, R. Frunzio, P. Mondola, F. Miot, P. Laccetti, M. Santillo, E. V. Avvedimento, Reactive oxygen species regulate the levels of dual oxidase (Duox1-2) in human neuroblastoma cells. *PLOS One* **7**, e34405 (2012).
20. Z. Guo, S. Kozlov, M. F. Lavin, M. D. Person, T. T. Paul, ATM activation by oxidative stress. *Science* **330**, 517–521 (2010).
21. J. Chen, J. Stubbe, Bleomycins: Towards better therapeutics. *Nat. Rev. Cancer* **5**, 102–112 (2005).
22. A. Shibata, O. Barton, A. T. Noon, K. Dahm, D. Deckbar, A. A. Goodarzi, M. Löbrich, P. A. Jeggo, Role of ATM and the damage response mediator proteins 53BP1 and MDC1 in the maintenance of G_2/M checkpoint arrest. *Mol. Cell. Biol.* **30**, 3371–3383 (2010).
23. S. Bhattacharyya, J. Wei, W. G. Tourtellotte, M. Hinchcliff, C. G. Gottardi, J. Varga, Fibrosis in systemic sclerosis: Common and unique pathobiology. *Fibrogenesis Tissue Repair* **5** (Suppl. 1), S18 (2012).
24. H. Noh, E. Y. Oh, J. Y. Seo, M. R. Yu, Y. O. Kim, H. Ha, H. B. Lee, Histone deacetylase-2 is a key regulator of diabetes- and transforming growth factor-β1-induced renal injury. *Am. J. Physiol. Renal Physiol.* **297**, F729–F739 (2009).
25. H. Zhu, L. Shan, P. W. Schiller, A. Mai, T. Peng, Histone deacetylase-3 activation promotes tumor necrosis factor-α (TNF-α) expression in cardiomyocytes during lipopolysaccharide stimulation. *J. Biol. Chem.* **285**, 9429–9436 (2010).
26. N. Koshikawa, J. Hayashi, A. Nakagawara, K. Takenaga, Reactive oxygen species-generating mitochondrial DNA mutation up-regulates hypoxia-inducible factor-1α gene transcription via phosphatidylinositol 3-kinase-Akt/protein kinase C/histone deacetylase pathway. *J. Biol. Chem.* **284**, 33185–33194 (2009).
27. L. C. Huber, J. Distler, F. Moritz, H. Hemmatazad, T. Hauser, B. A. Michel, R. E. Gay, M. Matucci-Cerinic, S. Gay, O. Distler, A. Jüngel, Trichostatin A prevents the accumulation of extracellular matrix in a mouse model of bleomycin-induced skin fibrosis. *Arthritis Rheum.* **56**, 2755–2764 (2007).
28. F. Pacifico, C. Mauro, C. Barone, E. Crescenzi, S. Mellone, M. Monaco, G. Chiappetta, G. Terrazzano, D. Liguoro, P. Vito, E. Consiglio, S. Formisano, A. Leonardi, Oncogenic and anti apoptotic activity of NF-κB in human thyroid carcinomas. *J. Biol. Chem.* **279**, 54610–54619 (2004).
29. M. Bahassi el, S. Karyala, C. R. Tomlinson, M. A. Sartor, M. Medvedovic, R. F. Hennigan, Critical regulation of genes for tumor cell migration by AP-1. *Clin. Exp. Metastasis* **21**, 293–304 (2004).
30. F. Talotta, T. Mega, G. Bossis, L. Casalino, J. Basbous, I. Jariel-Encontre, M. Piechaczyk, P. Verde, Heterodimerization with Fra-1 cooperates with the ERK pathway to stabilize c-Jun in response to the RAS oncoprotein. *Oncogene* **29**, 4732–4740 (2010).
31. T. Hai, C. D. Wolfgang, D. K. Marsee, A. E. Allen, U. Sivaprasad, ATF3 and stress responses. *Gene Expr.* **7**, 321–335 (1999).
32. K. Y. Chung, A. Agarwal, I. Uitto, A. Mauviel, An AP-1 binding sequence is essential for regulation of the human α2(I) collagen (COL1A2) promoter activity by transforming growth factor-β. *J. Biol. Chem.* **271**, 3272–3278 (1996).
33. A. K. Ghosh, Factors involved in the regulation of type I collagen gene expression: Implication in fibrosis. *Exp. Biol. Med.* **227**, 301–314 (2002).
34. S. Morton, R. J. Davis, A. McLaren, P. Cohen, A reinvestigation of the multisite phosphorylation of the transcription factor c-Jun. *EMBO J.* **22**, 3876–3886 (2003).
35. M. Vinciguerra, I. Esposito, S. Salzano, A. Madeo, G. Nagel, M. Maggiolini, A. Gallo, A. M. Musti, Negative charged threonine 95 of c-Jun is essential for c-Jun N-terminal kinase-dependent phosphorylation of threonine 91/93 and stress-induced c-Jun biological activity. *Int. J. Biochem. Cell Biol.* **40**, 307–316 (2008).
36. C. E. Reddy, L. Albaniro, P. De Marco, D. Aiello, M. Maggiolini, A. Napoli, A. M. Musti, Multisite phosphorylation of c-Jun at threonine 91/93/95 triggers the onset of c-Jun pro/apoptotic activity in cerebellar granule neurons. *Cell Death Dis.* **4**, e852 (2013).
37. Y. Tanaka, A. Nakamura, M. S. Morioka, S. Inoue, M. Tamamori-Adachi, K. Yamada, K. Taketani, J. Kawauchi, M. Tanaka-Okamoto, J. Miyoshi, H. Tanaka, S. Kitajima, Systems analysis of ATF3 in stress response and cancer reveals opposing effects on pro-apoptotic genes in p53 pathway. *PLOS One* **6**, e26848 (2011).
38. M. Cebrat, L. Strzadala, P. Kisielow, Wnt inhibitory factor-1: A candidate for a new player in tumorigenesis of intestinal epithelial cells. *Cancer Lett.* **206**, 107–113 (2004).
39. J. W. Wen, J. T. Hwang, G. M. Kelly, Reactive oxygen species and Wnt signalling crosstalk patterns mouse extraembryonic endoderm. *Cell. Signal.* **24**, 2337–2348 (2012).
40. Z. Guo, R. Deshpande, T. Paull, ATM activation in the presence of oxidative stress. *Cell Cycle* **9**, 4805–4811 (2010).
41. C. Cosentino, D. Grieco, V. Costanzo, ATM activates the pentose phosphate pathway promoting anti-oxidant defence and DNA repair. *EMBO J.* **30**, 546–555 (2011).
42. A. Gabrielli, E. V. Avvedimento, T. Krieg, Scleroderma. *N. Engl. J. Med.* **360**, 1989–2003 (2009).
43. L. A. Rowe, N. Degtyareva, P. W. Doetsch, DNA damage-induced reactive oxygen species (ROS) stress response in *Saccharomyces cerevisiae*. *Free Radic. Biol. Med.* **45**, 1167–1177 (2008).
44. D. Lallemand, G. Spyrou, M. Yaniv, C. M. Pfarr, Variations in Jun and Fos protein expression and AP-1 activity in cycling, resting and stimulated fibroblasts. *Oncogene* **14**, 819–830 (1997).
45. Y. Chinenov, T. Kerppola, Close encounters of many kinds: Fos-Jun interactions that mediate transcription regulatory specificity. *Oncogene* **20**, 2438–2452 (2001).
46. L. Shu, K. C. Shen, Y. Wang, S. C. Brooks, Y. A. Wang, Impaired hepatocyte survival and liver regeneration in Atm-deficient mice. *Hum. Mol. Genet.* **14**, 3019–3025 (2005).
47. G. Liang, C. D. Wolfgang, B. P. Chen, T. H. Chen, T. Hai, *ATF3* gene. Genomic organization promoter, and regulation. *J. Biol. Chem.* **271**, 1695–1701 (1996).
48. K. Toualbi, M. C. Güller, J. L. Mauriz, C. Labalette, M. A. Buendia, A. Mauviel, D. Bernuau, Physical and functional cooperation between AP-1 and β-catenin for the regulation of TCF-dependent genes. *Oncogene* **26**, 3492–3502 (2007).
49. A. L. Delmas, B. M. Riggs, C. E. Pardo, L. M. Duer, R. P. Darst, E. G. Izumchenko, M. Monroe, A. Hakam, M. P. Kladde, E. M. Siegel, K. D. Brown, *WIF1* is a frequent target for epigenetic silencing in squamous cell carcinoma of the cervix. *Carcinogenesis* **32**, 1625–1633 (2011).
50. M. Kansara, M. Tsang, L. Kodjabachian, N. A. Sims, M. K. Trivett, M. Ehrich, A. Dobrovic, J. slavin, P. F. Choong, P. J. Simmons, I. B. Dawid, D. M. Thomas, Wnt inhibitory factor 1 is epigenetically silenced inhuman osteosarcoma, and targeted disruption accelerates osteosarcomagenesis in mice. *J. Clin. Invest.* **119**, 837–851 (2009).
51. E. V. Avvedimento, S. Obici, M. Sanchez, A. Gallo, A. Musti, M. E. Gottesman, Reactivation of thyroglobulin gene expression in transformed thyroid cells by 5-azacytidine. *Cell* **58**, 1135–1142 (1989).

52. B. L. Vaes, K. J. Dechering, E. P. van Someren, J. M. Hendriks, C. J. van de Ven, A. Feijen, C. L. Mummery, M. J. Reinders, W. Olijve, E. J. van Zoelen, W. T. Steegenga, Microarray analysis reveals expression regulation of Wnt antagonists in differentiating osteoblasts. *Bone* **36**, 803–811 (2005).
53. M. Bocchino, S. Agnese, E. Fagone, S. Svegliati, D. Grieco, C. Vancheri, A. Gabrielli, A. Sanduzzi, E. V. Avvedimento, Reactive oxygen species are required for maintenance and differentiation of primary lung fibroblasts in idiopathic pulmonary fibrosis. *PLOS One* **5**, e14003 (2010).
54. D. Y. Zhang, Y. Pan, C. Zhang, B. X. Yan, S. S. Yu, D. L. Wu, M. M. Shi, K. Shi, X. X. Cai, S. S. Zhou, J. B. Wang, J. P. Pan, L. H. Zhang, Wnt/β-catenin signaling induces the aging of mesenchymal stem cells through promoting the ROS production. *Mol. Cell. Biochem.* **374**, 13–20 (2013).
55. A. Milano, S. A. Pendergrass, J. L. Sargent, L. K. George, T. H. McCalmont, M. K. Connolly, M. L. Whitfield, Molecular subsets in the gene expression signatures of scleroderma skin. *PLOS One* **3**, e2696 (2008).
56. D. Wu, P. Wong, W. Li, C. F. Vogel, F. Matsumura, Suppression of *WIF-1* through promoter hypermethylation causes accelerated proliferation of the aryl hydrocarbon receptor (AHR) overexpressing MCF10AT1 breast cancer cells. *Toxicology* **285**, 97–103 (2011).
57. J. Behari, The Wnt/β-catenin signaling pathway in liver biology and disease. *Expert Rev. Gastroenterol. Hepatol.* **4**, 745–759 (2010).
58. M. Bonifazi, I. Tramacere, G. Pomponio, B. Gabrielli, E. V. Avvedimento, C. La Vecchia, E. Negri, A. Gabrielli, Systemic sclerosis (scleroderma) and cancer risk: Systematic review and meta-analysis of observational studies. *Rheumatology* **52**, 143–154 (2013).

Acknowledgments: We thank P. Verde for the AP1 expression vectors, M. L. Bocchino for primary cultures isolated from idiopathic lung fibrosis patients, A. Leonardi for the NF-κB repressor-expressing vector (*25*), and S. Saccomanno for the human histological sections. **Funding:** This work was supported by a Young Investigator Award from Gruppo Italiano Lotta alla Sclerodermia to G.M., by grants from Ministero Italiano per l'Università e la Ricerca Scientifica, Fondazione Cariverona, Fondazione Italiana Ricerca Artrite, Fondazione di Medicina Molecolare e Terapia Cellulare, Università Politecnica delle Marche, Ancona, Italy, and from Associazione Italiana Ricerca sul Cancro (AIRC) IG. 11364, from Epigenomics Flagship Project—EPIGEN to C.N.R., and from POR Campania FSE 2007-2013, Project CRÈME. **Author contributions:** G. Marrone and A.P. carried out the ChIP assays, the analysis of AP1 transcription factors, posttranscriptional modifications, and transfections. S.A. performed the immunohistological and immunofluorescence experiments. S.S. performed Western blot assays, interpreted results, and assisted in manuscript preparation. T.S. performed the cellular assays and RT-PCR. A.J. and O.D. provided the mouse histological sections. A. Grieco and G. Moroncini contributed to primer design and experiments using recombinant SSc-IgG. D.G. and M.V. conducted the experiments with A-T cells. A.M.M. supervised the experiments with AP1 transcription factors and generated the c-Jun mutants. A. Gabrielli and E.V.A. supervised the project and wrote the manuscript. **Competing interests:** The authors declare that they have no competing interests.

Submitted 5 August 2013
Accepted 28 July 2014
Final Publication 2 September 2014
10.1126/scisignal.2004592
Citation: S. Svegliati, G. Marrone, A. Pezone, T. Spadoni, A. Grieco, G. Moroncini, D. Grieco, M. Vinciguerra, S. Agnese, A. Jüngel, O. Distler, A. M. Musti, A. Gabrielli, E. V. Avvedimento, Oxidative DNA damage induces the ATM-mediated transcriptional suppression of the Wnt inhibitor WIF-1 in systemic sclerosis and fibrosis. *Sci. Signal.* **7**, ra84 (2014).

Science Signaling
AAAS

Oxidative DNA damage induces the ATM-mediated transcriptional suppression of the Wnt inhibitor WIF-1 in systemic sclerosis and fibrosis

Silvia Svegliati, Giusi Marrone, Antonio Pezone, Tatiana Spadoni, Antonella Grieco, Gianluca Moroncini, Domenico Grieco, Maria Vinciguerra, Savina Agnese, Astrid Jüngel, Oliver Distler, Anna Maria Musti, Armando Gabrielli and Enrico V. Avvedimento

(September 2, 2014)
Science Signaling **7** (341), ra84. [doi: 10.1126/scisignal.2004592]